A neutronic model of the PMR200 prismatic modular reactor using MCNP5

SF Sihlangu

24868507

Dissertation submitted in fulfilment of the requirements for the degree *Magister Scientiae* in Nuclear Engineering at the Potchefstroom Campus of the North-West University

Supervisor: Dr VV Naicker
Co-Supervisor: Prof S Chirayath

May 2016

Abstract

The PMR200 reactor is a prismatic modular High Temperature Reactor. The High Temperature Reactor is a near term Generation IV reactor with the capability of producing electricity, and its high outlet temperature enables thermochemical hydrogen production. This makes the PMR200 one of the candidates for the Nuclear Hydrogen Development and Demonstration plant in Korea and the Next Generation Nuclear Project. The most desirable aspect of the PMR200 is its range of safety features.

It is imperative to determine whether the reactor meets the required safety standards. In this work a neutronic analysis of the PMR200 core is performed. The model of the pre-conceptual design for the PMR200 is modelled using radiation transport and simulation code, MCNP5. The temperature of all the materials is set at 300 K and the pre-conceptual model is found to be supercritical. The reactor is made into a critical configuration by controlling the mass fraction of boron carbide to 4.2% so that the neutron multiplication factor, $k_{eff} \cong 1$.

The fuel temperature coefficients are computed for the coated particle and the fuel compact and are found to be negative. The moderator coefficient, total temperature coefficient and isothermal temperature coefficients are all found to be negative. Reactivity of the PMR core is controlled by three banks of control rods and burnable neutron poisons. Control rod worth and SCRAM reactivity are assessed for the three banks of control rods and the rods are found to have enough reactivity to change the reactor from a supercritical to a subcritical state. The effect of the neutron absorbers on the neutron economy is assessed by analysing the flux distribution in response to an insertion of absorbers. The neutron economy decreases when the control rods are fully inserted or are at the critical position. The same behaviour can be seen when the mass fraction of the boron carbide in the control rods is altered.

Keywords

High Temperature Reactor, Prismatic Modular Reactor, PMR200, neutronic analysis, criticality, reactivity worth, Doppler Coefficient, Temperature Coefficient, MCNP5

Declaration

I, the undersigned, hereby declare that the work contained in this project is my own original work.

Sinenhlanhla F. Sihlangu
Date: 20 April 2016
Potchefstroom

Acknowledgement

Firstly I would like to thank the Lord Almighty for the strength, for his mercy and his love. All that I am comes from you, Thank You.

I am sincerely grateful to my supervisor Dr V Naicker for the hours, expertise and useful commentary put into this work. I am also extremely grateful for his patience and encouragement throughout the course of this dissertation.

I would like to extend my gratitude to my co-supervisor Dr Sunil Chirayath for his expertise and input that has made this work possible.

I would also like to thank my loved ones for their love and support throughout this entire process.

My studies were funded by the DST Chair in Nuclear Engineering and its contribution to this work is acknowledged.

I am also thankful to the lecturers and the staff at the North-West University. Your teaching and assistance has been valuable and greatly appreciated.

Table of Contents

Table of Contents 5

List of Tables 8

List of Figures 9

List of Abbreviations 11

1. Introduction 13
   - 1.1. Background 13
     - 1.1.1. South African Energy 13
     - 1.1.2. High Temperature Gas Cooled Reactors 15
   - 1.2. Motivation 20
   - 1.3. Reactor Analysis 21
   - 1.4. Problem Statement 21
   - 1.5. Aim 21
   - 1.6. Objectives 21
   - 1.7. Research Benefits 22
   - 1.8. Outline of Dissertation 22
2. Literature Survey and Reactor Details 24
   - 2.1. MCNP5 Theory 24
     - 2.1.1. Introduction 24
     - 2.1.2. Neutron Transport Equation 24
     - 2.1.3. Simulation Tools 25
     - 2.1.4. Analog Simulation for Neutron Transport 26
     - 2.1.5. Criticality Problem 26
     - 2.1.6. MCNP Code Outline 27
     - 2.1.7. Verification and Validation of MCNP 27
     - 2.1.8. Nuclear data library 28
     - 2.1.9. Cross-section 29
     - 2.1.10. Source Specification 29
     - 2.1.11. MCNP Tallies 29
     - 2.1.12. Uncertainty Analysis 30
     - 2.1.13. Coefficients of Reactivity 32
     - 2.1.14. Doppler Effect 33

2.1.15. Treatment of Thermal Neutrons 34
2.1.16. Criticality Calculation in MCNP 34
2.1.17. Convergence and the Shannon Entropy 34
- 2.2. Reactor Details 36
2.2.1. Introduction 36
2.2.2. Safety Design 36
I. Fission product release 36
II. Chemical stability 37
III. Decay heat removal 37
IV. Mechanical stability 37
2.2.3. Core Layout 37
I. Side bottom and top reactor configuration 39
II. Fuel block, burnable poisons, coolant channels and block handling hole 40
III. Basic fuel form and fuel compact 41
IV. Control rods 42
3. Methodology 45
- 3.1. General Details Regarding MCNP Input 45
3.1.1. Introduction 45
3.1.2. Message Block 45
3.1.3. Title Cards 45
3.1.4. Cell Cards 46
3.1.5. Surface Cards 46
3.1.6. Data Cards 47
- 3.2. Full Core Model of the PMR200 51
3.2.1. Model Development Overview 51
3.2.2. Geometry 51
3.2.3. Materials 59
3.2.4. Tallies 60
- 3.3. Estimation of Accuracy and Precision 61
3.3.1. Model Limitation 61
3.3.2. Factors Affecting MCNP Accuracy 64
3.3.3. Factors Affecting MCNP Precision 64
- 3.4. Verification 65
- 3.5. Discretisation 67

4. Results and Discussion 68
- 4.1. Convergence 68

Convergence of K-eff 68
- 4.2. Full core model 70

Initial effective multiplication factor of the pre-conceptual PMR200 model design 70

Mass fraction of absorber material 71

Temperature coefficients (PMR200-TC) 72

Control rod worth 79
- 4.3. Time Economy of MCNP5 88

5. Conclusion 89

6. Recommendations for Future Work 90

7. Bibliography 91

8. Appendices 97
- Appendix 1: Boltzmann equation 97
- Appendix 2: Probability distribution function 98
- Appendix 3: Cumulative distribution function 98
- Appendix 4: URAN card in MCNP5 98

List of Tables

Table 1-1:Data on seven High Temperature Reactors which have been built and operated 19
Table 2-1: Major design parameters of PMR200 40
Table 2-2: Fuel block design parameters for the PMR200 41
Table 2-3: Geometry and material data for the Coated particle of the PMR200 42
Table 2-4: Control rod design parameters for the PMR200 43
Table 3-1: List of Geometry cards in MNCP 47
Table 3-2: The material composition of the reactor components 59
Table 4-1: The multiplication factors obtained from MCNP for the full core model 71
Table 4-2: A comparison of the multiplication factor for different operating control rod depths 71
Table 4-3: A comparison of the effective multiplication factor for different mass fractions of B_4C in the burnable poisons 72
Table 4-4: Temperature coefficients for a temperature rise from 300 K to 320 K 77
Table 4-5: The effect of the shutdown system on reactivity 81

List of Figures

Figure 1-1: The reactor core of the FSV HTGR 17
Figure 2-1: Doppler broadening of a resonance cross-section 33
Figure 2-2: The PMR core configuration 38
Figure 2-3: The horizontal view of the standard fuel block 39
Figure 2-4: Axial view of the fuel block 39
Figure 2-5: PMR fuel block, fuel rod, fuel compact and TRISO particle 42
Figure 2-6 : Standard fuel block and control fuel block 44
Figure 3-1: MCNP model of the PMR200 core 53
Figure 3-2: MCNP5 model of PMR200 core configuration 54
Figure 3-3: (A) The graphite block (B) The standard fuel block (C) The control fuel block 55
Figure 3-4: (A) MCNP representation of the outer fuel compact with a packing fraction of 27.5% (B) inner fuel compact with a packing fraction of 23.5% 56
Figure 3-5 : MCNP modelling procedure showing the three different lattices 57
Figure 3-6: MCNP5 model of the TRISO particle 58
Figure 3-7: (A) Randomly packed coated particles (B) Centred coated fuel particles 61
Figure 3-8: MCNP representation of the dispersion of fuel particles in the fuel rods of the PMR200 with (A) an infinite lattice (B) a finite lattice 63
Figure 3-9: A comparison of the number densities calculated number densities to the number densities computed by NWURCS 65
Figure 3-10 : A comparison of calculated nuclide ratios vs nuclide ratios computed by NWURCS 66
Figure 4-1: H_{src} vs. number of cycles 68
Figure 4-2: K-eff vs number of cycles 69
Figure 4-3: (A) standard fuel block (B) Control rod fuel block 71
Figure 4-4: The response of $keff$ on the variation of the temperature of the TRISO particle 74
Figure 4-5: The Doppler coefficient of the coated particle 74
Figure 4-6: The response of the effective multiplication factor to a variation in temperature of the fuel compact 75
Figure 4-7: Doppler coefficient of the fuel compact 75
Figure 4-8: Effective multiplication factor of the moderator at different temperatures 76
Figure 4-9: Temperature coefficient for a variation in moderator temperature 76
Figure 4-10: Effect of temperature on the effective multiplication factor 78
Figure 4-11: Isothermal temperature coefficient 78
Figure 4-12: Isothermal temperature coefficients of the PMR200 (Sihlangu) and 600 MWth GT-MHR (Jo,Noh et al) 79
Figure 4-13: Operational control rod worth in the active core 80
Figure 4-14 The effect of the presence of absorber material on the flux 82
Figure 4-15: Comparison of the effect of the control rod position on flux 83
Figure 4-16: Neutron flux vs. core height for the controls rods fully inserted at different thetal directions 84
Figure 4-17: Neutron flux vs. core height for the controls rods fully inserted at multiple thetal directions 84
Figure 4-18: Neutron flux for the controls placed at the critical rod control position 85

Figure 4-19: Comparison of control rod position vs. no control rod position for the control rods fully withdrawn 86
Figure 4-20: Comparison of different concentrations of B_4C in control rods 87

List of Abbreviations

AGR	Advanced Gas Cooled Reactor
AVR	Arbeitsgemeinschaft Versuchsreaktor (working group test reactor)
BISO	Bistructural Isotropic
BP	Burnable Poison
CDF	Cumulative Distribution Function
DOE	Department of Energy
EPR	European Pressurised Reactor
FOAK	First-Of-Its-Kind
FOM	Figure of Merit
FSD	Fractional Standard Deviation
FSV	Fort St.Vrain
GT-MHR	Gas Turbine-Modular Reactor
HEU	High Enriched Uranium (>20% U^{235})
HTR	High Temperature Reactor
HTR-10	High Temperature Reactor-10 MW
HTTR	High Temperature Test Reactor
IAEA	International Atomic Energy Agency
KAERI	Korea Atomic Energy Research Institute
LEU	Low Enriched Uranium (<20% U^{235})
LOCA	Loss of Coolant Accident
NERSA	National Energy Regulator of South Africa
NGNP	Next Generation Nuclear Plant

NHDD	Nuclear Hydrogen Development and Demonstration
NWURCS	North-West University Reactor Code Suite
PBMR	Pebble Bed Modular Reactor
PMR	Prismatic Modular Reactor
PDF	Probability Distribution Function
PyC	Pyrolytic Carbon
RSS	Reactor Shutdown System
SA	South Africa
THTR	Thorium Hochtemperatur Reaktor/Thorium High Temperature Reactor
TRISO	Tristructural Isotropic
USA	United States
VHTR	Very High Temperature Reactor
VVER	Vodno-Vodyanoi Energeticheshy Reactor (Water-Water Power Reactor)

1. Introduction

1.1.Background

1.1.1. South African Energy

The South African public began to feel the repercussions of the country's strained energy supply in 2005. Nearly 10 years later the power supply has become stretched and the energy crisis in the country seems to have worsened. Electrical power supply in South Africa is in the hands of state-owned Eskom and the company decided that the way to alleviate this shortage was to introduce load shedding. Load shedding began in the province of the Western Cape and by 2008 the blackouts were felt country-wide.

In the past South Africa has had electricity generation capacity with a reserve margin of around 40%. Today this figure has withered down to zero (Trollip, Butler, Burton, Caetano, & Godinho, 2014). The international norm for electricity supply companies is to have a minimum of 15% spare capacity to accommodate additional power demands. In addition, Eskom has a net self-generated capacity of 41194 MW (Eskom, 2015). 29.3% of this generating capacity is unavailable for supplying electricity due to repair and maintenance work (Mantahantsha, 2014), (Calldo, 2008). Eskom has recently requested an electricity tariff hike of 25.3% in an already stressed economy to assist with the maintenance of the power plants. The power cuts have cost the economy approximately 30 billion dollars since 2008 and big businesses are feeling the repercussions of the unreliable energy supply.

According to the IRP 2010-2030, South Africa plans to mitigate the electricity crisis by adding 9600 MWe by 2030 through the introduction of nuclear power stations (Intergrated Resource Plan For Electricity 2010-2030, 2011). Currently, the country's nuclear generating capacity is provided by the Koeberg Nuclear Power Station, which has a net output of 1830 MW (Cop17 fact sheet, 2011) and consists of two pressurised water reactors. South Africa's nuclear procurement programme is to begin in 2015.

Approximately 90% of the country's energy demand is supplied by coal-fired power stations, 5% is supplied by the nuclear power station, Koeberg and the remainder comes from hydroelectric power. Thus South Africa's large population relies heavily on coal. The coal sector is responsible for the bulk of CO_2 emissions, SO_2 emissions and nitrous gas emissions. The country accounts for about 45% of Africa's CO_2 emissions (Lin & Wesseh Jr., 2014) and is the 7th largest emitter of greenhouse gases per capita in the world (Menyah & Wolde-Rufael, 2010).

However, although nuclear power presents a good solution to South Africa's energy needs, one should also be aware of the apprehensions regarding nuclear power. These include long term storage of nuclear waste; the fact that uranium fuel is a non-renewable resource; and the finite although small probability of a nuclear accident occurring. Uranium reserves are a limited resource and will last approximately 50-70 years with the current demand (Mez, 2012). Nuclear accidents have been a longstanding public concern. Following the Fukushima Daiichi accident in March 2011, nuclear power has lost a lot of public favour.

Despite this, the disadvantages of coal-fired power far outweigh those of nuclear power. It is noteworthy that new generations of reactors will be built to be accident-proof with the intention of eradicating public fears in this regard.

Eskom has already taken a step forward in the new nuclear build; it has announced plans to build a new nuclear power station at Thyspunt, South East of Port Elizabeth. By 2030 the South African energy pool should consist of 48% coal, 13.4% nuclear, 6.5% hydroelectric and 14.5% other renewables (Intergrated Resource Plan For Electricity 2010-2030, 2011) .

GEN III reactors such as the VVER reactor and the European Pressurized Reactor (EPR) would most probably be the best candidates for mitigating the national energy crisis. High Temperature Reactors are in a pre-conceptual phase and are not available for commercial use. The First–Of-Its-Kind (FOAK) prismatic reactor is only scheduled for startup in the early 2020s (Areva HTGR, 2014).

1.1.2. High Temperature Gas Cooled Reactors

There are two design concepts for the High Temperature Gas-Cooled Reactor (HTGR). One is the pebble bed reactor and the other is the prismatic block type reactor. The pebble bed concept has numerous coated uranium particles embedded in a graphite matrix and then formed into a spherical fuel element. Since the modular reactor concept is the focus of this writing, the pebble bed reactor will not be discussed further.

The prismatic modular reactor is a graphite moderated, helium cooled, low enriched uranium fuel reactor. Low enrichment means that the fuel enrichment is less than 20%. The core is composed of hexagonal structured fuel blocks and blocks consisting only of graphite.

The fuel blocks house the fuel. The basic fuel form is coated uranium particles which are located in the fuel compacts. These compacts are stacked vertically to form fuel rods, and subsequently the fuel rods are inserted into vertical channels in the hexagonal blocks. The modular reactor design is explained in section 2.2.3.

The HTGR has an outlet coolant temperature of 700 – 1000°C to produce electricity and hydrogen efficiently.

HTGRs have a wide range of industrial applications ranging from electricity generation to hydrogen production. Moreover this technology boasts inherent safety, safeguards and sustainability features, which include high efficiency, very high burn-up, proliferation resistance, economical competiveness (IAEA, 2010) and a negative temperature coefficient of reactivity (Gee, 2002). The main development in HTGR technology is the coated particle as a fuel; the coated particles are either BISO particles, which are two layers of pyrolytic carbon, or TRISO particles, which are layers of pyrolytic carbon with a layer of silicon carbide surrounding the fuel kernel. These ceramic layers covering the fuel kernel aid in the retention of fission products. Further safety aspects of the PMR concept are discussed in section 2.2.1.

There are seven well-known HTGR plants with a reasonable operation history that are similar to the proposed future units[1]. These plants can be categorised into first and second generation. The first generation HTGR plants were operational from 1960 to 1990 and the second generation are the High Temperature Test Reactors (HTTR) and High Temperature Reactors-10 MW (HTR-10), which are still in operation (Mcdowell, Mitchell, Pugh, Nickolaus, & Swearingen, 2011). Four of these plants use prismatic block type fuel and three use the pebble bed fuel design.

In Great Britain, the development of HTGR reactors began with the MAGNOX[2], which was the first commercial gas cooled reactor. The 50 MWe reactor had pressurised carbon dioxide as coolant and magnesium alloy cladding for the fuel (IAEA, 2010).

1 Other smaller reactor units have been built and operated but do not have a substantial operation history as well as a substantial impact on current and planned HTGR projects (Mcdowell, Mitchell, Pugh, Nickolaus, & Swearingen, 2011).

2 The first commercial gas cooled reactor was the MAGNOX, but it utilised carbon dioxide as a pressurised coolant and magnesium alloy cladding. The gas cooled version was switched to stainless steel alloy and enriched fuel as a means of increasing efficiency (IAEA, 2010)

Later designs aimed at increasing the efficiency, so the gas cooled concept switched to stainless steel cladding and enriched uranium fuel. The next British HTGR was the DRAGON[3] reactor which was a 20 MW thermal power reactor that was operational between 1966 and 1975; it was an experimental reactor which demonstrated rod-type fuel elements with tristructural isotopic (TRISO) fuel particles. Originally the reactor was operated with a fuel load of highly enriched uranium (HEU); this was later replaced with low enriched uranium (LEU) due to questions of availability of HEU (Mcdowell, Mitchell, Pugh, Nickolaus, & Swearingen, 2011). This was the first of the the seven reactors mentioned in this writing to use a helium coolant. Today the reactor is in a state of safe enclosure for financial and political reasons.

The Peach Bottom reactor was the first HTGR developed in the USA and operated successfully between 1965 and 1988; this reactor delivered 40MW of electrical power. Peach Bottom Unit 1 was the first in the world to produce electrical power. The operation of this reactor was terminated due to the operation of Fort St.Vrain. One of the reported hurdles experienced by the Peach Bottom reactor was a large release of fission products due to the earlier design of the fuel particle, which was a thorium kernel covered with a single layer of pyrolitic carbon (PyC). Later this was replaced by bistructural isotropic (BISO) particles.

Fort St. Vrain is a medium sized reactor with block type fuel element design, producing 342 MW of electrical power. The reactor first achieved criticality in 1975 (Pavlou, et al., 2012) and operated between 1976 and 1989. This was the first reactor to have hexagonal fuel and provided important experience and understanding of hexagonal block type reactors.

3 The DRAGON reactor was a prototype of a smaller 5MWt reactor. This reactor was the first to operate with a helium coolant (IAEA, 2010).

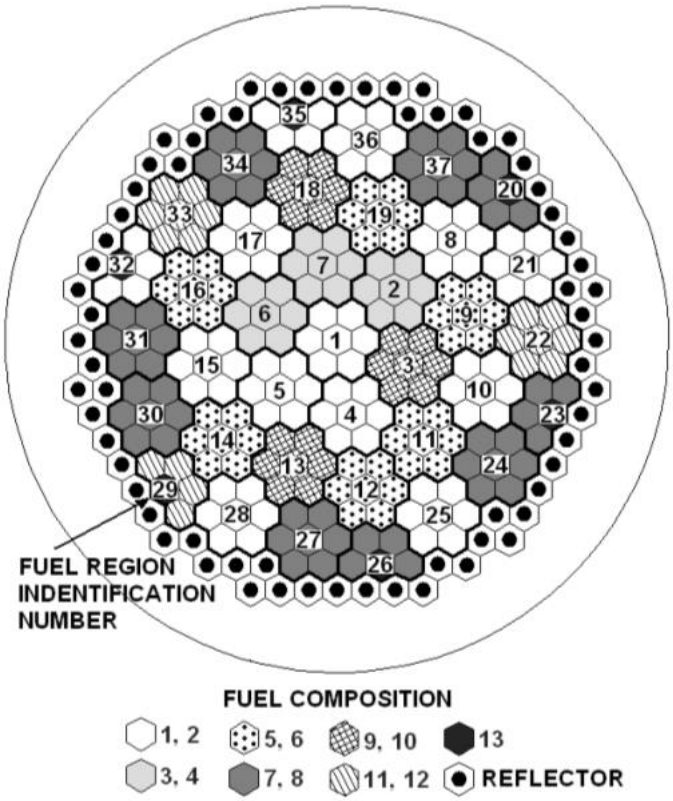

Figure 1-1: The reactor core of the FSV HTGR (Martin, June 2012)

The FSV reactor core is shown in Figure 1-1. It is partly decommissioned for various technical reasons as well as a change in public mindset regarding nuclear power in the USA.

The first pebble bed reactor, the AVR, was built in Germany in 1959 (Kuppers, Hahn, Heinzel, & Weil, 26 March 2014). This reactor was an experimental reactor, operational between 1967 and 1988 and delivering 15 MW of electrical power. From 1985 a TRISO particle with UO_2 kernel was used and prior to that the BISO fuel with UC_2 fuel kernel was used (Moormann, 2008).

Germany also built another pebble bed reactor, the THTR-300, which operated between 1985 and 1988. Thorium was used to supplement the uranium fuel. ^{232}Th absorbs a neutron from the chain reaction of ^{235}U, and ^{233}Th decays into the fissile ^{233}U, which participates in the chain reactions. The reactor delivered 308 MW of electrical power. Following the events arising from the nuclear accident in Chernobyl the reactor was shut down (NUCL 878 course, 2014).

The second generation of HTGRs has been operational since 1998. The HTTR has been successfully developed and operated in Japan. It is a block-type reactor that delivers 30 MWt of thermal power. The HTR-10 was built in China and is based on the pebble bed concept. Data on the seven rectors is tabulated in Table 1-1.

The PMR200 is a pre-conceptual design by the Korea Atomic Energy Research Institute (KAERI) and is a candidate for the Next Generation Nuclear Plant (NGNP) (Bae, Hong, & Kim, 2012), (Tak, Kim, Lim, Jun, & Jo, 2010). The NGNP Project was established by the US Department of Energy, with the objective of developing safe, clean and economical nuclear energy. Additionally the NGNP supports the US National Hydrogen Fuel Initiative (NHI), which aims to acquire technologies that are free of

greenhouse gas emissions (International Atomic Energy Agency). The HTGR is one of the nuclear reactors identified as a candidate for the NGNP Project; in addition it is a Generation IV reactor. The goals of the GEN IV project are proliferation resistance, passive safety, superior economics, reduced waste and better fuel utilisation (LaBar, Simon, Shenoy, & Campbell; Slabber, 2004). HTGR reactors far surpass these goals (Southworth, et al., 2003). The PMR200 is one of the candidates for a nuclear hydrogen development and demonstration (NHDD) plant in Korea (Tak, Kim, Lim, Jun, & Jo, 2010). KAERI plans to demonstrate enormous production of hydrogen by the 2020s and the 200 MWth power is selected because it is the proper size for a hydrogen production plant as well as for an oil refinery plant (Chang, et al., 2007). Additionally the block type reactor cores that are candidates for the NHDD and NGNP have a similar design concept to the Fort St. Vrain HTGR core (Tak, Kim, Lim, Jun, & Jo, 2010).

Other prismatic NHDD cores include the PMR 600 and PMR 350, while the pebble bed NHDD core is the PBR 200. The prismatic core is favoured by the NGNP alliance because it has a design limitation of 625 MWt per module in comparison to the pebble bed core which has a design limitation of 200 MWt per unit (Areva HTGR, 2014).

Table 1-1:Data on seven High Temperature Reactors which have been built and operated (LaBar, Simon, Shenoy, & Campbell); (NUCL 878 course, 2014); (Mcdowell, Mitchell, Pugh, Nickolaus, & Swearingen, 2011)

	Thermal Power	Electrical Power	Fuel Element Type	Fuel + Fertile Material	Coated Particles	Enrichment	Primary Inlet/Outlet Temperature (℃)	Mean He Pressure (MPa)	Years of Operation	Status
DRAGON	20	-	Cylindrical	UO_2,ThO_2	TRISO	LEU/HEU	350/750	2	1964-1975	Safe Enclosure
Peach Bottom	115	40	Cylindrical	UO_2,ThO_2	BISO	HEU	327/700-726	2.5	1966-1974	Safe Enclosure
AVR	46		Spherical	UO_2,ThO_2	BISO	HEU	275/950	1	1967-1988	Defueled
FSV	842	330	Hexagonal	ThC_2,UC_2	TRISO	HEU	450/777	4.5	1976-1989	Decommissioned
THTR	750	300	Spherical	UO_2,ThO_2	BISO	HEU	404/777	6	1985-1991	Safe Enclosure
HTTR	-	30	Hexagonal	-	TRISO	LEU	-	4	1998[4]-	In Operation
HTR-10	-	10	Spherical	-	TRISO	LEU	250/700	3	2000[4]	In Operation

4 Still operational as of date of writing

1.2.Motivation

South Africa is one of the highest greenhouse gas contributors in the world. An increasing electrical power demand and the construction of more coal powered stations aggravates the problem.

HTGRs have a higher burn-up of fuel compared to a Light Water Reactors (LWR). A LWR has a typical fuel burnup of 30 000 to 50 000 MWd/T (Stacey, 2007, p. 205). The Gas Turbine-Modular Helium Reactor (GT-MHR), which is a prismatic block type HTGR, has a typical burn-up of 100 000 MWd/T (Stacey, 2007, p. 268). Plutonium fuelled HTGRs have an ultra-high fuel burn-up of up to 700 GWd/T (Kuijper, et al., 2006).

HTGRs achieve a higher efficiency and have reduced capital cost (Lohnert, 2004). Additionally the prismatic modular reactor (PMR) is small in size. Hence the main components of the reactor can be manufactured remotely and this reduces costs (Gee, 2002). Therefore there is a need to diversify or explore a more recent generation of reactor technology (Gen IV reactors).

South Africa has the biggest economy in Africa and provides about half of the continent's energy (Menyah & Wolde-Rufael, 2010). Therefore it has an influence on the social, technological and economic decisions of other African countries (Lin & Wesseh Jr., 2014). This implies that the advancement of nuclear technology in South Africa sets the trend for the rest of Africa. There is a concern about the capital cost of nuclear power stations; however they may be expensive to build but they are cheaper to run.

The HTGR and VVER are uranium fuelled and South Africa is rich in uranium. It has one of the largest uranium reserves in the world (van Wyk, 2013) and contributes up to 45% of total African uranium reserves. The country relies on international companies such as Areva, Westinghouse Electric Company, Tenex and Urenco (van Wyk, 2013) to enrich fuel. This leaves room for skills development in this particular field as well as job creation opportunities[5].

The HTGR is a candidate for the NGNP. It is the only near-term concept that delivers process heat at high enough temperatures to produce hydrogen very efficiently (Saurwen, 2007). Heat from the helium coolant is used in the production of hydrogen, which has a number of industrial applications such as petroleum refining, metals treating, chemical production and electrical applications (Southworth, et al., 2003). Hydrogen can be produced through thermochemical splitting of water and thermally assisted electrolysis of water. Other potential applications for HTR are oil extraction from oil shales, coal gasification, desalination and heat applications using waste heat from the HTGR (IAEA, 2010).

In addition the HTGR has increased proliferation resistance because the uranium oxide kernel is situated deep within layers of ceramic (coated particle), which makes the reprocessing of fuel very difficult.

5 South Africa's unemployment rate was recorded at 25% in 2014 (Employment, unemployment,skills and economic growth, 2014).

For Gen IV technology, skills localisation is required. This opens doors for skills development in HGTR technology. Construction of an HGTR plant could create about 270 permanent jobs at the site during plant operation (Areva HTGR, 2014).

Given all of these factors, further study of the HTGR is important.

1.3.Reactor Analysis

The PMR200 input was developed firstly from the analysis of the Monte Carlo N=Particle Transport Code (MCNP) input model of the VHTR obtained from (Chirayath, 2013). This analysis contributed to an understanding of the modelling of the hexagonal fuel block in MCNP.

The PMR200 input was modelled accurately with design specifications described in the reference (Lee, Jo , Shim, Kim, & Noh, 2010). Number densities for the materials were computed manually and then later generated by North-West University Reactor Code Suite (NWURCS) for verification. The geometry of the model was assessed repeatedly and later compared to the input file generated by NWURCS to assess the accuracy of the MCNP model.

One of the assumptions made about the core model was that the reactor is critical ($k_\infty \approx 1$) at a temperature of 300 K. Although this will not be a true reflection of the real case, it provides a good starting point in terms of developing the model. MCNP delivered a supercritical value ($k_\infty > 1$), so adjustments were made to the concentration of absorber material in the poisons as well as to the position of the absorbers, so the reactor was critical($k_\infty \approx 1$). Convergence of the model is assessed followed by the analysis of control rod reactivity worth, temperature coefficients and neutron fluxes of the full core model.

1.4.Problem Statement

As discussed in section 1.2, the deployment of the HTGR as a nuclear reactor system in South Africa is a possible scenario. To this end, adequate localised analysis techniques for this type of reactor must be developed.

Recognising this need, this dissertation focuses specifically on developing and analysing the MCNP5 neutronic model for the PMR200.

1.5. Aim

An MCNP5 is used to perform criticality calculations for the PMR 200 reactor. Additionally calculations are performed for temperature coefficients, control worths and the effect of the absorbers rods on the neutron flux is analysed.

1.6.Objectives

The objectives of this dissertation are to:

- Construct an input model of the PMR200.

    - Test the material and geometry of the model by comparing material specifications (density and elemental atom fractions) with the density obtained from the NWURCS. NWURCS is the acronym for North-West University Code Suite (Naicker, du Toit, & Nyalunga, 2015). It was developed at NWU School of Mechanical and Nuclear Engineering. It is a FORTRAN script that generates an MCNP input for a reactor system.

    - Check convergence of MCNP results.

    - Perform criticality analysis calculations and reactivity calculations for the full core.

    - Assess the time economy when using MCNP.

1.7.Research Benefits

The Mechanical and Nuclear Engineering School at the North West University (NWU) commenced research on Prismatic High Temperature Reactors, including neutronic and thermal fluids research projects. A neutronic Monte Carlo simulation for hexagonal fuel assemblies had not been done before at the NWU.

1.8.Outline of Dissertation

The Prismatic Modular Reactor is modelled and the results are obtained using radiation transport code, Monte Carlo N-Particle 5, (MCNP5) version 1.60 release.

Chapter Two is the literature survey, which details the background and physics of the Monte Carlo simulations. The physics of the MCNP code includes nuclear data libraries, particle transport methodology, radiation source definitions and scoring tallies. The second part of Chapter Two discusses the geometry description of the PMR200.

Chapter Three discusses the construction of the PMR model; verification of the model includes material and geometry verification using NWURCS.

Chapter Four is a presentation of the results using the methods mentioned in Chapter Three. This chapter begins with testing for convergence.

Chapter Five gathers up all the results and contains the concluding remarks.

Chapter Six discusses the recommendations for future work.

Chapter Seven is the bibliography.

Chapter Eight is the appendix, which gives background theory and also explains theory which was not explained in Chapter Two.

2. Literature Survey and Reactor Details

2.1.MCNP5 Theory

2.1.1. Introduction

This section discusses the physics of Monte Carlo simulations that apply to the MCNP model of the PMR200.

2.1.2. Neutron Transport Equation

Neutron transport and neutron interaction within matter is fundamental to understanding reactor core physics. Solving the neutron transport equation can predict the distribution of neutrons in the core; it is the neutron balance equation that has its origin in the Boltzmann equation. The Boltzmann equation is used in the kinetic theory of gases and is discussed further in the appendix.

Neutron transport solves a number of different problems and this writing focuses on the criticality problem.

The neutron transport equation can be simplified as follows (Kulikowska, 2000):

Rate of change of neutrons = net rate of generation of neutrons in collisions

+ rate of introduction of source neutrons

– net rate of outflow of neutrons

The neutron transport equation is as follows (Stacey, 2007):

$$\frac{\partial N}{\partial t}(\boldsymbol{r},\boldsymbol{\Omega},\mathrm{t})d\boldsymbol{r}d\boldsymbol{\Omega} = \mathrm{v}\big(N(\boldsymbol{r},\boldsymbol{\Omega},\mathrm{t}) - N(\boldsymbol{r}+\boldsymbol{\Omega}dl,\boldsymbol{\Omega},\mathrm{t})\big)dAd\boldsymbol{\Omega}\int_{\mathbf{0}}^{4\pi} d\boldsymbol{\Omega}'\Sigma_s(\boldsymbol{r},\boldsymbol{\Omega}'\rightarrow\boldsymbol{\Omega})\mathrm{v}N(\boldsymbol{r},\boldsymbol{\Omega}',\mathrm{t})d\boldsymbol{r}d\boldsymbol{\Omega} + \frac{1}{4\pi}\int_{0}^{4\pi} d\boldsymbol{\Omega}'\nu\Sigma_f(\boldsymbol{r})\mathrm{v}N(\boldsymbol{r},\boldsymbol{\Omega}',\mathrm{t})d\boldsymbol{r}d\boldsymbol{\Omega} + \mathrm{S}_{ex}(\boldsymbol{r},\boldsymbol{\Omega})d\boldsymbol{r}d\boldsymbol{\Omega} - (\Sigma_a(\boldsymbol{r})+\Sigma_s(\boldsymbol{r}))\mathrm{v}N(\boldsymbol{r},\boldsymbol{\Omega},\mathrm{t})d\boldsymbol{r}d\boldsymbol{\Omega} \quad (1.1)$$

where:

$r(x,y,z)$ is the position vector

v is the neutron velocity (Mansour, Saad, & Aziz, 2013)

Ω is the direction of motion

t is the time

Σ_s is the macroscopic neutron scattering cross-section

Σ_t is the total neutron cross-section

$N(\boldsymbol{r}, \boldsymbol{\Omega}, \mathrm{t})d\boldsymbol{r}d\boldsymbol{\Omega}$ is the number of neutrons at position $\boldsymbol{r}$ and direction $\boldsymbol{\Omega}$ in the differential volume **dr**

$\frac{\partial N}{\partial t} d\boldsymbol{r}d\boldsymbol{\Omega}$ is the rate of change of $N(\boldsymbol{r}, \boldsymbol{\Omega}, \mathrm{t})$ within the volume element

$\int_0^{4\pi} d\boldsymbol{\Omega}' \Sigma_s(\boldsymbol{r}, \boldsymbol{\Omega}' \rightarrow \boldsymbol{\Omega}) \mathrm{v} N(\boldsymbol{r}, \boldsymbol{\Omega}', \mathrm{t}) d\boldsymbol{r}d\boldsymbol{\Omega}$ is the rate at which neutrons traveling in direction $\boldsymbol{\Omega}$ are being introduced into the volume element by scattering of neutrons within the differential volume from different directions $\boldsymbol{\Omega}'$

$\int_0^{4\pi} d\boldsymbol{\Omega}' \nu \Sigma_f(\boldsymbol{r}) \mathrm{v} N(\boldsymbol{r}, \boldsymbol{\Omega}', \mathrm{t}) d\boldsymbol{r}d\boldsymbol{\Omega}$ is the rate at which neutrons are produced by fission

$\mathrm{S}_{ex}(\boldsymbol{r}, \boldsymbol{\Omega}) d\boldsymbol{r}d\boldsymbol{\Omega}$ is the rate at which neutrons produced by an external source are introduced into the volume element

$(\Sigma_a(\boldsymbol{r}) + \Sigma_s(\boldsymbol{r})) \mathrm{v} N(\boldsymbol{r}, \boldsymbol{\Omega}, \mathrm{t})$ is the rate at which neutrons within the volume element travelling in the direction $\boldsymbol{\Omega}$ are being scattered into a different direction $\boldsymbol{\Omega}'$ or being absorbed

The neutron transport equation holds under the following assumptions (Lewis & Miller, Computational Methods of Neutron Transport, 1985):

- Particles may be considered as points
- Particles travel in straight lines between points
- Particle-particle interactions may be neglected
- Collisions may be considered as instantaneous
- The material properties are considered to be isotropic
- The properties of nuclei and the composition of materials under consideration are assumed to be known and time-independent unless explicitly stated
- Only the expected or mean value of the particle density distribution is represented

2.1.3. Simulation Tools

Neutronics is the modelling and simulating of neutron transport and interactions in a reactor. The two existing methods are deterministic and stochastic and are discussed in more detail below.

Deterministic method

Deterministic methods solve the Boltzmann transport equation either in an analytic or a numerical manner. The diffusion method is one of the deterministic methods and is especially accurate when applied to low-heterogeneous systems such as the LWR.

There are a few deterministic codes available for HTGR physics analysis, examples being the VSOP code (Kim, Cho, Lee, Noh, & Zee, 2007) and HELIOS.

Monte Carlo method

The Monte Carlo method is useful when it is difficult to describe physical phenomena using deterministic methods. It is a statistical approach and is used to approximate the probability of certain outcomes by performing multiple runs utilising different random variables. To execute Monte Carlo calculations one would have to provide the probability density functions (PDFs) that describe a system and the simulation proceeds by random sampling from the PDFs. A number of particle histories are performed and the final answer is taken as the average of the particle histories. The variance is also predicted with this average result.

The Monte Carlo code can be coupled with a thermal hydraulic code to obtain 3D power and thermal hydraulic solutions for the core.

Monte Carlo is advantageous because in principle it can be used for an accurate prediction of the core characteristics of Very High Temperature Reactors (VHTRs) (Kim, Cho, Lee, Noh, & Zee, 2007). Conversely the code can be impractical since it requires a lot of CPU time and can be expensive. Some of the current Monte Carlo codes include McCard, Serpent, KENO in SCALE, MASTER, MVP and MCNP.

Hybrid methods or combining both methods

It is becoming common practice to combine the capabilities of deterministic methods with Monte Carlo to overcome the undesirable characteristics or short-comings of each technique, such as the two step procedure in (Kim, Cho, Lee, Noh, & Zee, 2007) which utilises the HELIOs and MASTER codes for a physics analysis of the VHTR core.

2.1.4. Analog Simulation for Neutron Transport

Neutrons in a Monte Carlo simulation have a stochastic nature governed by random numbers. The Monte Carlo codes have random number generators but the source in the first cycle is in some cases user-specified (Montwedi, 2014).

The problem begins with a neutron source, which has a spatial distribution, a distribution in energy and an isotropic distribution in direction. The distributions are described by cumulative distribution functions (CDFs) and PDFs. The neutron variables such as position, direction cosines, energy, next collision distance, scattering probabilities, next collision nuclide, etc. contained in the probability density functions of linearised integral Boltzmann particle transport equation, are sampled appropriately using a random number generator for each particle history simulated.

2.1.5. Criticality Problem

The neutron transport equation is applied to fixed source problems (shielding calculations) and criticality problems. There are two important eigenvalues when discussing criticality, the effective

neutron multiplication factor, k_{eff} and the time-absorption eigenvalue, α. These eigenvalues indicate whether a system is critical or not and by how much.

The k_{eff} eigenvalue is most commonly used to assess the steady state criticality problem. The k eigenvalue can be adjusted by changing the geometry of the reactor, changing densities of materials (particularly the absorber material) or typically by insertion or withdrawal of control rods.

The k eigenvalue can be expressed as follows (Stacey, 2007):

$$k = \frac{\nu\Sigma_f/\Sigma_a}{1 + L^2B_g^2} = k_\infty P_{NL} \tag{2.3}$$

where

P_{NL} = nonleakage probability

k_∞ is the multiplication constant for an infinite assembly with no leakage and can be defined by the four factor formula

$$k_\infty = \eta f \varepsilon p \tag{2.4}$$

This aids in understanding the single effects. ε is the fast fission factor, p is the resonance escape probability and is the probability that the neutron is not captured during the slowing down process. f is the thermal utilisation and η is the product of the fission probability for a neutron absorbed in the fuel and the average number of neutrons released per fission.

The criticality calculation procedure in MCNP is discussed in section 2.1.16.

2.1.6. MCNP Code Outline

MCNP is a general purpose, continuous-energy, generalised-geometry, coupled n particle (neutron, photon and electron) Monte Carlo transport code (Seker & Colak, 2003). MCNP is developed at the Oak Ridge National Laboratory and distributed for Los Alamos by the Radiation Safety Information Computational Centre (RSICC) (http://www-rsicc.ornl.gov/rsic.html). In this writing MCNP version 5, release 1.60 is used.

The MCNP code package includes a plotting referred to as the Visual Editor or Vised. Vised is designed to assist the user by displaying the geometry specified in the input file. The user can also create an input in Vised (Schwarz, Schwarz, & Carter, 2011)

2.1.7. Verification and Validation of MCNP

MCNP is a verified and validated code for various benchmarks. Verification is performed by code developers to determine if the code accurately solves the equations as well as the models it is designed to solve (Brown, Mosteller, & Sood, 2003). It may also include comparison to older versions of MCNP. In the reference (Brown, Mosteller, & Sood, 2003), MCNP5 is compared to MCNP4C2 and

four sets of verification problems are used to ensure correctness. Tests include 42 regression tests, a suite of 26 criticality benchmark problems, a suite of 10 analytic benchmarks for criticality and 19 radiation shielding validation problems. It is concluded that MCNP5 is verified to be as reliable and accurate as previous versions and that all previously existing capabilities have been preserved (Brown, Mosteller, & Sood, 2003).

Validation suites are performed to provide an indication of the degree of accuracy of MCNP and its libraries. The MCNP verification test suite gives 97% coverage of the code (Hendricks, et al., 2000). Results obtained from using the new release of MCNP are compared to results from benchmark experiments as well as previous releases of MCNP. The verification process is extensive and tedious; furthermore cash rewards are given for any bugs found in the code (Brown, Mosteller, & Sood, Verification of MCNP5, 2003).

In the criticality validation suite a number of cases are considered, including a variety of fissile materials and neutron energy spectra, low enriched uranium, intermediate enriched uranium, highly enriched fuel as well as fuels in configuration that provide fast, intermediate and thermal spectra (Mosteller).

2.1.8. Nuclear data library

MNCP utilises continuous-energy atomic and nuclear data libraries. These are evaluated from the Evaluated Nuclear Data File (ENDF/B-VII) system, Advanced Computational Technology Initiative (ACTI), Evaluated Nuclear Data Library (ENDL), Evaluated Photon Data Library (EPDL), Activation Library (ACTL) compilations and evaluations from Nuclear Physics (T–16) Group 6, 7, 8. Version 5 includes updates from ENDF/B-VI.6, ACTI and EPDL97. Certain codes are used to process the evaluated data into an ACE (A Compact ENDF) format suitable for MCNP. As of this writing version 6 of MCNP has been released but it was not necessary to use version 6 since this research does not include burn-up calculations and hence a previous version, MCNP5 was used.

MCNP has over 836 neutron interactions for approximately 100 different isotopes and elements. Some of the isotopes or elements have neutron cross-sections at different temperatures. The neutron data tables include data that is collected at different temperatures and different processing tolerances. Neutron data tables also exist for photon interactions, neutron-induced photons, neutron dosimetry or activation and thermal particle scattering. Each data table has a unique identifier termed ZAID, where Z is the atomic number, A is the mass number and ID is the library specifier. Photon interaction tables exist for all elements from the atomic number 1 to atomic number 100. Neutron-induced photon interactions are recorded as part of the neutron interaction tables.

Cross section data exists for approximately 200 dosimetry or activation reactions involving more than 400 target nuclei in ground and excited states. Thermal data for the S(α,β) treatment to consider the chemical binding and crystalline effects are included. The S(α,β) treatment data is available for benzene, graphite, zirconium, beryllium oxide, beryllium metal, light water, heavy water, polyethylene and hydrogen in zirconium hydride.

2.1.9. Cross-section

The cross-section stored in units of barns (10^{-24} cm^2) is the degree to which neutrons interact with the nuclei. When a neutron interacts with a nucleus, it can either scatter or be absorbed. The absorption cross-section is denoted by σ_a, therefore

$$\sigma_a = \sigma_\gamma + \sigma_f + \sigma_p + \sigma_\alpha + \ldots \quad (2.5)$$

where σ_p and σ_α are the cross-sections for (n,p) and (n,α) reactions[6] respectively, σ_f is the fission cross-section and σ_γ is the capture cross-section. The total cross-section is

$$\sigma_t = \sigma_s + \sigma_i + \sigma_\gamma + \sigma_f + \ldots + \ldots \quad (2.6)$$

where σ_s and σ_i are the elastic scattering and inelastic cross-sections respectively.

The MCNP package has nine sets of nuclear data sets which include:

- Neutron interaction data (there is one neutron interaction table per element)
- Photon interaction cross sections
- Electron Interaction data
- Neutron dosimetry cross-section
- Neutron thermal $S(\alpha, \beta)$ tables
- Multigroup cross-section libraries

For this writing, only the neutron interaction cross-sections and the neutron thermal $S(\alpha, \beta)$ tables are used. The neutron interaction cross-sections are split into continuous energy and discrete cross-sections which have the form ZAID.nnC and ZAID.nnD respectively. In particular the continuous energy data has been used from ENDF/B-VII.

2.1.10. Source Specification

In MCNP, the source is specified by the user and there are three ways in which the user can specify the source. All three methods allow the user to specify various source conditions without making a change in the input model. Source variables of energy, position, time and direction are specified. Information about the geometrical extent of the source and the parameters starting cell or surface can also be specified.

2.1.11. MCNP Tallies

Tallies are recordings of average flux behaviour. The basic types of tallies are current at a surface, flux at a surface, flux at a point or ring and flux averaged over a cell. In this study F4 mesh tallies are used. They will be discussed in section 3.1.

[6] (n,p) and (n,α) reactions are charged particle reactions that result in the absorption of neutrons. These reactions can be exothermic or endothermic (Lamarsh, 2nd edition)

2.1.12. Uncertainty Analysis

It is important to assess the accuracy and precision of the results obtained from a Monte Carlo code. Factors such as tally type, variance reduction techniques and number of histories have an effect on the precision of results. MCNP has a lot of quantities to assess the accuracy and quality of the results and these quantities are discussed below.

I. Tally mean

The tally mean is the average of all histories calculated in a run and is given by

$$\overline{x} = \frac{1}{N}\sum_{i=1}^{N} x_i \tag{2.7}$$

where

N = the number of histories

$x_i =$ the total contribution from the ith starting particle

$\overline{x} =$ the average value of the scores for all histories calculated.

The sample mean $\bar{x}$ estimates the true mean and is given by $E(x) = \int xf(x)$. The relation between these two is given by the law of large numbers. $f(x)$ is the distribution of x.

II. Variance and standard deviation

The variance is a measure of the spread in values and is given by

$$\sigma^2 = \int \big(x - E(x)\big)^2 f(x)dx \tag{2.8}$$

The standard deviation is denoted by σ.

III. Relative error

MCNP prints out the relative error, which is also called the fractional standard deviation (FSD). It is the value that is always reported with the tally result $\overline{x}$, (Hussein, 1997) and is defined as

$$R = \frac{S_{\bar{x}}}{\bar{x}} \tag{2.9}$$

where $S_{\bar{x}}$ is the estimated standard deviation, $S_{\bar{x}} = \frac{S}{\sqrt{N}}$. . The relative error is an indication of the precision of the tally mean.

IV. Figure of merit

The figure of merit (FOM) is defined by the following:

$$FOM \equiv \frac{1}{R^2 T} \tag{2.10}$$

T is the computer time (in minutes) of the calculation and $R^2 \approx \frac{1}{N}$ and $R^2 T$ is approximately a constant in Monte Carlo. The figure of merit indicates the reliability and behavior of the tallies. For a well behaved tally FOM is approximately constant except for the possibility of statistical fluctuations, which vary in the problem. The possible statistical fluctuations have a FOM of approximately 2R. The FOM also determines the quality of the mean $\overline{x}$. A large value of the FOM is preferable as it reduces the computer time.

V. Variance of the variance

The variance of the variance (VOV) is the estimated relative variance of the relative error R. VOV helps the MCNP user with determining the reliability of the confidence intervals. VOV approximates σ in the central limit theorem and is defined by

$$VOV = \frac{s^2\left(S_{\bar{x}}^2\right)}{S_{\bar{x}}^4} \tag{2.11}$$

$s^2\left(S_{\bar{x}}^2\right)$ = is the estimate variance in $S_{\bar{x}}^2$((X-5 Monte Carlo Team, 2003), page 2-122).

Variance of variance for the tally bin is

$$VOV = \frac{\sum(x_i - \bar{x})^4}{(\sum(x_i - \bar{x})^2)^2} \tag{2.12}$$

VI. Central limit theorem

The central limit theorem states that for large values of N, and identically independent random variables, with finite means and variances, the distribution of $\bar{x}'$s approaches a normal distribution (X-5 Monte Carlo Team, 2003).

The purpose of the central limit theorem is to define the confidence intervals [ ].

$$\lim_{V\to\infty} P_r\left[E(x) + \alpha\frac{\sigma}{\sqrt{N}} < \bar{x} < E(x) + \beta\frac{\sigma}{\sqrt{N}}\right] = \frac{1}{\sqrt{2\pi}}\int_{\alpha}^{\beta} e^{\frac{-t^2}{2}dt} \tag{2.12}$$

α and β are arbitrary, and $P_r[Z]$ is the probability of attaining Z.

In terms of estimated standard deviation of $\bar{x}$ and $S_{\bar{x}}$

$$\lim_{V\to\infty} P_r\left[\alpha S_{\bar{x}} < \frac{\bar{x} - E(x)}{\frac{\sigma}{\sqrt{N}}} < \beta\frac{\sigma}{\sqrt{N}}\right] \approx \frac{1}{\sqrt{2\pi}}\int_{\alpha}^{\beta} e^{\frac{-t^2}{2}dt} \tag{2.13}$$

$$\lim_{V\to\infty} P_r\left[\alpha S_{\bar{x}} < \frac{\bar{x} - E(x)}{\frac{\sigma}{\sqrt{N}}} < \beta\frac{\sigma}{\sqrt{N}}\right] \approx \frac{1}{\sqrt{2\pi}}\int_{\alpha}^{\beta} e^{\frac{-t^2}{2}dt} \tag{2.14}$$

2.1.13. Coefficients of Reactivity

Neutron reactivity is affected by the changes in the state of the coolant, by the movement of the control rods, by changing densities and mainly by changes in temperature. A change in temperature has an effect on the value of k_{eff} and in turn that has an effect on the neutron reactivity of the reactor. The temperature coefficient is defined (Stacey, 2007) as:

$$\alpha_T \equiv \frac{\delta\rho}{\delta T} \tag{2.15}$$

where *T* is the temperature, and ρ is the reactivity which is defined as (Lamarsh, 2nd edition)

$$\rho = \frac{k-1}{k} = 1 - \frac{1}{k} \tag{2.16}$$

and by differentiation (Lamarsh, 2nd edition)

$$\alpha_T = \frac{1}{k^2}\frac{\delta k}{\delta T} \cong \frac{1}{k}\frac{\delta k}{\delta T} \tag{2.17}$$

In this approximation the value of *k* is close to unity so $k^2 \cong k$.

For $\alpha_T > 0$, an ever increasing *T*, leads to an ever increasing *k* and ultimately a meltdown. An ever decreasing T leads to an ever decreasing k and ultimately a shutdown. A positive temperature coefficient leads to an unstable reactor.

For $\alpha_T < 0$, an increase in temperature leads to a decrease in power (decrease in *k*) and leads to a decrease in reactor temperature and in turn returns the reactor back towards the original state. A

decrease in reactor temperature leads to an increase in power (increase in *k*), which decreases the reactor temperature and reactor is returned back to its original state. A negative reactor coefficient is self-regulating and therefore leads to a stable reactor.

Since the fuel, moderator and reflectors are not at the same temperature nor at the same physical position, each component has its own reactivity coefficient i.e. moderator temperature coefficient α_m, reflector coefficient, α_R, and fuel temperature coefficient, α_f. The fuel temperature coefficient of reactivity is also known as the Doppler temperature coefficient of reactivity.

The moderator coefficient is negative or positive depending on whether the particular moderator "moderates more than it absorbs" or "absorbs more than it moderates.

2.1.14. Doppler Effect

- Most nuclear reactors have a negative Doppler temperature coefficient due to the nuclear Doppler Effect.
- The change in shape of the resonance with temperature is known as Doppler broadening. As seen in Figure 2-1, as the temperature of the fuel increases the cross-section of fuel specifically spreads out or broadens. This feedback effect has its origin in the resonance cross-section of heavy nuclei such as ^{238}U. The cross-sections of heavy nuclei exhibit resonances at particular energies, mainly as a result of absorption.

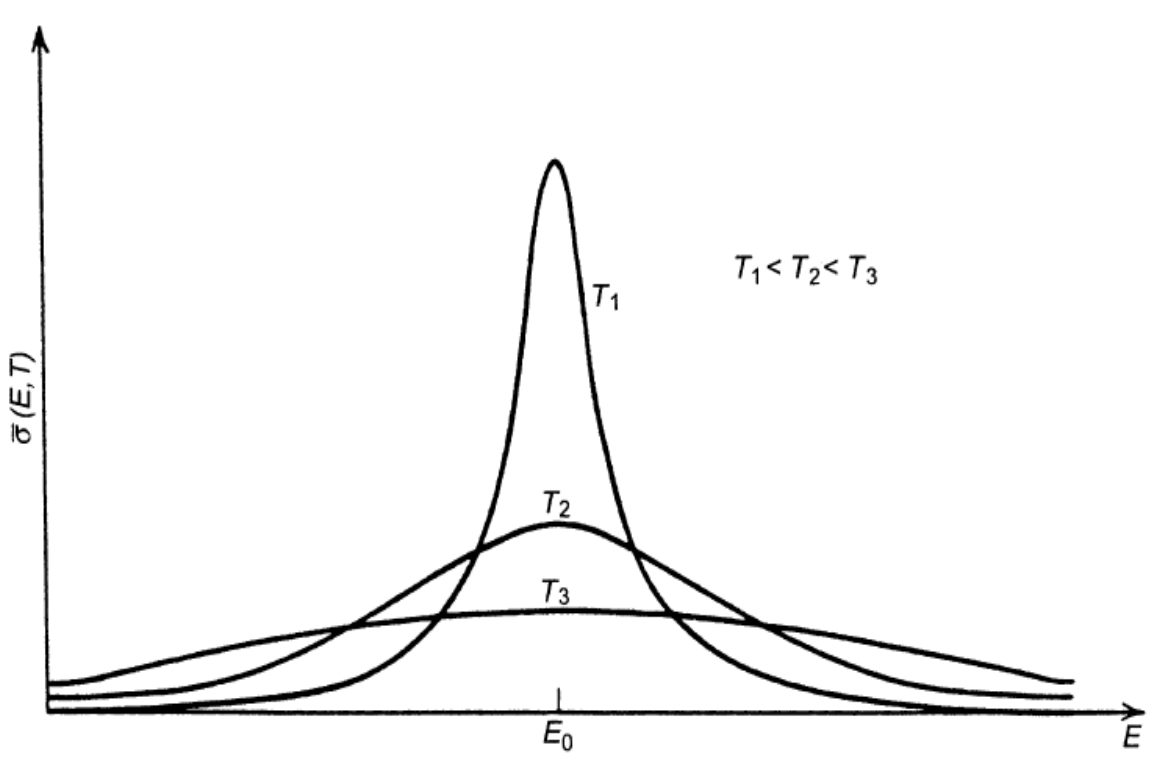

Figure 2-1: Doppler broadening of a resonance cross-section (Stacey, 2007)

2.1.15. Treatment of Thermal Neutrons

Thermal neutrons are described by both the free gas and S(α,β) models. In the free gas thermal treatment it is assumed that the medium is a free gas. The thermal free gas treatment in MCNP is applicable to elastic scattering only and the S(α,β) thermal scattering treatment applies to both elastic and inelastic scattering.

2.1.16. Criticality Calculation in MCNP

The criticality calculations in Monte Carlo are based on the iterative procedure called power iteration ((X-5 Monte Carlo Team, 2003), page 2-169). It has the following characteristics:

- The initial guess for fission source spatial distribution (first generation) as well as the initial value of k_{eff} is user specified.
- The source for the next fission generation is produced by the histories that follow and a new value for k_{eff} is estimated.
- The new fission source distribution is used to follow histories in the second generation producing another fission distribution and estimate for k_{eff}.
- The cycles or generations are repeated until the source spatial distribution has converged.
- The multiplication constant is computed from

$$k_{eff} = \frac{fission\ neutrons\ in\ generation\ i+1}{fission\ neutrons\ in\ generation\ i} \tag{2.18}$$

$k_{eff} > 1$	supercritical
$k_{eff} = 1$	critical
$k_{eff} < 1$	subcritical

2.1.17. Convergence and the Shannon Entropy

MCNP calculates the value of k_{eff} using the power-iteration procedure (Brown, 2006) discussed in section 2.1.16. So it is vital to ensure that the power-iteration procedure has converged to ensure that contamination of the source is negligible.

In order to obtain the correct results whilst performing criticality calculations, it is imperative to address the convergence of k_{eff} and the fission source distribution prior to completing the tallies. Convergence of the fission source distribution and the estimated value of k_{eff}((X-5 Monte Carlo Team, 2003), page 2-169) can be written as

$$\vec{S}^{(n+1)} \approx \overrightarrow{s_0} + a\left(\frac{k_1}{k_0}\right)^{n+1}\overrightarrow{s_1} + \cdots \tag{2.19}$$

$$k_{eff}{}^{(n+1)} \approx k_0 \left[1 - b\left(\frac{k_1}{k_0}\right)\left(1 - \frac{k_1}{k_0}\right)^n + \cdots\right]$$

(2.20)

where $\overrightarrow{s_0}$ and k_0 are the eigenfunction and eigenvalue of the fundamental mode, $\overrightarrow{s_1}$ and k_1 are the eigenfunction and eigenvalue of the first higher mode, a and b are constants, and n is the number of cycles performed in the power iteration procedure ((X-5 Monte Carlo Team, 2003),page 2-169).

The Shannon entropy is available in MCNP to assist the user with examining the convergence of the fission source spatial distribution. As the fission source distribution becomes stationary, the Shannon entropy, H_{src} approaches a single steady-state value (Brown, Nease, & Cheatham, 2007).

The Shannon entropy H_{src} is calculated from the following:

$$H_{src} = -\sum_{j=1}^{N_s} P_j \cdot ln_2(P_j)$$

(2.21)

where P_j is the fraction of the source distribution in bin J and N_s is the number of tally bins for the source distribution.

Although MCNP reports whether the source has passed the convergence test or not, it is still essential that the plot of H_{SRC} vs. cycle be examined to further verify that the number of inactive cycles is adequate for fission source convergence (X-5 Monte Carlo Team, 2003).

In a criticality calculation, there are a user-defined number of cycles which are to be skipped. These cycles are labelled the in-active cycles; this is where the spatial source changes from the initial guess to the appropriate distribution for the problem. After an MCNP run has completed, MCNP makes a recommendation for the number of cycles that should be skipped. An adequate number of initial cycles must be discarded before the tallies are estimated for neutron flux so that the contamination of the initial source is negligible (Brown, 2009).

2.2.Reactor Details

2.2.1. Introduction

The prismatic modular reactor is a graphite moderated, helium cooled, low enriched uranium fuel reactor. The core is composed of hexagonal structured fuel blocks, which house the fuel. The basic fuel form is a coated particle. The PMR200 fuel block has the same dimensions as the GT-MHR reactor (Kim & Lim, 2011). The reactor fuel is double-heterogeneous; this is due to the heterogeneity of the coated particle in the fuel compact and the heterogeneity of the fuel compact in the fuel block. In addition, the fuel block has axial heterogeneity due to the non-fuel zones filled with graphite at the top and bottom (Han, Lee, Jo, & Noh, 2013). This heterogeneity of the reactor core makes it complex to model. This section discusses the inherent safety features of the PMR as well as the design specifications.

2.2.2. Safety Design

The PMR has unique and inherently safe features; mainly the core is durable, the reactor fuel has good retention of fission products and the core cannot melt under a LOCA. The components of the reactor such as the fuel and moderator are designed to be invulnerable to chemical and irradiation damage.

I. Fission product release

There are four barriers against fission product release. The first and outermost barrier is the reactor containment building. This is followed by the reactor pressure vessel (RPV), followed by the fuel element, and lastly the coated particle. The reactor containment building is a reinforced concrete building that protects the reactor from outside impacts. In addition the reactor containment building stays intact during a depressurisation accident (Kunitomi, Katanishi, Takada, Takizuka, & Yan, 2004). The reactor pressure vessel is made of cast steel and houses the reactor internals. The boundary of the RPV protects against product release. The fuel element is made from graphite which has high durability at very high temperatures.

A coated particle is the last and very efficient fission barrier. The layers of ceramic have an excellent fission retention capability. The very tiny fuel kernel is pre-stressed externally by the graphite matrix of the fuel elements and can be considered as a pressure vessel. These pressure vessels are very tiny with very tight walls and can retain fission products very well (NUCL 878 course, 2014). The buffer layer (see Figure 2-5) functions as a storage for fission products that have escaped the kernel. The SiC carbide layer prevents the migration of fission products and pyrolytic layers maintain their integrity at high temperatures.

II. Chemical stability

Helium is an excellent coolant because it is an inert gas and will not react chemically or radiologically with other materials of the core or with any ingress elements. Due to the great retention of fission products in the coated particle, the circuits of operating HTGR plants that have been operated were very clean (NUCL 878 course, 2014). N_2, O_2, H_2O, CO_2, CO, CH_4 and H_2 are the impurities that can be found in the helium circuit, but in very minute levels.

The N_2, O_2 and H_2O originate from air contamination during refuelling and maintenance. Further H_2O contamination is caused by water ingress. Carbon monoxide and carbon dioxide contamination stem from carbon oxidation, where miniscule amounts of carbon dioxide enter during air contamination. H_2 contamination is from water vapour and some hydrogen is produced in the form of tritium. Moreover the dominant tritium source in the coolant gas is the neutron activation. Methane arises from hydro-gasification (Kissane, 2009).

III. Decay heat removal

The reactor contains two independent shutdown systems, i.e. control rods and a reserve shut down system. The prismatic modular reactor has a passive cooling system, the Reactor Cavity Cooling System to remove decay heat when the Shutdown Cooling System and Heat Transport System are non-operational. The passive cooling system prevents the reactor temperature from surpassing 1600^0C. Removal of decay heat is self-acting and is possible through self-reliant mechanisms such as heat conduction, heat radiation and free convection. The reactor has a negative temperature coefficient of reactivity, which inherently shuts down the reactor above normal operating temperatures. The reactor pressure vessel is uninsulated to allow for decay removal under accident conditions.

IV. Mechanical stability

Graphite stays stable up to 3600^0C.

- The cold gas temperature has to be above 250^oC (for all HTGR concepts) to reduce the Wigner effect significantly. At irradiation temperatures below 200^oC, the inner energy of the graphite lattice is raised up, which results in spontaneous annealing effects and a sudden release of energy (NUCL 878 course, 2014).
- The graphite structures can be damaged by fast neutrons, causing material shrinkage and a later stage material expansion. In HTGR concepts, the reflector system is designed to limit the amplitude of the fast flux, so that the reflector is changed after a longer period of operation (NUCL 878 course, 2014).

2.2.3. Core Layout

The PMR200 core is an annular core with 66 fuel columns, each with six fuel blocks stacked axially. The standard fuel block contains 12 burnable poison holes, 102 coolant channels and 204 fuel holes as shown in

Figure **2-3**. The inner fuel has a packing fraction of 23.5% and the outer fuel has a packing fraction of 27.5%. The packing fraction is the ratio or percentage of the TRISO particle in the fuel pin. The fuel reload scheme used is the three batch fuel shuffling scheme. (Lee, Jo , Shim, Kim, & Noh, 2010) The reactor is fuelled with UO_2. The inlet and outlet temperatures of helium are $490℃$ and $950℃$ respectively (Tak, Kim, Lim, Jun, & Jo, 2010).

The core has three sets of control rods, 12 start-up control rods, 24 operating control rods and 12 reserve shut-down control rods as illustrated in Figure 2-2.

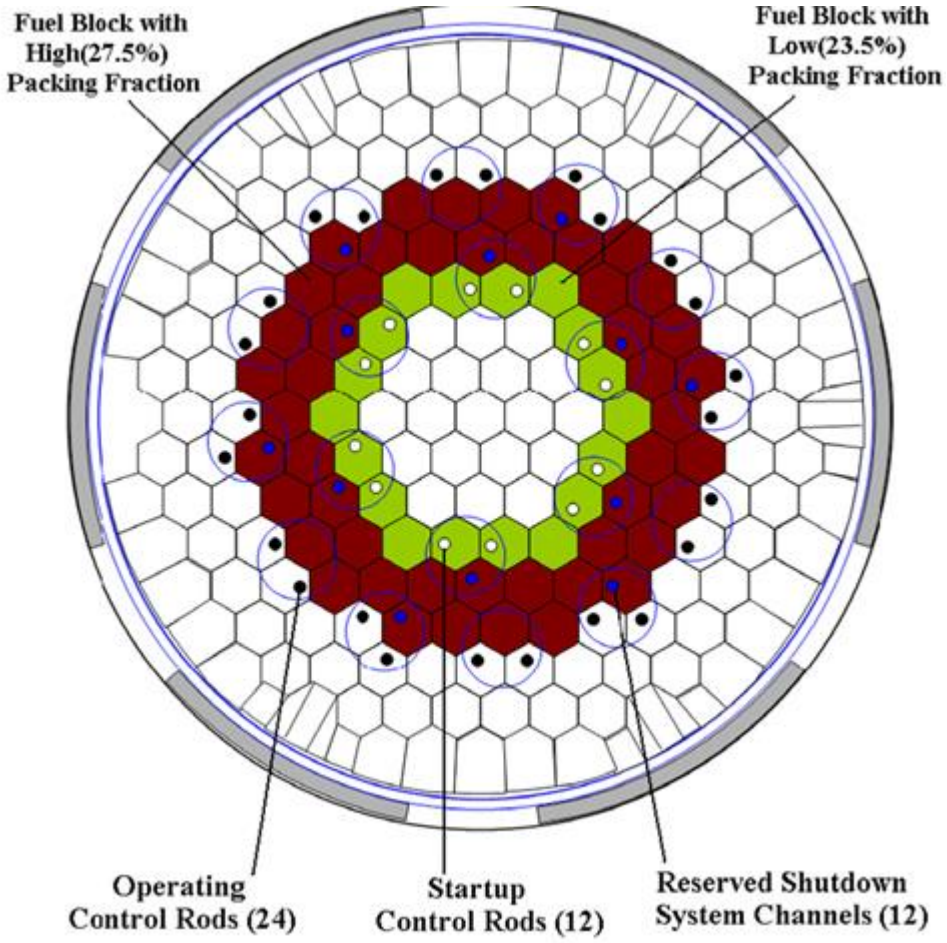

Figure 2-2: The PMR core configuration (Lee, Jo , Shim, Kim, & Noh, 2010)

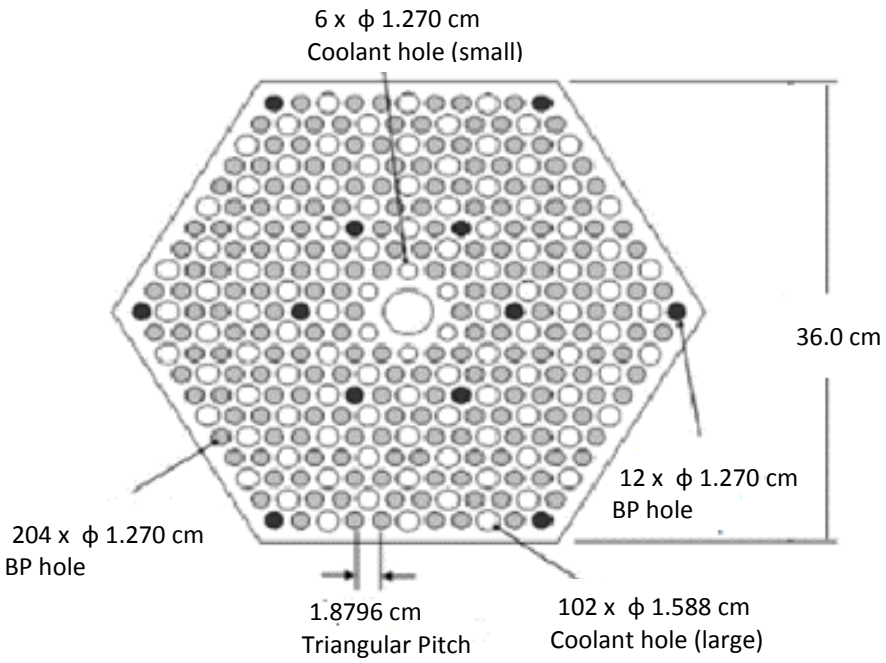

Figure 2-3: The horizontal view of the standard fuel block (Lee, Jo , Shim, Kim, & Noh, 2010)

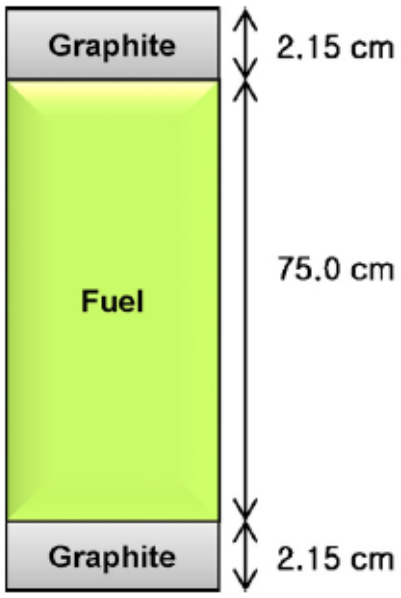

Figure 2-4: Axial view of the fuel block (Han, Lee, Jo, & Noh, 2013)

I. Side bottom and top reactor configuration

The active core height is 475.8 cm with a top and bottom reflector, with heights of 120cm and 160 cm respectively.

Table 2-1: Major design parameters of PMR200 (Lee, Jo , Shim, Kim, & Noh, 2010)

Parameters	Values
Thermal Power ($\boldsymbol{MWth}$)	200
Specific power density ($\boldsymbol{W/g}$)	74.96
Average power density ($\boldsymbol{W/cc}$)	5.67
$\boldsymbol{UO_2}$ enrichment ($\boldsymbol{w/o}$)	12
No of fuel columns	66
No of axial layers	6
Active core height ($\boldsymbol{cm}$)	475.8
Top/Bottom reflector height ($\boldsymbol{cm}$)	120/160
Inner/Outer fuel ring volume fraction (%)	27.5/23.5

II. Fuel block, burnable poisons, coolant channels and block handling hole

There are 12 burnable poisons (BPs) in the standard fuel block with a diameter of 1.270 cm. The BPs are rod-type and are inserted vertically into the fuel assembly. They are made from a sintered mixture of boron carbide and graphite. The standard fuel block of the PMR200 is shown in

Figure **2-3** and Figure 2-4. The design parameters of the fuel block are listed in Table 2-2.

Table 2-2: Fuel block design parameters for the PMR200 (Lee, Jo , Shim, Kim, & Noh, 2010)

Parameter	Value
Block face to face width (cm)	36.000
Gap thickness between blocks (cm)	1.000
Fuel Block height (cm)	79.300
Active fuel block height (cm)	75.000
Fuel Block graphite density (g/cc)	1.730
Block handling hole radius (cm)	1.8796
Fuel hole radius (cm)	0.6350
Fuel compact radius (cm)	0.6225
Coolant hole radius (cm)	0.7940
BP hole radius (cm)	0.6350
Hole pitch (cm)	1.880
$\boldsymbol{B_4C}$ and graphite mixture density (g/cc)	1.735
Mass fraction of $\boldsymbol{B_4C}$ (%)	1.241

III. Basic fuel form and fuel compact

The basic fuel form is a TRISO particle, which consists of a UO_2 kernel and layers of ceramic that act as a protection barrier and keep fission products contained. The fuel kernel is covered by a low density porous graphite buffer layer, a dense inner pyrolytic carbon, a silicon carbide layer and a dense outer pyrolytic layer. The fuel kernels are randomly embedded in a graphite fuel compact. The fuel compacts are stacked axially in the fuel rod casing and the fuel rods are inserted into the fuel holes of the hexagonal graphite fuel block shown in Figure 2-5. The design parameters for the coated particle are tabulated in Table 2-3.

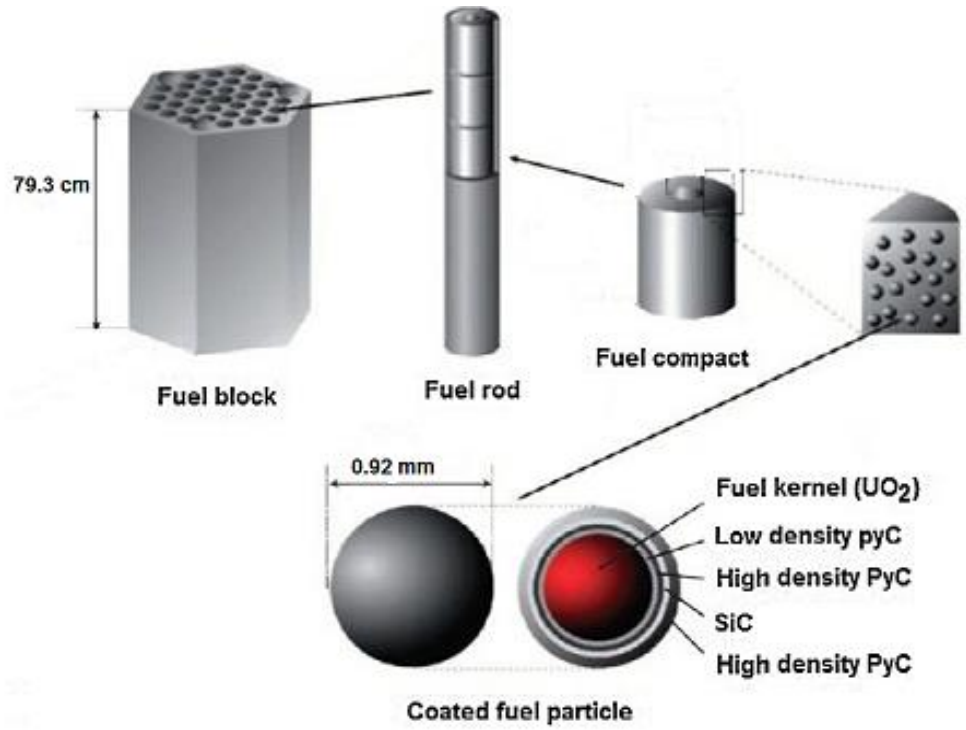

Figure 2-5: PMR fuel block, fuel rod, fuel compact and TRISO particle (Sousa, et al., 2014)

Table 2-3: Geometry and material data for the Coated particle of the PMR200 (Lee, Jo , Shim, Kim, & Noh, 2010)

Parameter	Thickness ($\boldsymbol{\mu m}$)	Density ($\boldsymbol{g/cm^3}$)
Kernel radius	250	10.4
Buffer layer	100	1.0
Inner PyC coating thickness	40	1.9
Silicon Carbide coting thickness	35	3.2
Outer PyC coating thickness	40	1.9

IV. Control rods

HGTRs rely on only two systems of reactivity controls, the burnable poisons and the control rods. The pre-conceptual design for the PMR200 shows three sets of control rods. The start-up control rods are situated in the inner fuel ring of the core; they are only used at the start-up and shutdown. They are removed during normal operation to overcome the power defect. The operating rods are placed in the graphite blocks and serve to maintain criticality during normal operation. They are

partially inserted and are driven in or out to maintain criticality. (Reitsma, Personal communication, 2014).

The third set of rods is the reserve shutdown system which has enough reactivity to shut down the system from operation to subcriticality condition. In the case of emergency shutdown, control rods can be dropped into the cavity (Reitsma, Personal communication, 2014).

All the control rods have the same design; they are made from a sintered mixture of B_4C and carbon sandwiched between two layers of graphite. Each control rod is housed in the control fuel block as shown in Figure 2-6 and the design specifications are presented in Table 2-4.

Table 2-4: Control rod design parameters for the PMR200

Parameters	Values
Inner radius of inner graphite tube (cm)	2.478
Thickness of inner graphite tube (cm)	0.127
Thickness of annular $\boldsymbol{B_4C}$ + graphite absorber (cm)	1.635
Thickness of outer graphite tube (cm)	0.127
Graphite tube density (g/cc)	1.730
Mass fraction of $\boldsymbol{B_4C}$ in absorber region (%)	1.316
Control rod hole radius (cm)	5.080
Control rod hole position from the block center (cm)	9.767

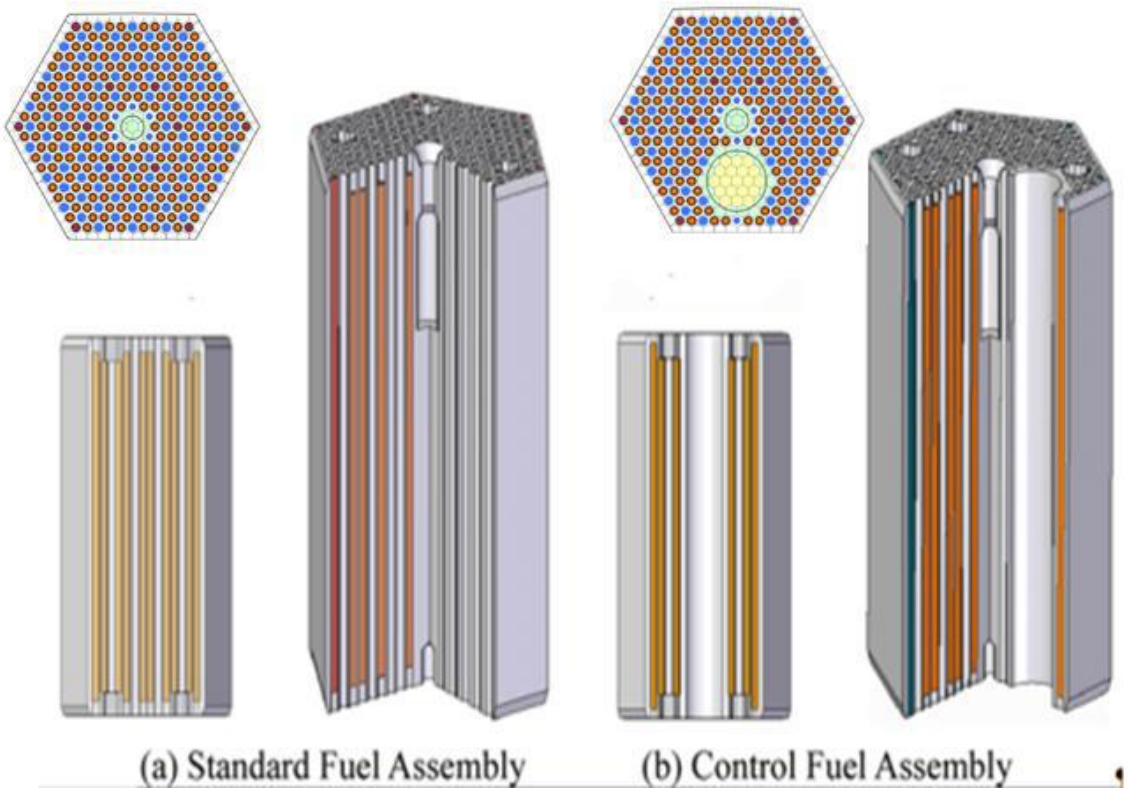

Figure 2-6 : Standard fuel block and control fuel block ((Kim & Lim, 2011) (Tak, Kim, Hong, & Noh, 2011))

3. Methodology

3.1.General Details Regarding MCNP Input

3.1.1. Introduction

MCNP is a general purpose, continuous-energy, generalised-geometry, time-dependent, coupled neutron/photon/electron Monte Carlo transport code ((X-5 Monte Carlo Team, 2003), page 1-1).

The user constructs an input file which specifies the geometry, materials and tallies. MCNP reads the input file and produces an output with the specified results.

The input file follows the following format:

Optional Message Block

Blank Line Delimiter

Title Card

Cell Card

Blank Line Delimiter

Surface Card

Blank Line Delimiter

Data Cards

Blank Line Delimiter

Anything

All the input files are limited to 72 columns and data entries are separated by blanks. The dollar sign ($) indicates the end of a data entry. Comments can be entered after the dollar sign ($) and a C is also used for a comment card. The C should be entered anywhere in columns 1-5.

3.1.2. Message Block

This part of the input is optional. It serves to give MCNP an execution message and it starts with the string “MESSAGE:”

3.1.3. Title Cards

Title cards specify the title of the input file e.g. HTR Prismatic Power Core.

3.1.4. Cell Cards

Cell cards contain information about the material of the surface; cell cards have the format

j m d geo param

"j" represents the cell number, which is a positive number not greater than 99999.

"m" denotes the material number which specifies the type of material (see section 3.1.6 (IV)), similarly the material number must a positive number less than 99999.

"d" is the density; a negative entry is interpreted as a mass density in units of grams per cubic centimetre. A positive entry for the density is interpreted as the atomic density in units of 10^{24} atoms per cubic centimetre.

"geo" denotes the geometric location of the material. Boolean operators (plus sign is optional) as well as allocated surface numbers are used to describe how surfaces bind regions of space to form a cell.

"param" is an optional specification of cell parameters on the cell card instead of the data card section of the input card.

Example:

3 21 0.0065 (-91 92)

The above example is a definition of cell card 3, which contains material card 21 (see material cards) and the atomic number density of 0.0065. The numbers in parentheses define the geometry of the cell.

91, 92 define two different surfaces (see surface card) and in this case they are concentric spheres. Cell three is inside of 91 (negative sign) but outside of 92 (positive sign).

3.1.5. Surface Cards

Surface cards contain information about the type and dimension of the surface. A Boolean operator and a number indicate the coordinate, while the mnemonics define the type of surface. The coordinates of the surface are also defined. MCNP has a wide selection of surfaces, i.e. planes, spheres, cylinders, cones, ellipsoids, hyperboloids and torus. Surfaces can also be defined by macrobodies and reflecting surfaces.

Example: 5 pz 0.060734

6 pz -0.060734

The numbers 5 and 6 are surface numbers and these are the numbers that appear in the cell card definition.

“pz” is a plane in Cartesian coordinates, normal to the Z-axis. In surface card 6, the negative sign and numerical value indicate that the surface cuts the z-axis at Z=-0.060734. In surface card 5, Z=0.060734 indicates that this surface cuts the z-axis at Z = 0.060734.

3.1.6. Data Cards

Data cards consist of a mode card, cell and surface parameter cards, source specification cards, tally specification cards and material specification.

I. MODE card

MCNP can be run in several different modes including neutron transport only, neutron and neutron-induced photon transport, photon transport only, electron transport only, photon and electron transport and neutron, neutron induced, photon and electron transport. If the user omits the mode card, then neutron transport only is assumed.

II. Geometry card

The geometry cards are used to specify cell volumes, surface area, universe, cell transformation, type of lattice and stochastic geometry.

Table 3-1: List of Geometry cards in MNCP

Mnemonic	Card Type
VOL	Cell Volume
AREA	Surface area
U	Universe
TRCL	Cell Transformation
LAT	Lattice
FILL	Fill
TRn	Coordinate Transformation
URAN	Stochastic Geometry

Cell volume and surface cards are optional cards. MCNP calculates the volume of all cells because some tallies require volume or masses of cells. Additionally MCNP calculates the area of surfaces as a result of volume calculations.

The universe card specifies which universe a cell belongs to. The universe can be a collection of cells or a lattice. In addition to a hexahedral lattice (a lattice that is made of hexagonal prisms), there is also the option of defining a Cartesian lattice. The fill card is used to specify how a lattice is filled.

III. Source specification card

There are four available methods of defining a starting particle. For this study the SDEF card is used and has the format: POS CEL ERG WGT TIME PAR

POS - xyz, starting position with default(0,0,0)

CEL - Starting cell number, this entry is not always required for an isotropic source. MCNP will determine the starting cell number and its default starting direction

ERG - Energy of the particle and the default starting energy is 14MeV

WGT - Starting weight, the default is 1

TIME - The time when the particle started and the default is zero

PAR - The particle type emitted by the source, if the run is executed in MODE N, then a neutron is emitted

IV. Material specification

The material card specifies the different materials that make up the reactor. It has the form

M*n* $ZAID_i$ $fraction_i$ $ZAID_2$ $fraction_2$ ... keyword=value

"n" is the material number of the cell cards

"ZAID" is the Nuclide Identification Number, which has the form ZZZAAA.nnX and is used to identify a particular nuclide.

- ZZZ is the atomic number of a nuclide
- AAA is the mass number of the nuclide for naturally occurring elements AAA=000
- nn is the cross-section evaluation identifier and a default cross-section is used if this card is omitted
- X is the class of data

"Fraction" is the atomic fraction or weight fraction of the element/nuclide i in the material Mn.

Example:

M2	14028.70c	4.6115E-01
	14029.70c	2.3416E-02
	14030.70c	1.5436E-02
	6000.70c	5.000E-01

This example is a material card for silicon carbide using individual atom fractions since fractions are entered as positive numbers. If entered with a minus sign then it is read by MCNP as weight fractions.

The material card can be associated with an MTm card, with an $S(\alpha,\beta)$ data set provided that the data set exists.

Form: MT*m* X_1 X_2

m = material number
X_i = $S(\alpha,\beta)$

Example:

m21	92235.70c	4.0450E-02
	92238.70c	2.9288E-01
	8016.70c	6.6667E-01
mt21	o2/u.10t	u/o2.10t

V. Tally specification card

Tally cards are used to specify the outcome required from a Monte Carlo calculation. The MCNP can provide the following results:

- Current across a surface (tally type 1)
- Flux at a surface (tally type 2)
- Track length estimate of cell flux (tally type 4)
- Flux at a point (tally type 5)
- Track length estimate of energy disposition (tally type 6)
- Track length estimate of fission energy disposition (tally type 7)
- Energy distribution of pulses created in a reactor (tally type 8)

Tallies are given tally numbers 1, 2, 4, 5, 6, 7, 8 as mentioned above and all tallies thereof are given increments of 10. For this work type 4 tallies are used, therefore F4:N, F14:N, F24:N, F34, F314 etc. are all type 4 tallies but apply to different energy or multiplier bins. Tallies may only be assigned a tally number with a maximum of three digits.

The FMESH tally or superimposed mesh tally can only be used with type 4 tallies. It has the form FMESH*n*:pl, where "n" is the type 4 tally number and "pl" is the particle type i.e. N or P or E. The FMESH tally calculates the track length estimate of cell flux averaged over a mesh cell. The output is given in units of particles/cm^2.

The user has to describe the geometry of the reactor, the location of coarse meshes in the r, θ and z direction and the corresponding fine meshes in those directions. The tally results are printed in the meshtal file.

Example:

FMESH4:n	GEOM=cycl	ORIGIN= 0 0 -17
	IMESH = 8 12	IINTS= 8 4
	JMESH = 10 20	JINTS= 9 6
	KMESH = 0.5 1	KINTS = 1 2
	AXS= 1 0 0	VEC = 0 0 1

The example above describes a cylindrical mesh tally along the z-axis. The lower plane of the reactor is at -17. The tally is divided into 8 bins for r=0 to r=8, 4 bins for r=8 to r=12, 9 bins for z =-17 to z=-7, 6 bins from z=7 to z=17, 1 bin from $\theta = 0°$ to $\theta = 180°$ and 2 bins from $\theta = 180°$ to $\theta = 360°$.

3.2.Full Core Model of the PMR200

The MCNP5 model of the PMR200 has been modelled precisely to the reactor design specified in chapter 2.3 and in (Lee, Jo , Shim, Kim, & Noh, 2010). The dimensions, structure and form of the reactor core components were modelled in detail and all components of the PMR200 core are explicitly modelled. Adjustments were made where necessary to meet certain assumptions/conditions, particularly in the material modelling of the neutron absorbers, and these are discussed in the subsequent section.

3.2.1. Model Development Overview

The construction of the PMR200 core model is divided into several steps and all steps were subjected to thorough accuracy and precision tests. The modelling is divided into three phases. The first is the geometry modelling followed by the materials and the tallies. A homogenous model of the core is first modelled, followed by a heterogeneous model without neutron absorbers and finally a full fuel assembly model and a full PMR200 core model.

A fuel assembly of the PMR is also modelled, beginning with a homogenous model and followed by a heterogeneous model without absorbers. The NGNP fuel block data specified in (Kim, Cho, Lee, Noh, & Zee, 2007) is used to verify the MCNP5 modelling of the fuel block. The NWURCS code was used to verify the materials and geometry design.

The following assumptions were made and subsequently modifications were made in the pre-conceptual PMR core design to meet some of the following assumptions/conditions.

- The reactor temperature is 300 K
- The reactor is critical
- Steady state
- The coolant is at 1 atmosphere
- Fresh fuel core
- The moderator is pure graphite absent of impurities
- Control rods are inserted 1/3 into the core

3.2.2. Geometry

Firstly the homogenous model of the reactor was modelled; thereafter the homogenous model was subjected to careful geometric tests. The same procedure was followed for the full core model. A fuel assembly was also modelled to aid in verification of the geometry. This is discussed further in section 3.4.

I. The full core model

The full core model was constructed from outwards to inwards, the first universe defines the reflectors and the last universe defines the coated particle. The annular core is represented by a cylindrical body and is sectioned into 6 axial layers. The vertical view of the model is shown in Figure 3-1. This figure was obtained using Vised Version 24E.

The model is built in such a way that the core is represented by a hexagonal lattice as shown in Figure 3-2. Each of the units represents a standard fuel assembly (see Figure 3-3A), a control fuel assembly or graphite blocks.

The fuel assembly units are filled by a smaller hexagonal lattice representing the fuel pins. This smaller lattice must be necessarily rotated by 90 degrees otherwise the smaller lattice will not fit snugly into the bigger lattice. Each element of the smaller hexagonal lattice is therefore populated either by a coolant channel, a burnable poison or a fuel compact. The two types of fuel assemblies are shown in Figure 3-3B (standard fuel block) and Figure 3-3C (control fuel block).

The fuel compact is made up of coated uranium particles. In order to model this, a 3-D cartesian lattice (cubic) is constructed to fit into the compact. Each element of this lattice therefore contains a single coated particle. The dimensions of the lattice element (the cube) are calculated so that the required packing fraction of the coated particles in the compact is achieved. The MCNP view of outer fuel compact with a packing fraction of 27.5% is shown in Figure 3-4A and the MCNP view inner fuel compact with a packing fraction of 23.5% is shown in Figure 3-4B. The model of the fuel particle is shown in Figure 3-6.

I. The control rods

The three types of identical control rods discussed in section 2.2.3 (IV) are modelled accurately into the MCNP5 model of PMR200. The sintered boron carbide is sandwiched between two graphite layers and for this model the graphite is assumed to be absent of impurities. It also assumed that this graphite has the same density as the moderator graphite (see section 3.2.3). Each control rod is housed in the control rod fuel block. The MCNP model of PMR200 is summarized in Figure 3-5.

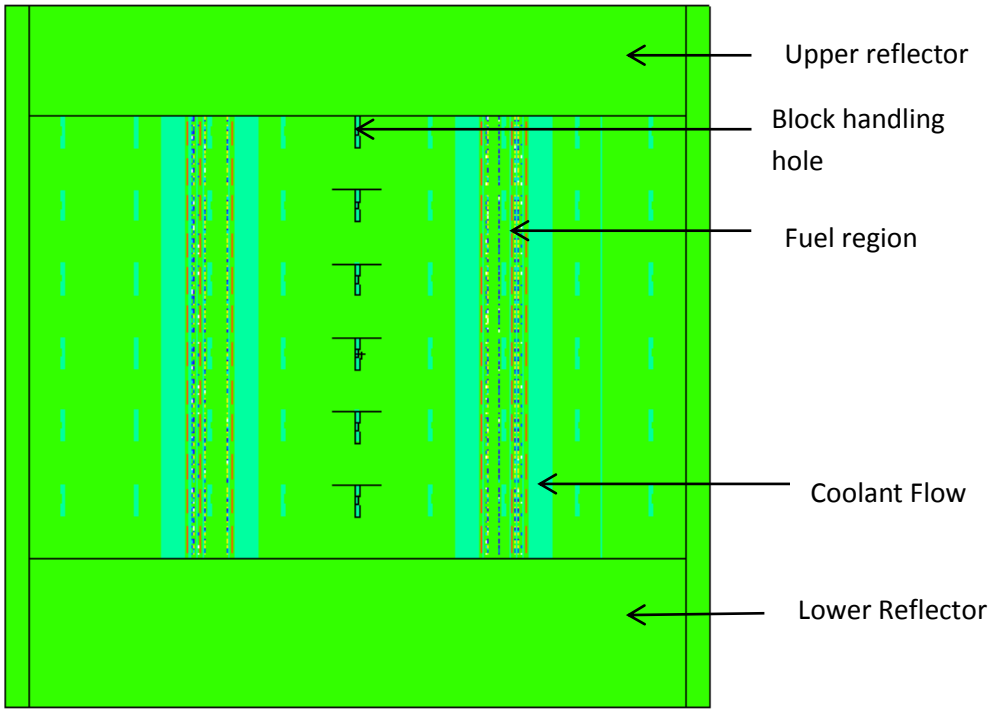

Figure 3-1: MCNP model of the PMR200 core

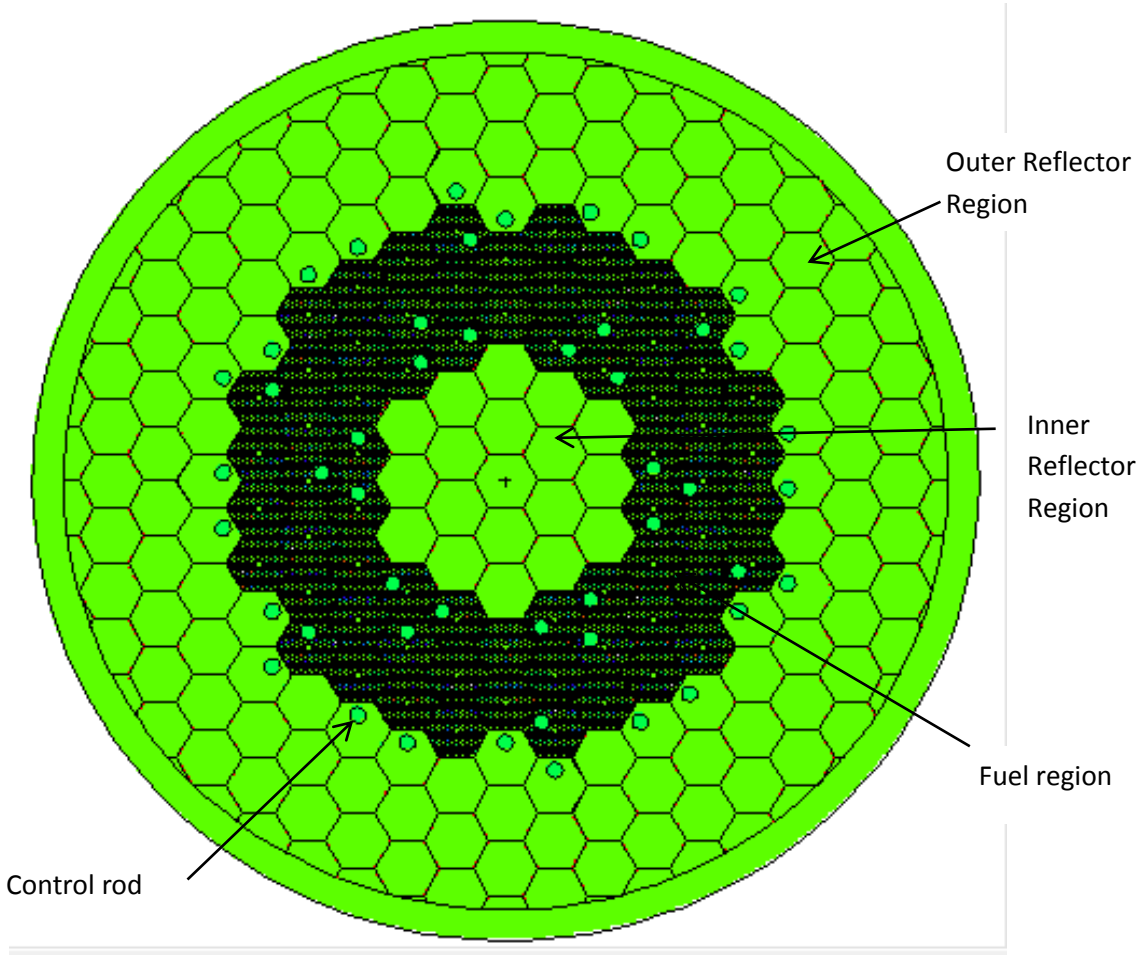

Figure 3-2: MCNP5 model of PMR200 core configuration

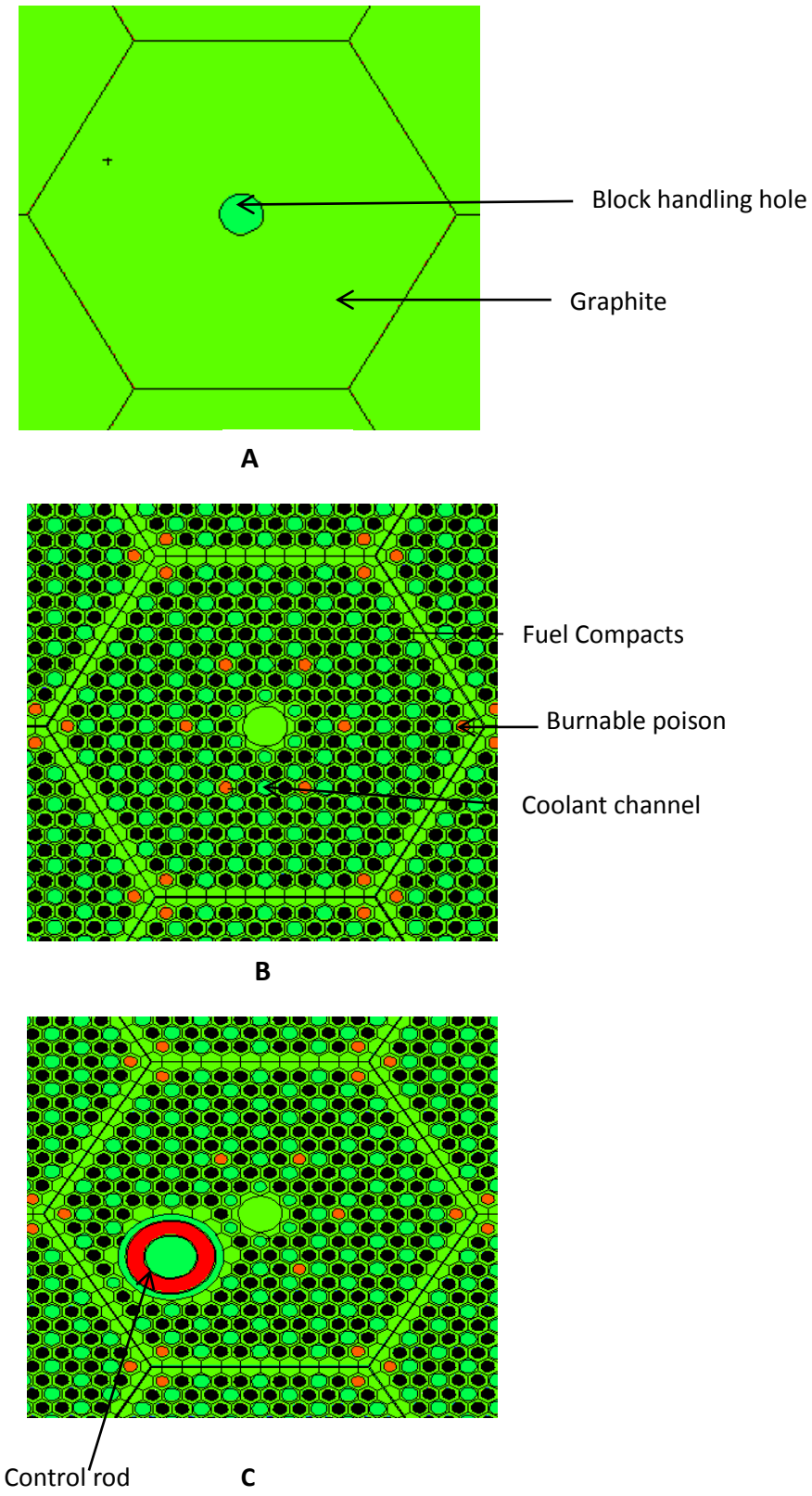

Figure 3-3: (A) The graphite block (B) The standard fuel block (C) The control fuel block

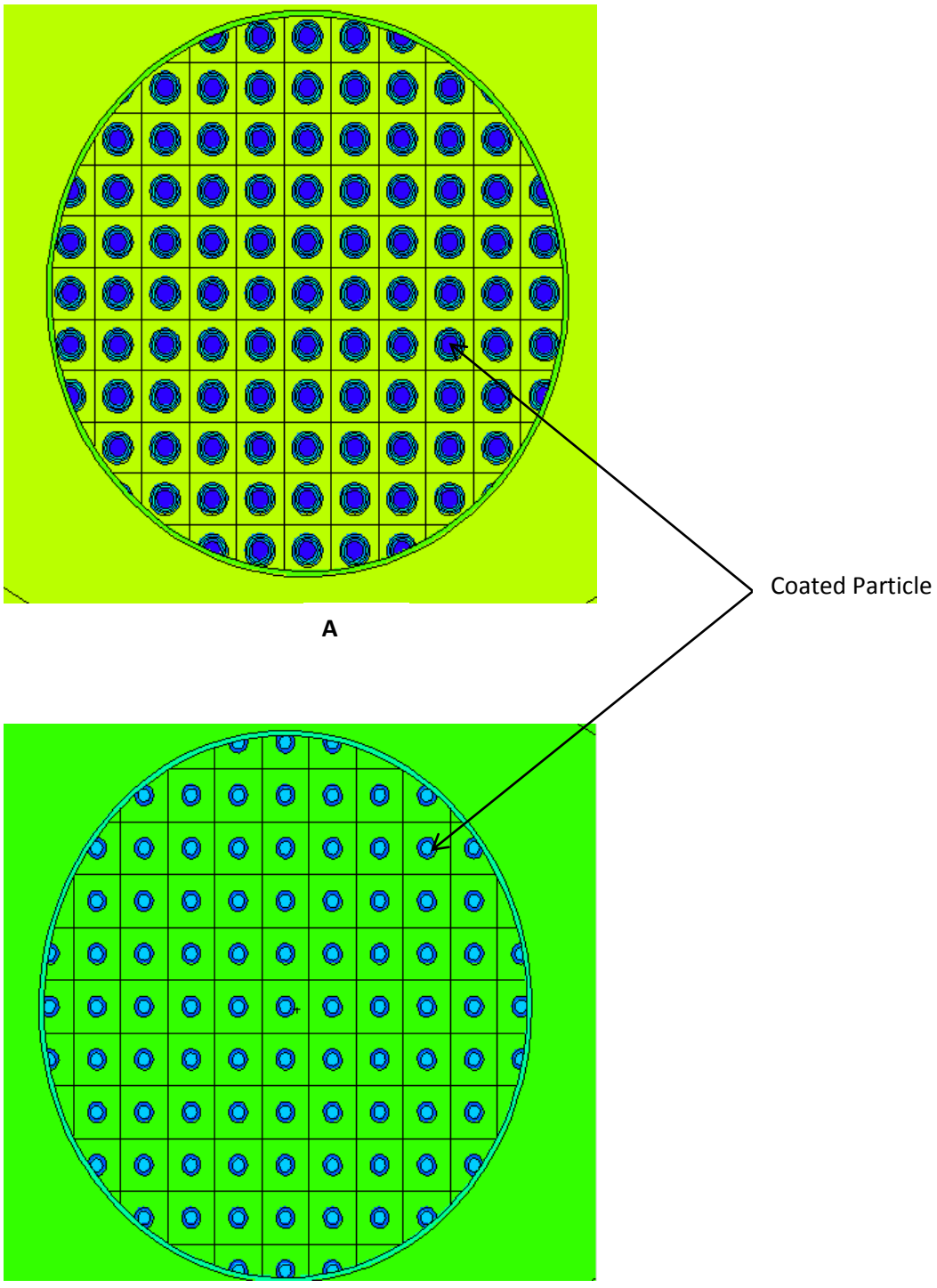

Figure 3-4: (A) MCNP representation of the outer fuel compact with a packing fraction of 27.5% (B) inner fuel compact with a packing fraction of 23.5%

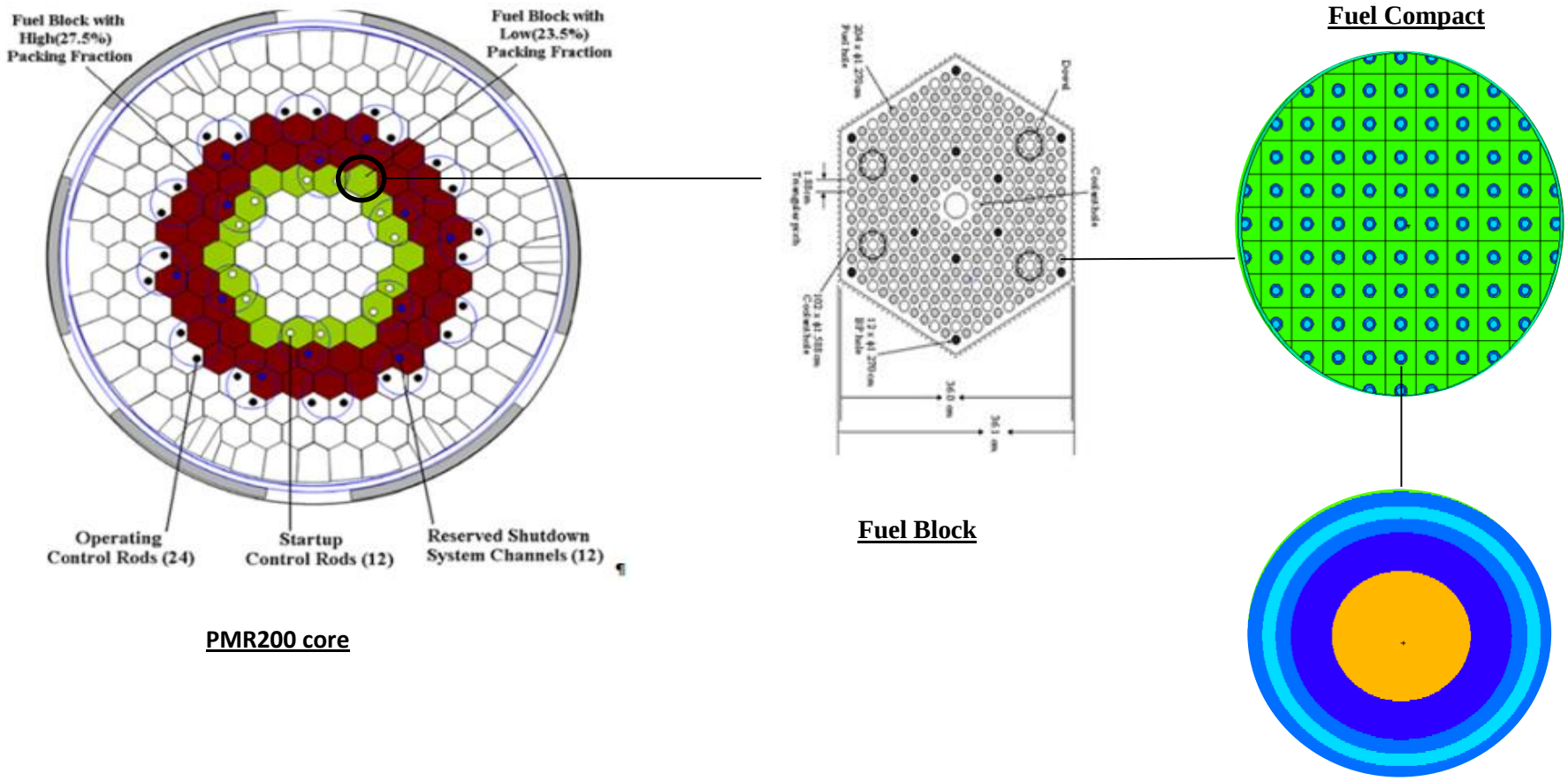

Figure 3-5 : MCNP modelling procedure showing the three different lattices

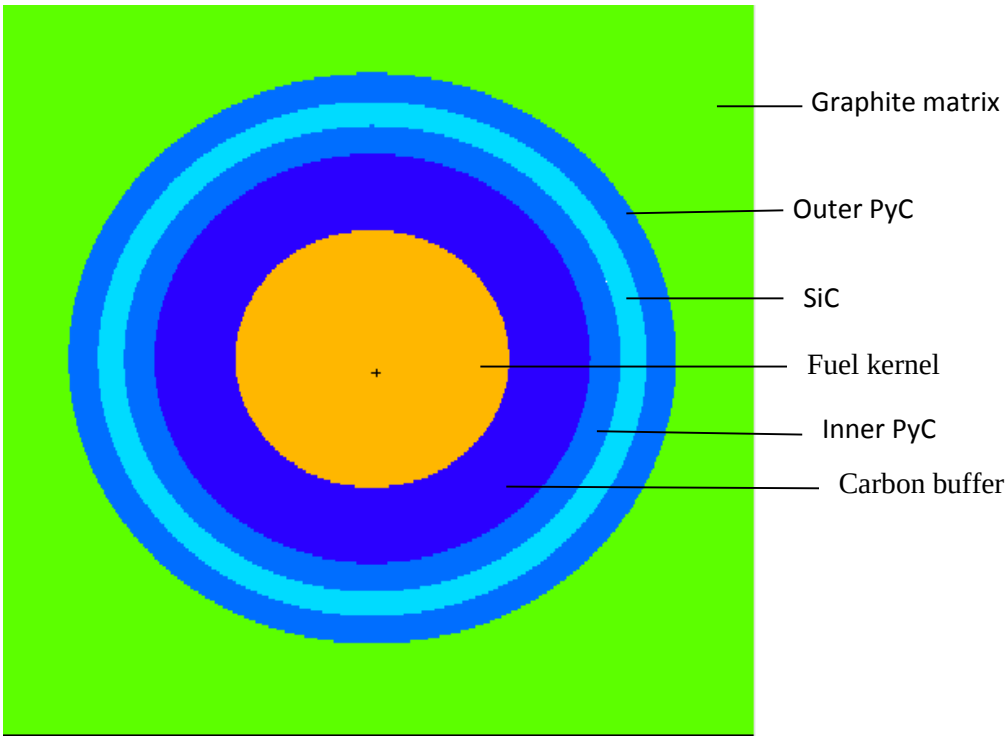

Figure 3-6: MCNP5 model of the TRISO particle

3.2.3. Materials

The list of reactor materials is tabulated in Figure 3-2 along with the atomic density. Each of the calculated material constituent elements and their ratios are listed. The figures presented in Table 3-2 are compared to the nuclide densities and ratios acquired from NWURCS to verify the input model (see section 3.4)

Table 3-2: The material composition of the reactor components

Reactor Component	**Unit** ($\times 10^{24} atoms/cm^3$)	**Isotopes**	**Ratio**
Graphite	0.0868	^{12}C	1.0000
Helium coolant	0.000257	He	1.0000
Burnable poisons (1.241%)	0.0871	^{10}B	1.3154E0-3
		^{11}B	5.2946E-03
		^{12}C	9.947054E-01
Control rods (1.316%)	0.0870	^{10}B	1.3948E-03
		^{11}B	5.6143E-03
		^{12}C	9.9299E-01
Fuel kernel	0.0697	^{238}U	2.9288E-01
		^{235}U	4.0450E-02
		^{16}O	6.6667E-01
Carbon buffer	0.0502	^{12}C	1.000E-01
Inner and outer PyC	0.0953	^{12}C	1.000E-01
Silicon coating	0.0962	^{28}Si	4.6115E-01
		^{29}Si	2.3416E-02
		^{30}Si	1.5436E-02
		^{12}C	5.0000E-01

3.2.4. Tallies

For the F4mesh tallies, the theta direction is divided into 25 angular bins from $\theta = 0$ to $\theta = 60$℃, so only 1/6 of the core is analysed. The height of the core is divided into 16 tally bins from the bottom of the core to the top of the core. The radial direction is divided into 10 tally bins from the centre of the core to the outer core.

3.3. Estimation of Accuracy and Precision

3.3.1. Model Limitation

The model limitations alter the results and affect the accuracy of the results obtained from MCNP.

I. Stochastic geometry

In reality, the coated fuel particles are packed randomly in the graphite matrix. In this MCNP model the fuel particles are ordered in a face centred cubic (FCC) arrangement with the coated particle in the centre of each lattice block as illustrated in Figure 3-7B.

The URAN card in MCNP is the stochastic geometry card for high temperature reactors. It operates by assigning randomly selected numbers to a universe in a lattice that is flagged as stochastic (X-5 Monte Carlo Team, 2003). For this writing, any randomness has been ignored. The effect of using randomly selected fuel particles versus centred fuel particles is negligible (Brown & Martin, Stochastic geometry capability in MCNP5 for the analysis of particle fuel, 2004). In the work by (Brown, Martin, Conlin, & Lee, 2005) it is reported that the result of k-effective is lower by 0.1% – 0.2% in stochastic geometry in comparison to centred particle geometry. See appendix for a further discussion and format of the URAN card.

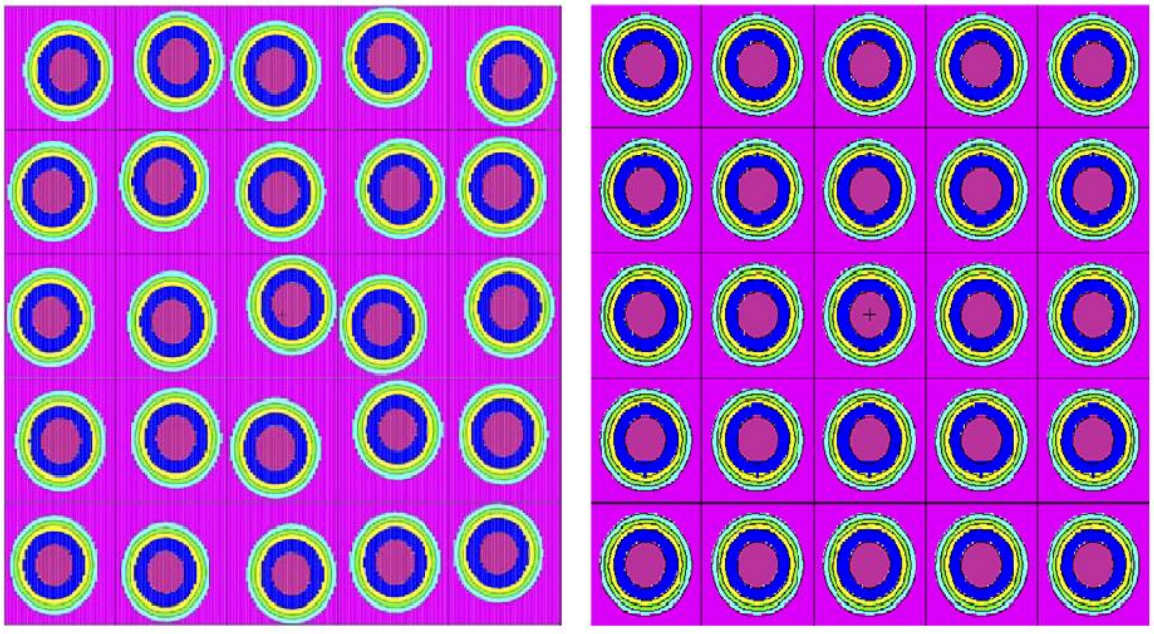

Figure 3-7: (A) Randomly packed coated particles (B) Centred coated fuel particles (Brown & Martin, 2004)

II. Finite versus infinite lattice

The MCNP user has a choice between an infinite lattice and a finite lattice (see Figure 3-8). The user defines a lattice (finite or infinite), spheres and a cylindrical body to represent the fuel kernels embedded in a fuel compact.

The infinite lattice is an inaccurate representation of the fuel rods since the cylinder slices the fuel spheres at the perimeter of the cylinder, leaving some of the fuel spheres in fragments. This is visible in Figure 3-8 A.

Figure 3-8 B shows a model with a finite lattice, which is a more realistic representation as it only has whole fuel particles. In (Brown, Martin, Conlin, & Lee, 2005), the effect of using a random coated particle arrangement and a finite lattice versus the use of a centred (FCC) coated particle arrangement and an infinite lattice is investigated. It is found that stochastic geometry with an infinite lattice reduces the multiplication factor by approximately 0.06%.

In this study, the infinite lattice was used; the finite lattice should be investigated in further studies.

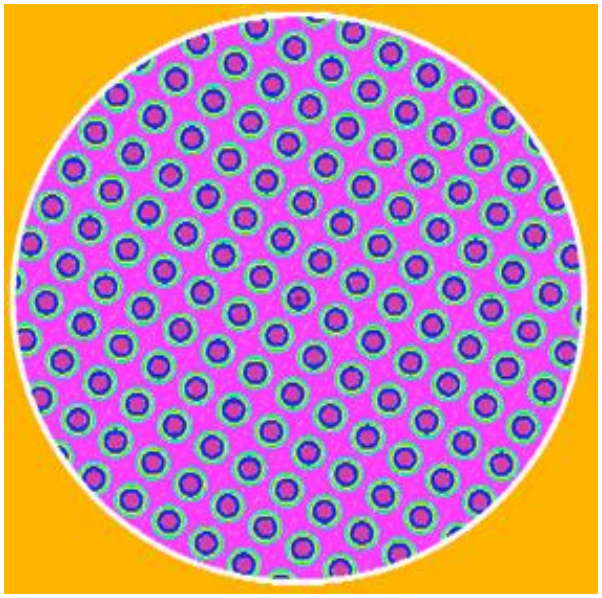

A

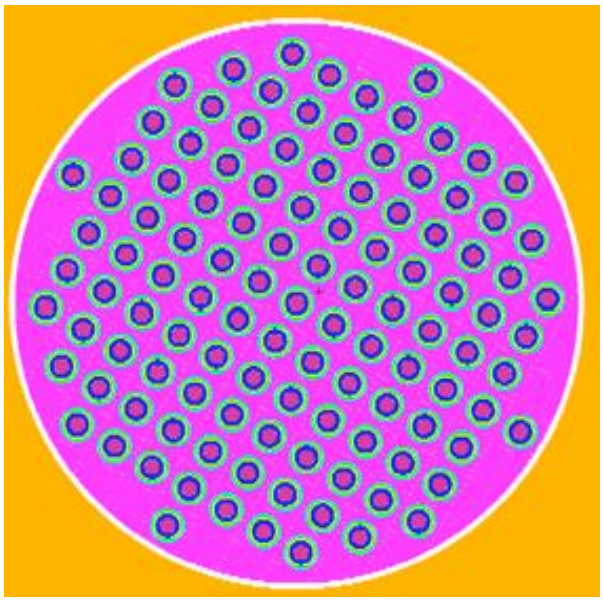

B

Figure 3-8: MCNP representation of the dispersion of fuel particles in the fuel rods of the PMR200 with (A) an infinite lattice (B) a finite lattice (Brown, Martin, Conlin, & Lee, 2005)

VI. Temperature

For this model any variation in temperature throughout the core has been neglected. The base calculations are performed at 300 K and it is assumed that all reactor materials are at this constant temperature. To determine the temperature distribution of the PMR200, a thermal fluid calculation is required but this is not within the scope of this project.

3.3.2. Factors Affecting MCNP Accuracy

Accuracy depends on:

- The model
- The code
- The user
- Model factors include the physical characteristics and geometric description of the model which may be inadequate or incorrect, resulting in inaccurate results.
- Secondly code factors include the physics features as well as the mathematics of the problem, for example atomic densities, Avogadro's number, transport and reaction cross-sections and coding bugs.

Lastly user errors include problems with the construction of the input; these can be reduced by thoroughly checking the input. Another user error is abuse of the variance reduction technique, which can lead to portions of the physical space not being allowed to contribute to the results. Variance reduction techniques were not used because all of the geometry modelled was considered important for neutron transport.

3.3.3. Factors Affecting MCNP Precision

Precision refers to the uncertainty of a result; precision is affected by variance reduction techniques, forward vs. adjoint calculation, the number of histories (N) as well as the appropriateness of the selected tally.

The tally type and variance reduction techniques increase the efficiency of the calculation and were discussed in Chapter 2.1 under variance reduction techniques.

Precision of MCNP calculations is affected by the number of histories run (*N*) because precision is proportional to $1/\sqrt{N}$. Increasing the number of histories to improve precision is usually the last resort because it is costly in computer time.

The MCNP result is printed with a fractional standard deviation. This fractional standard deviation is the statistical error associated with the number of histories run. Furthermore there are three fundamental concerns which must be addressed in MCNP to ensure that calculations are performed correctly. These are convergence of k_{eff} ,a bias in k_{eff} and tallies and a bias in statistics on tallies (Brown, 2009). Shannon entropy vs cycle as well as k_{eff} can both determine convergence of the power iteration process; this is shown in chapter 4.1.

3.4.Verification

The full core model for the PMR200 was assessed and checked repeatedly. The geometry, materials and tallies were compared to those generated by NWURCS. Using this script in place of manually constructing an MCNP input reduces human error. It is currently being verified. Therefore, comparison with this code will give confidence in the calculated values in this work.

Material verification and geometry verification

The input model generated by NWURCS was consistent with the PMR200 model. The material definition for the PMR200 and the material definition generated by NWURCS are in good agreement and as illustrated in.

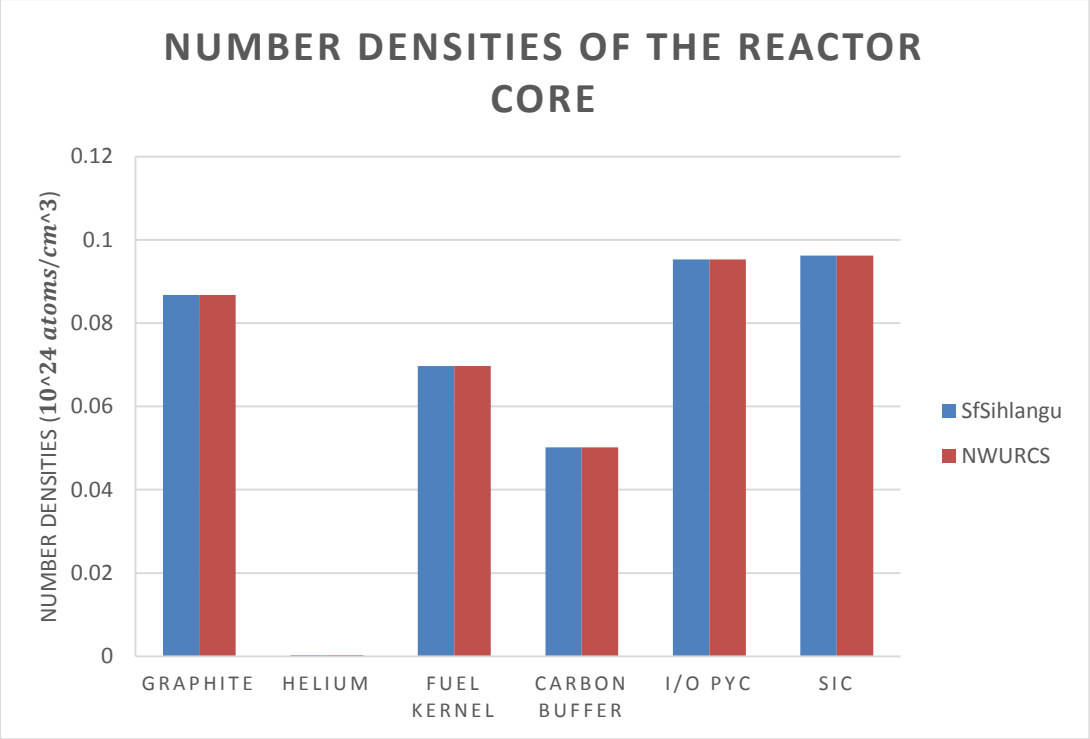

Figure 3-9: A comparison of the number densities calculated number densities to the number densities computed by NWURCS

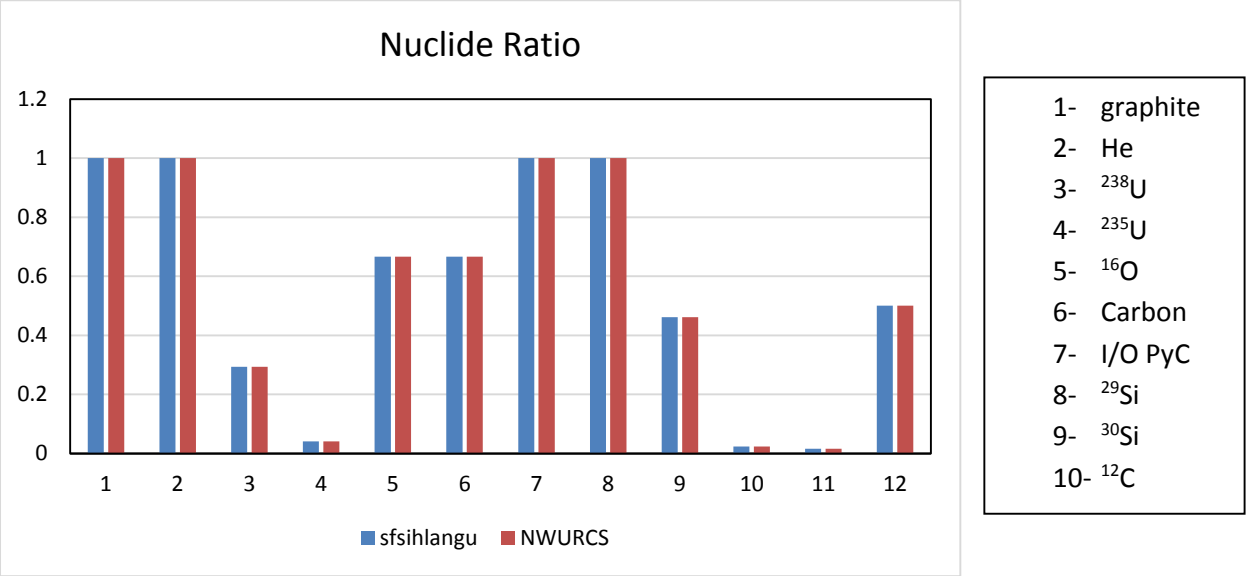

Figure 3-10 : A comparison of calculated nuclide ratios vs nuclide ratios computed by NWURCS

Each of the material constituent elements and their ratios are listed in Figure 3-9 and Figure 3-11 respectively. The calculated nuclide densities and ratios are in agreement with the densities and ratios computed by NWURCS.

3.5.Discretisation

The temperature profile of this PMR core is not known since a thermal fluids calculation has not been done. Discretisation is crucial when performing temperature-dependent calculations. Essentially, as the neutron history is tracked through the material, care must be taken to ensure that changes in the material due to the temperature are taken into account. For example, the material cross-sections and densities would be a function of temperature. Since a single temperature was assumed throughout the materials, spatial discretisation is therefore not needed.

Correspondingly discretisation is also crucial in burn-up calculations for a similar reason to the one stated above. For this model, the fresh fuel did not contain any of the isotopes that are produced only after a neutron flux is present. Therefore discretisation was not necessary at this stage of the work.

4. Results and Discussion

This chapter covers results from all the models, beginning with the homogenous model, the fuel block model, the PMR200 without absorbers and finally the full core model. MCNP5 results are used to evaluate initial criticality, absorber material concentration, temperature coefficients and reactivity and control rod worth. Tally results were used to evaluate the effect of the burnable poisons and control rods on the power profile of the reactor. Prior to the completion of the calculations convergence of the model is assessed

4.1.Convergence

The results below show a convergence assessment for the full core model, with all the control rods withdrawn. The convergence test is done because a sufficient number of initial cycles should be skipped before proceeding with tally calculations, so any contamination of the source guess is negligible. This translates to running the calculation twice if it happens that the first calculation of the tally calculations was started before the source converged. In the second calculation, the number of skipped cycles is increased to the required number.

Convergence of K-eff

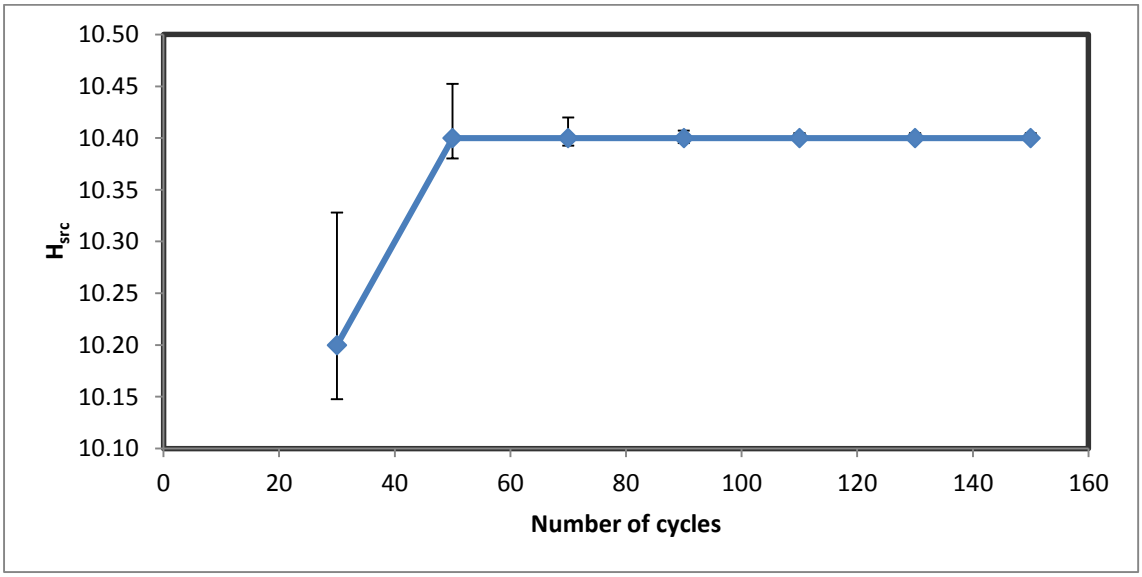

Figure 4-1: H_{src} vs. number of cycles

It can be seen from the H_{src} vs. number of cycles plot (see Figure 4-1) that at 30 cycles H_{src} is 10.20 and increases to 10.40. Convergence is reached after approximately 70 cycles and after 110 cycles the error bars get smaller. From visual examination, approximately 110 cycles would be sufficient for

the source to converge and is approximately the right number of cycles to discard so that there is no bias in the tally results.

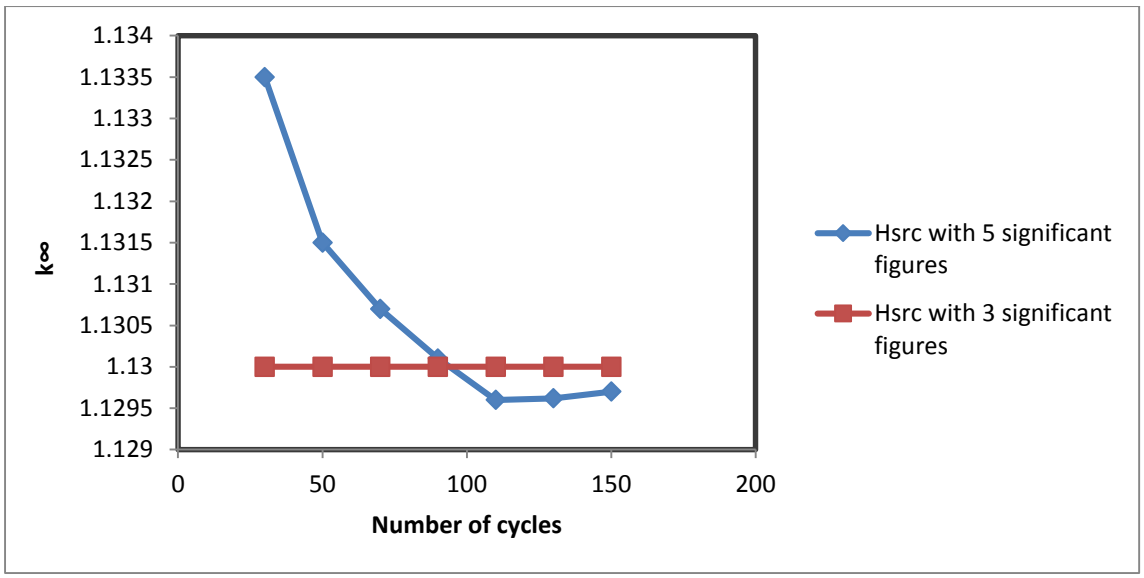

Figure 4-2: K-eff vs number of cycles

MCNP gives the values of k_{eff} in five significant figures and the values of H_{src} in three significant figures. When k_{eff} is plotted at three significant figures as shown in Figure 4-2, it converges as early as 30 cycles. This is an unreliable result for convergence.

4.2.Full core model

The effective multiplication factor for the pre-conceptual design is assessed. It is assumed that the reactor is critical so the concentration of the poisons is adjusted to obtain a critical value of k_{eff}. When the reactor is actually running, this will not be so, since the temperature will be greater than 300 K, and hence k_{eff} at 300 K will be larger than 1 so that the reactor can be critical at the operating temperature. However, since this study is the first step in producing the final model, the temperature set at 300 K was deemed acceptable.

Temperature coefficients of reactivity, reactivity and control rod worth are computed for the full core model. It is vital to calculate the reactivity of the core to ensure that the energy requirements are met. The control rod worth is computed for safety analysis and is a critical calculation for new reactor designs (Tyobeka, Ivanov, & Pautz, 2008). Temperature coefficients are computed because it is necessary to know a model's response to temperature variation; this is also important for safety analysis. An inherently safe reactor should have a total negative coefficient of reactivity. In addition the neutron flux distribution is determined to provide data for safety analysis. The neutron flux is proportional to the power output of the reactor and the power distribution is essential for safety analysis. In a real reactor the power distribution would be calculated at the beginning of life, during depletion through to the End of Life (EOL).

Initial effective multiplication factor of the pre-conceptual PMR200 model design

The full core calculations are performed for the core configuration discussed in chapter 3.2 and chapter 2.2. The first three models based on the pre-conceptual design of the PMR200 are discussed below:

- A full core calculation is performed, beginning with a core model consisting of all the standard fuel blocks only (shown in Figure 4-3a) and a packing fraction of 23.5% for the inner ring and 26.5% for the outer ring (model A). The burnable poisons are filled with graphite in place of B_4C/C.
- Model B is the same as the previous model but the burnable poisons are filled with B_4C-carbon composite.
- Model C is the pre-conceptual design as shown in Figure 2-2. It has same packing fractions for the fuel rings as model A. Both the standard and control fuel assemblies (Figure 4-3) are included and the control rods are removed.
- As mentioned in section 2.2.3 (IV), the operating control rods must be placed at a certain depth at start-up. For model D the operating rods are placed 1/3 into the core.

Table 4-1: The multiplication factors obtained from MCNP for the full core model

Model	Description	k_{eff}
A	Standard fuel blocks only and BP are filled with graphite	*1.44424 ± 0.00021*
B	Standard fuel assemblies only	*1.14212 ± 0.00039*
C	Control rods removed	*1.21062 ± 0.00022*
D	Control rods placed at 1/3 in the core	1.19789± 0.00027

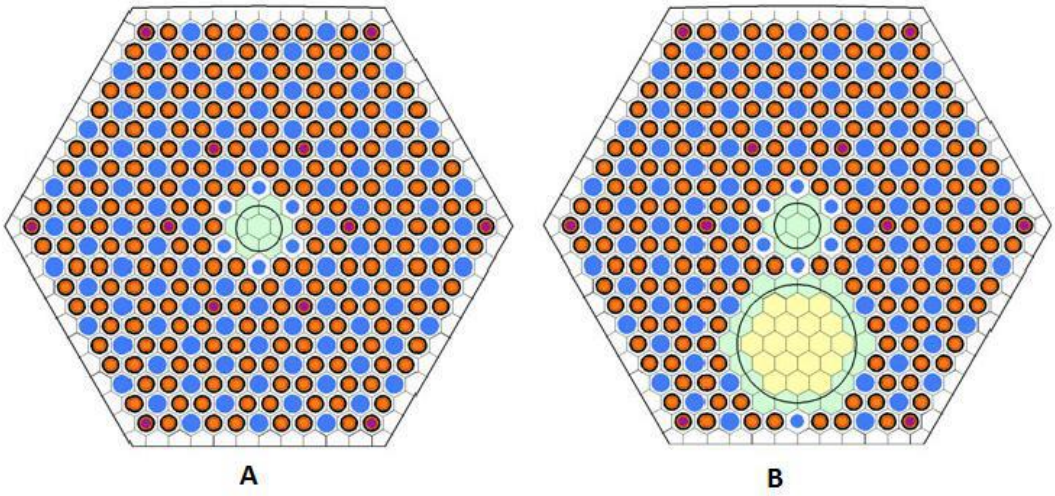

Figure 4-3: (A) standard fuel block (B) Control rod fuel block (Tak, Kim, Hong, & Noh, 2011)

Mass fraction of absorber material

Table 4-2: A comparison of the multiplication factor for different operating control rod depths

Depth of operating rods in the core	k_{eff}
1/6	1.20553 ± 0.00024
1/3	1.19789± 0.00027
1/2	1.18681 ± 0.00022
2/3	1.16968± 0.00023

It can be seen from Table 4-1 that the MCNP model of the pre-conceptual design renders a supercritical value of *1.19789*, with the operating control rods placed a third into the core. It is assumed that the reactor is critical at 300 K, so the mass fraction of absorber material is adjusted

until MCNP returns a result of k_{eff} that is approximately equal to 1. Table 4-2 shows the behaviour of k_{eff} in response to a variation in the depth of insertion of the operating control rods in the core. An insertion depth of 1/3 is chosen and the insertion depths greater than 1/3 are also tabulated in Table 4-2.

From Table 4-2, the result for k_{eff} for the different insertion depths of the operating controls is between 1.16968 and 1.20553. The similarity in the results can be explained by the disposition of the operating control rods in the core. The operating controls are placed in the graphite blocks, which are in a region of lower neutron flux. This can also be observed in Table 4-1, there is a small difference between the result of the multiplication factor of the full core model with the all control rods withdrawn ($k_{eff} = 1.21062$) and the result of the multiplication factor with operating controls rods placed a third in the core ($k_{eff} = 1.19789$).

Table 4-3: A comparison of the effective multiplication factor for different mass fractions of B_4C in the burnable poisons

Mass fraction of B_4C in absorber region (%)	k_{eff}
1.241	1.19789 ± 0.00027
3.9	1.01223±0.00025
4.2	**1.00020** ± **0.00026**
4.3	0.98920 ± 0.00027

The mass fraction of B_4C in the burnable poisons is set to 4.2% and the result of k_{eff} *is 1.00020.* Increasing the mass fraction of B_4C in the burnable poisons results in a lower excess reactivity.

As stated earlier, for a reactor that is producing power, the temperature will be higher than 300 K. This means that k_{eff} will be lower and the above calculation must be repeated to get a critical reactor state resulting in a different value for the mass fraction of B_4C in the burnable poisons. However this can only be done after the thermal fluids calculations are also set up.

Temperature coefficients (PMR200-TC)

For the effect of temperature to be analysed, the neutron multiplication factor k_{eff} of the reactor is computed at different temperatures. The control rod positions are kept at the critical position but when evaluating the operation of a real reactor, the critical control rod position should be changed (Evaluation of High Temperature Gas Cooled Reactor Performance: Benchmark Analysis Related to Intial Testing of the HTTR and HTR-10, 2003). All the materials are set at a uniform temperature of 300 K and only the part of the reactor that is being evaluated is altered by Δt.

The state of the reactor is sensitive to any changes in temperature. The deviation of the multiplication factor from the criticality is expressed in terms of reactivity ρ (Silva, Pereira, Veloso, & Costa, 2012).

$$\rho = \frac{k_1 - k_0}{k_1 \cdot k_0} \tag{4.1}$$

where k_0 is the value of the effective multiplication factor of the reactor at a steady state condition and at the critical position. k_1 is the effective multiplication constant due to a change in temperature (Δt). As mentioned earlier k_0= *1.00020 ± 0.00026.* Temperature coefficients can be defined as the change in reactivity with respect to the temperature and are obtained from the following relation (Silva, Pereira, Veloso, & Costa, 2012):

$$\alpha_T = \frac{k_1 - k_0}{k_1 \cdot k_0} \cdot \frac{1}{\Delta t} \tag{4.2}$$

The temperature is increased by Δt for each temperature coefficient computation. A rise in fuel temperature is due to fission heating. The fission heating is transported from the coated particle to the graphite of the fuel compact and the moderator. The temperature coefficients are analysed for the fuel and the moderator. Temperature coefficients for coolant are omitted because helium has a very low neutronic effect and is not affected significantly by the changes in temperature.

Doppler coefficient

To evaluate the Doppler coefficient, only the fuel temperature is varied by Δt, while the moderator temperature, moderator density and concentration of absorbers is kept constant. The Doppler coefficient is evaluated for the TRISO particle and the fuel compact. For the evaluation of the Doppler coefficient of the TRISO particle, the TRISO particle temperature is varied while the temperature of the other reactor components is kept constant. The Doppler coefficient of the compact is evaluated by varying the temperature of the compact, while the moderator and coolant temperatures are not altered. Note that the compact consists of the TRISO particles and the graphite matrix

The calculated values of k_{eff} are presented in Figure 4-4 and Figure 4-6 for the TRISO particle and the fuel compact respectively. The values of k_{eff} are presented with the standard deviation.

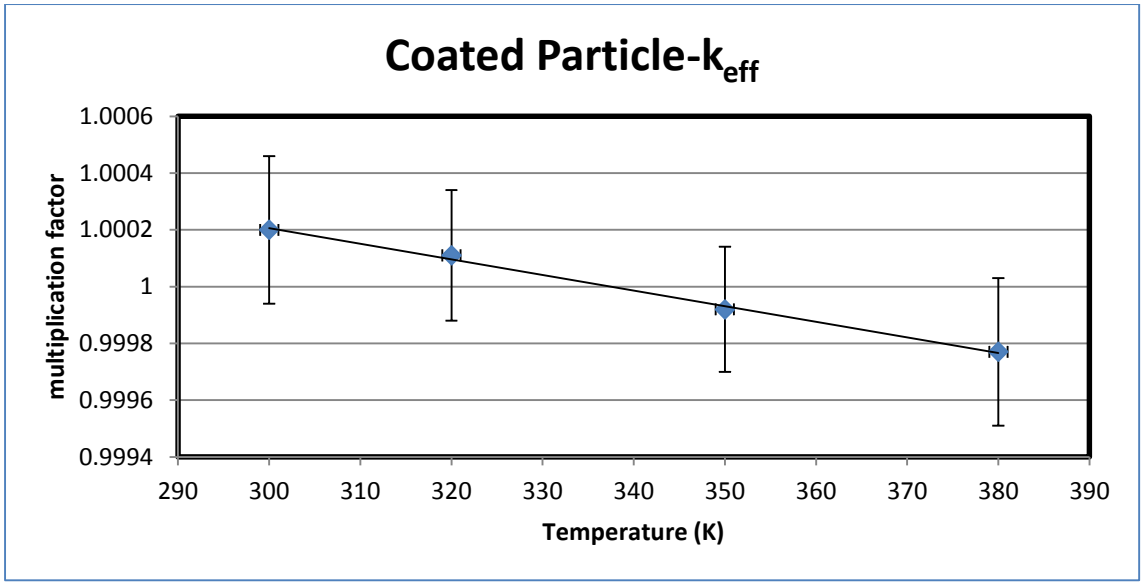

Figure 4-4: The response of k_{eff} on the variation of the temperature of the TRISO particle

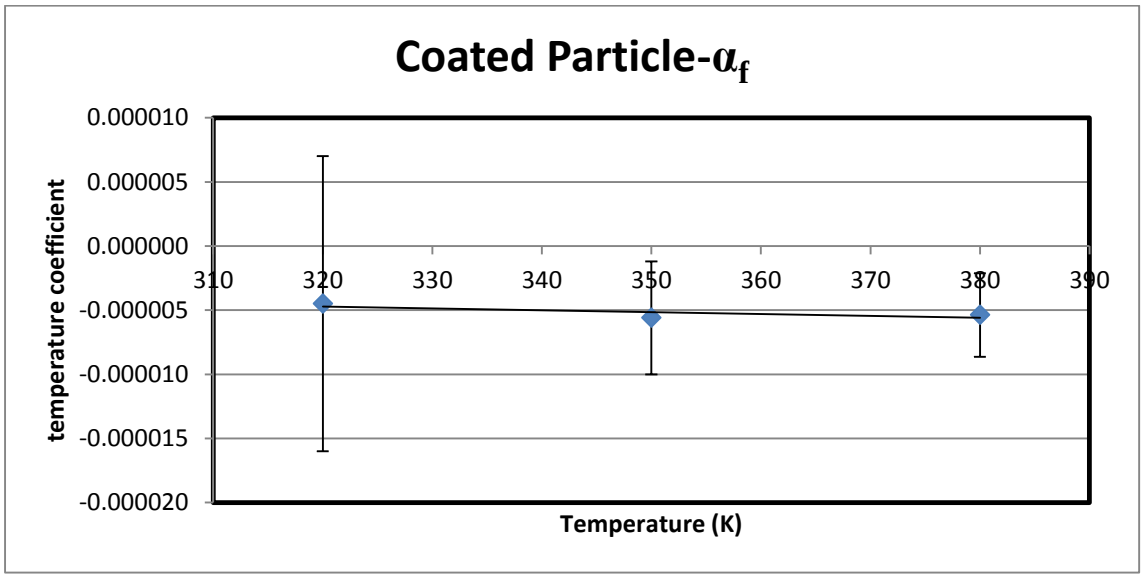

Figure 4-5: The Doppler coefficient of the coated particle

k_{eff} decreases with increasing temperature as shown in Figure 4-4 and Figure 4-6 respectively. However, this decrease is not larger than the statistical deviation. The reactivity of the coated particle and the fuel compact is negative regardless of all the temperature variations; hence the temperature coefficients are negative. This can be seen in Figure 4-5 and Figure 4-7.

The decrease of k_{eff} with increasing temperature is a result of the Doppler broadening of the resonance capture cross-sections of the ^{238}U. The fuel temperature increases, causing more neutrons to be absorbed in the fuel resonances of ^{238}U as they are being slowed down by the moderator. This results in a reduction in the resonance escape probability (p) and hence k_{eff}.

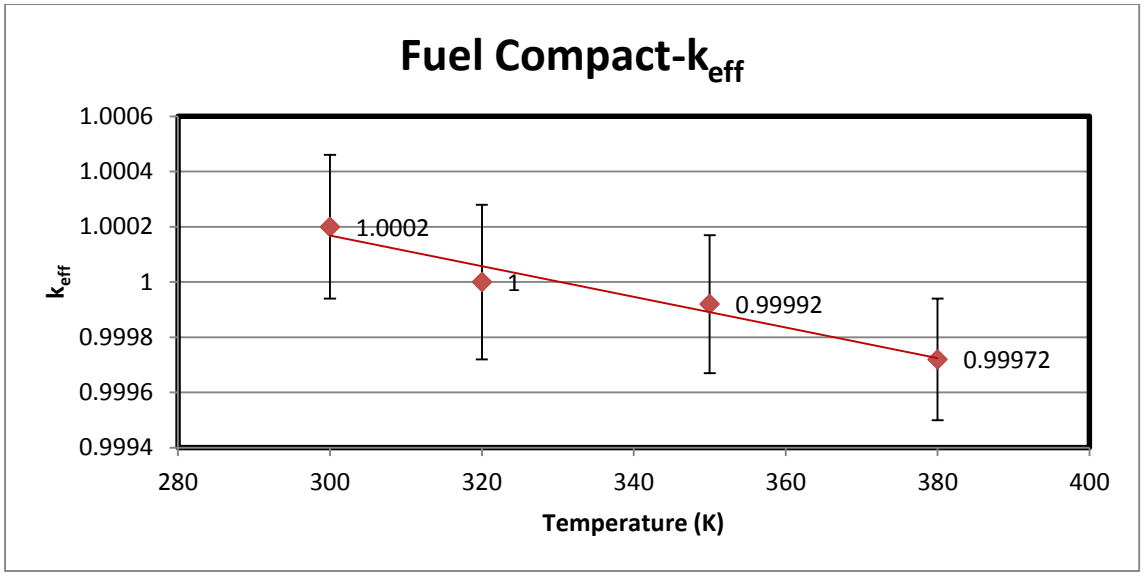

Figure 4-6: The response of the effective multiplication factor to a variation in temperature of the fuel compact

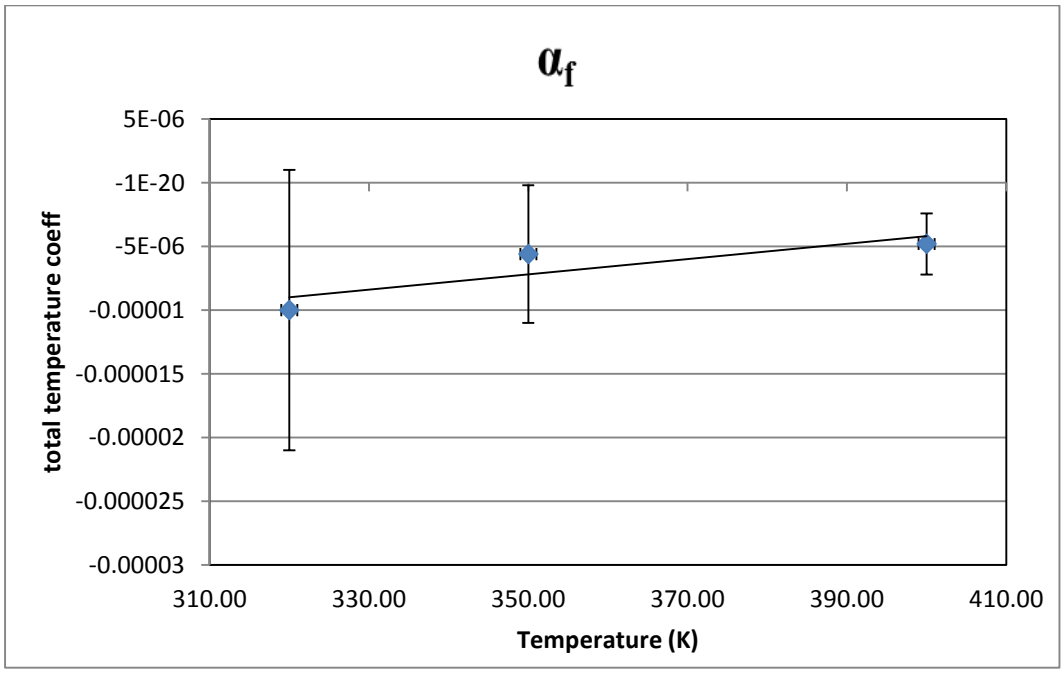

Figure 4-7: Doppler coefficient of the fuel compact

A negative Doppler coefficient indicates that the modelled reactor is stable and self-regulating, as discussed in section 2.1.14.

Moderator coefficient

To compute the moderator coefficient the temperature of the fuel compact as well as the temperature of the coolant is kept constant. Only the graphite, including the reflectors, is altered by *Δt*. The moderator coefficient is found to be negative, as presented in Figure 4-9. This indicates that the moderator moderates more than it absorbs. It should be noted that a solid moderator could be positive for some temperature and negative for others; however the fuel temperature coefficient must then be more strongly negative to compensate for this.

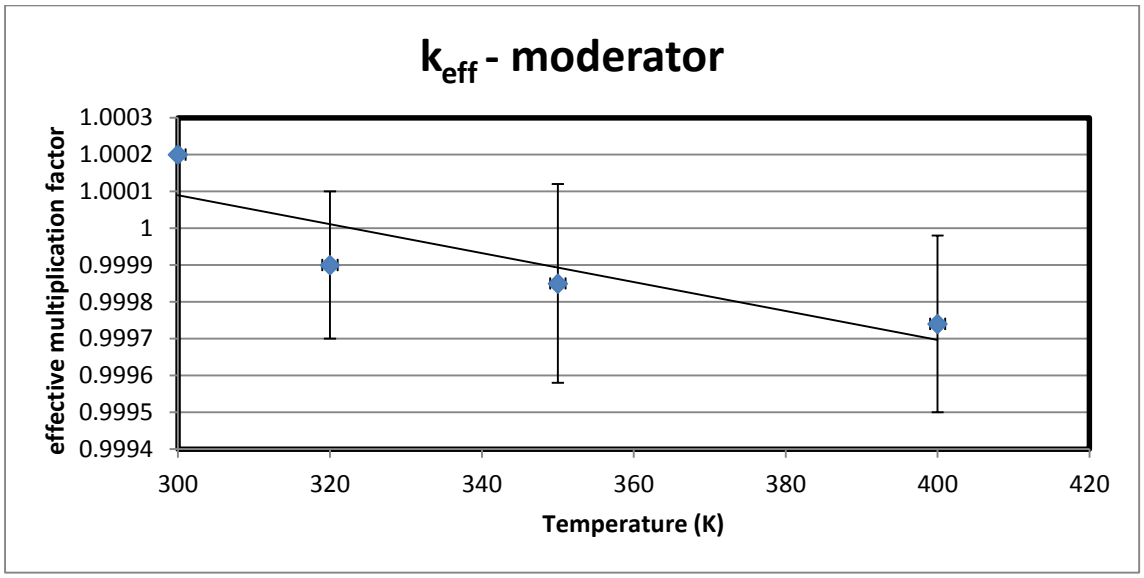

Figure 4-8: Effective multiplication factor of the moderator at different temperatures

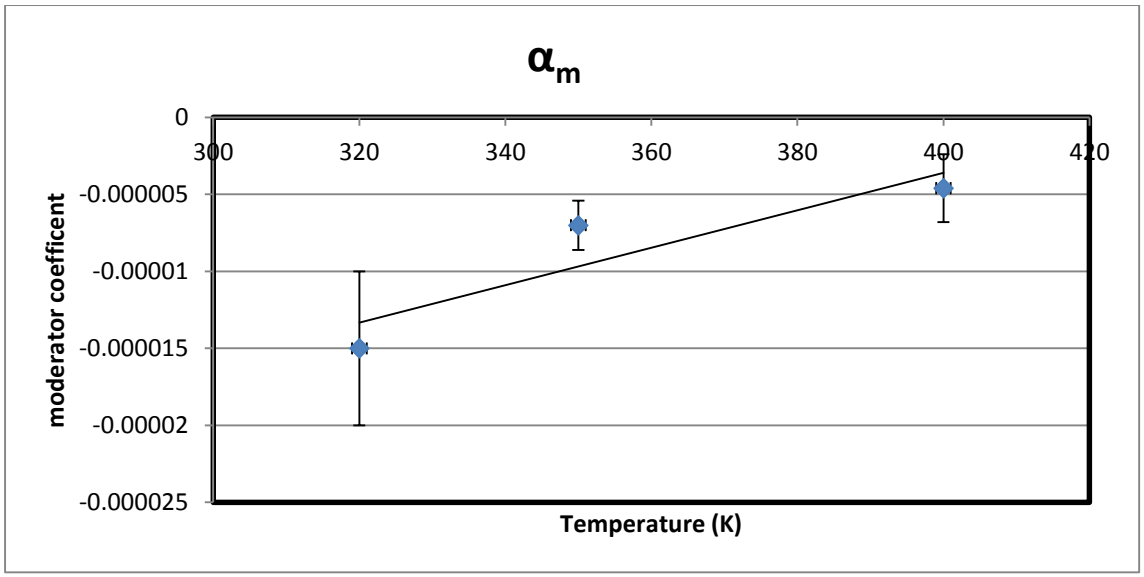

Figure 4-9: Temperature coefficient for a variation in moderator temperature

Calculated total temperature coefficient

The temperature coefficients of the fuel, moderator and reflector are compared in Table 4-4 for a temperature variation from 300 K to 320 K.

Table 4-4: Temperature coefficients for a temperature rise from 300 K to 320 K

α_F	-9.99988×10^{-6} K^{-1}
α_M	-1.59985×10^{-5} K^{-1}

The moderator coefficient is the most negative and has a large contribution to the negative reactivity. This is in agreement with the results presented in (Mulder & Teuchert, 2004) for the Pebble Bed Modular Reactor-400MW (PBMR 400). The total temperature coefficient can be calculated from

$$\alpha_T = \alpha_F + \alpha_M$$

The total temperature coefficient is found to be -25.9987×10^{-6}. K^{-1}, which is a desired negative value.

Isothermal temperature coefficients

For the computation of the isothermal temperature coefficients, the fuel and the moderator are at the same temperature. This is possible when the reactor is operated at very low temperatures to bring the core from room temperature to the operating inlet temperature of the helium coolant (Lewis, 2008). In Figure 4-10 the temperature is varied from 300 K to 400 K.

Figure 4-10, shows the value of k decreases steadily with increasing temperature and the total temperature coefficient is negative; therefore the model of the reactor is stable. These results are in agreement with results reported in (Jo, Noh, & Chang, 2005) as shown in Figure 4-12. The Doppler coefficient of the GT-MHR, which is a 600 MWth prismatic HTGR, is found to be negative under all operating conditions, namely the beginning of cycle (BOC), middle of cycle (MOC) and end of cycle (EOC). It should be noted that more histories should be run in order to increase the statistical accuracy of k_{eff}. However, this would be with the penalty that more computational time would be required. The same trend can be seen in (Evaluation of High Temperature Gas Cooled Reactor Performance: Benchmark Analysis Related to Intial Testing of the HTTR and HTR-10, 2003) for the HTTR where the temperature is varied from approximately 275 K to 480 K. The temperature increase is mostly due to the Doppler broadening of resonances, primarily of ^{238}U (Chiang, Wang, Sheu, & Liu, 2013). The isothermal temperature coefficients are negative because the reactivity is negative. A stable reactor should have a negative temperature coefficient.

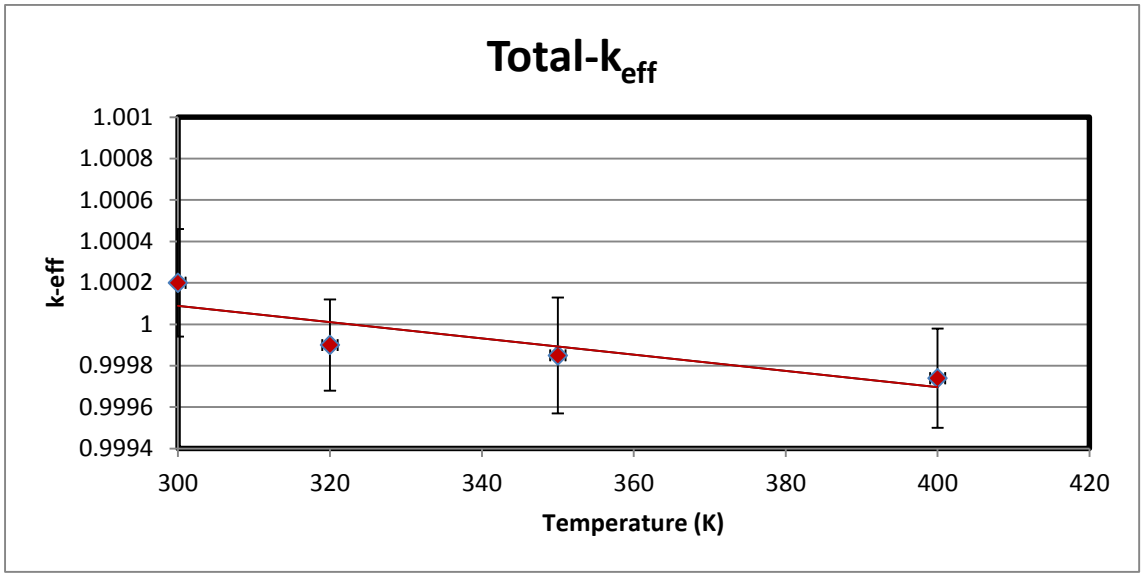

Figure 4-10: Effect of temperature on the effective multiplication factor

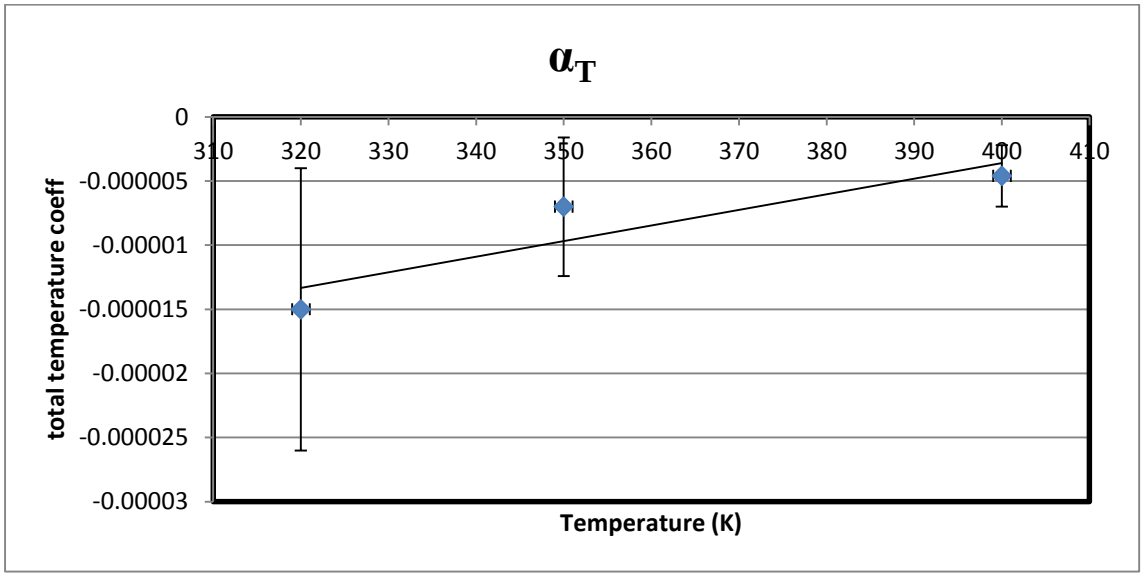

Figure 4-11: Isothermal temperature coefficient

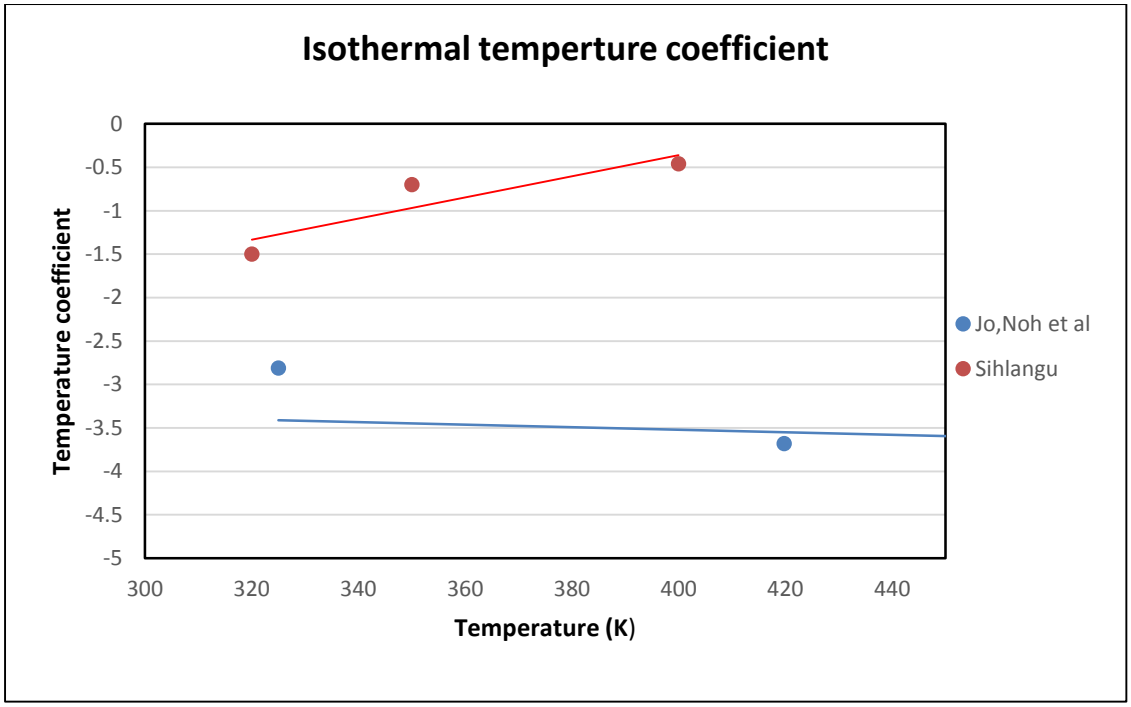

Figure 4-12: Isothermal temperature coefficients of the PMR200 (Sihlangu) and 600 MWth GT-MHR (Jo,Noh et al)

Control rod worth

The values for the control rod reactivity worth shown in Figure 4-13 are unique to the 24 operating control rods since these are the rods that control reactivity during operation. The x-axis reflects the vertical position in the core, with Z=0 being the top of the core and Z=475.8 being the bottom of the core. At start-up the controls are placed at a depth of 158.6 cm in the core and this is reflected by the zero reactivity. The operating control rods that are placed above 158.6 cm induce a positive reactivity value .

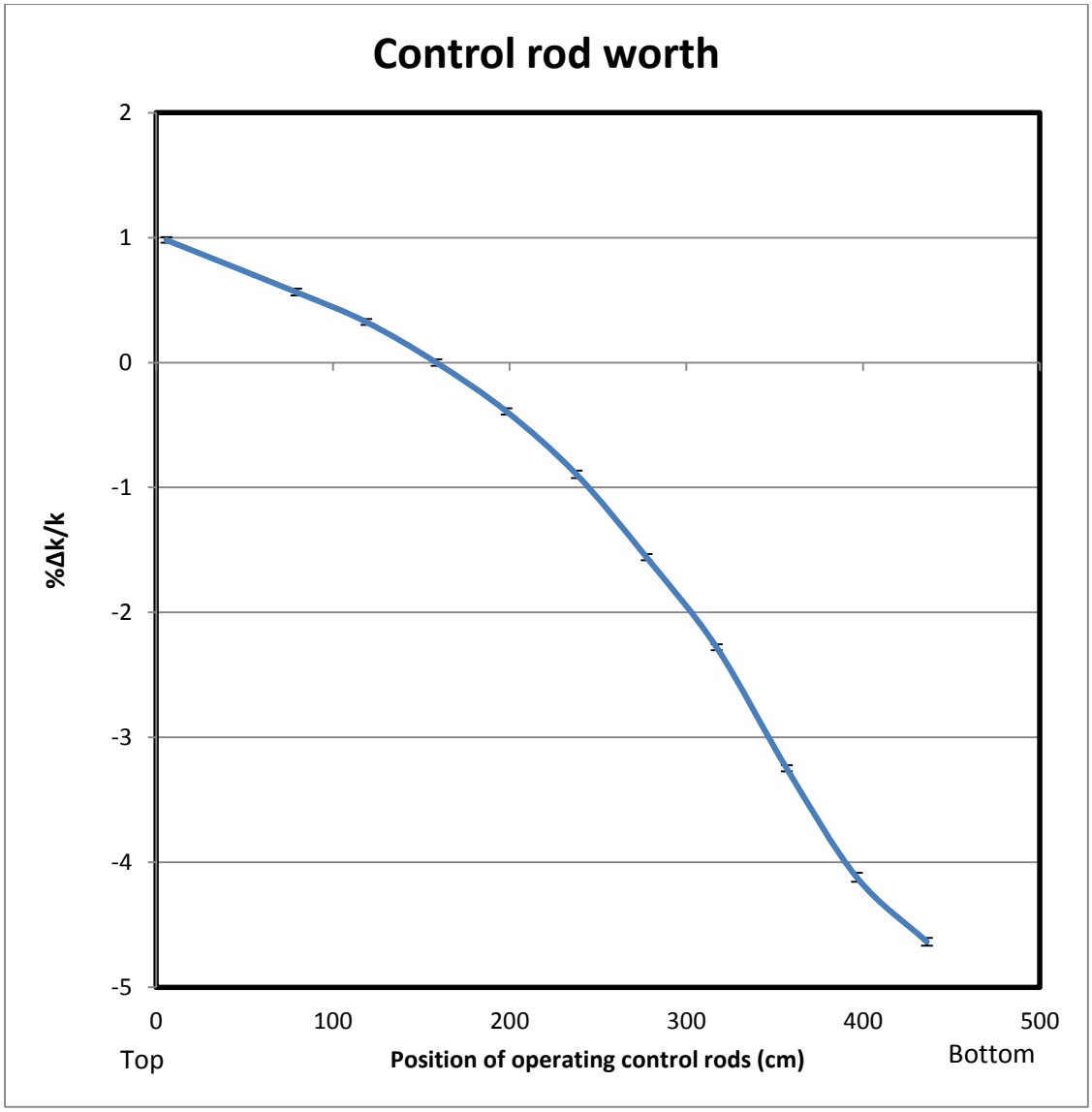

Figure 4-13: Operational control rod worth in the active core

The reactivity for the operational control rods is found to be between -4.635 and 0.98% $\frac{\Delta k}{k}$ so these rods have enough reactivity to change the reactor between a sub-critical state and a supercritical state. Analysis of the reactivity of the operating control rods is crucial since these rods are placed in the core during startup and overcome excess reactivity during startup.

SCRAM reactivity

Scram refers to the fast or emergency shutdown of a reactor (Kessler, 2012) . In order to study the scram reactivity, the operating control rods, which are placed at a certain position during operation, are all fully inserted into the reactor. The model is then modified so that only the reserve shutdown system is fully inserted into the core. Finally the model is modified so that both the operating rods and the RSS are fully inserted in the core. SCRAM reactivity is calculated from the criticality condition

when the operating rods are placed 1/3 into the core (317.2 cm). Reactivity is calculated using the following formula:

$$\rho = \frac{k - k_{crit}}{k.k_{crit}} \qquad (4.2)$$

where:

k_{crit} is the effective multiplication factor at the critical control rod position and has a value of *1.0020 ± 0.00026*

k is the *e*ffective multiplication factor after scram

Table 4-5: The effect of the shutdown system on reactivity

Description	**K_{eff}**	**Reactivity (%Δk/k)**
operating rods only	0.95396 ± 0.00023	-4.84619
RSS only	0.96292 ± 0.00031	-3.87078
Operating + RSS	0.91950 ± 0.00019	-8.77475
Operating + RSS + start-up	0.85451 ± 0.00023	-17.0461

The operating control rods have a more negative reactivity in comparison to the RSS. The RSS has the function of shutting down the reactor during emergency and accident conditions and the RSS in this model can effectively shut down the reactor. A combination of the two also effectively shuts down the reactor. The maximum insertion depth for all the control rods is 457.8 cm.

For the PBMR-400 the shutdown margin is chosen to be 1% for the RSS only (Reitsma, 2012) and the reactivity margin for the control rods is 5% for the GT-MHR (Kodochigov, et al., 2003). Using these limits as a guide, the shutdown margin of the reactor under study should be between 1 and 5%. The negative reactivity is 4.85% and 3.87% for the operating control rods and RSS respectively. Both the operating control rods and RSS lie within the margin.

Effect of the absorbers on flux

To evaluate the effect of the absorbers on the flux, the concentration of the absorber material is increased. Figure 4-14 is derived from the F4 mesh and considers the cylindrical geometry (r, z, θ) of the reactor. The angle θ and the radius R are kept constant and the relationship between the neutron flux and the height of the core is observed.

The tally results are divided into 11 tally bins in the radial direction, from the centre of the core (r=0) to the outer radius of the core (R=300). The tally bins in the Z-direction are divided into 17 tally bins from Z=0 to Z=755.8 (the top of the upper reflector) and the θ–direction is divided into 26 tally bins from 0 to 1 revolution.

At R=180.5 cm, the flux is depressed in comparison; this is because R=180.5 cm is in the vicinity of the control rod. R=36.1 cm is the radius extending to the inner reflector, where there is no absorber material. The operational control rods are at the critical control rod position.

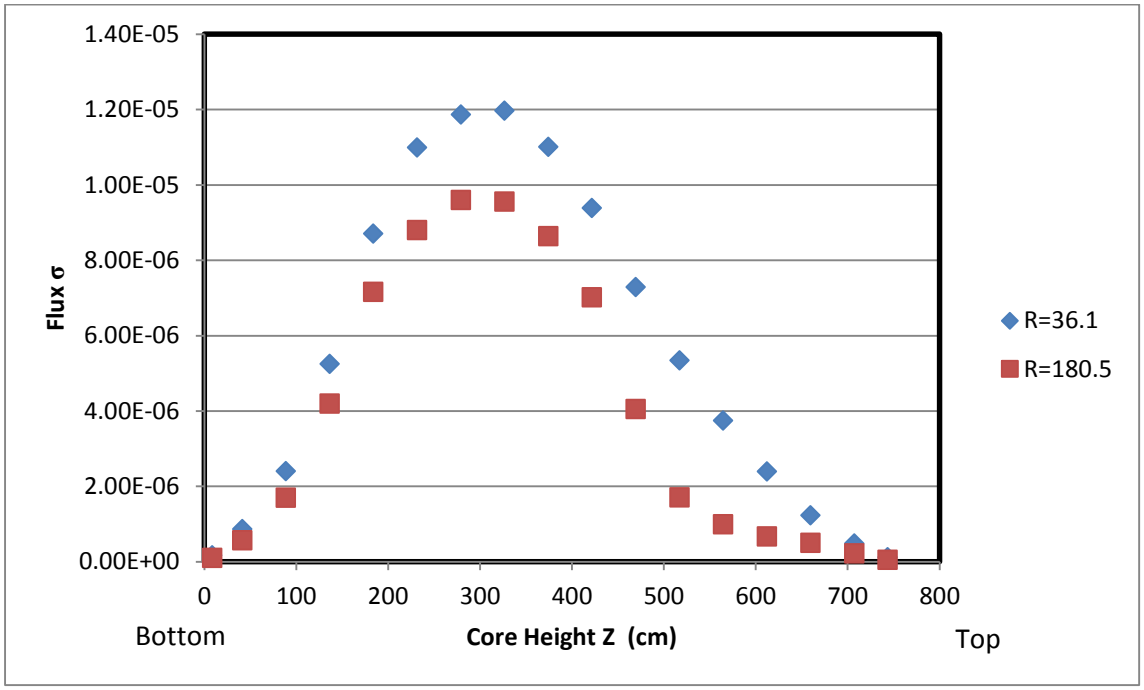

Figure 4-14 The effect of the presence of absorber material on the flux

To examine the effect of the control rods on the neutron flux, the neutron flux of the critical reactor model (CRIT CR) is compared to the flux of the model with the control rods withdrawn (CR OUT) and the flux of the model with the control rods fully inserted (CR IN). The density of the control rod material is multiplied by 4, to magnify the neutron flux results. In Figure 4-15 the parameters R=180.5 and θ= 0.006 are kept constant.

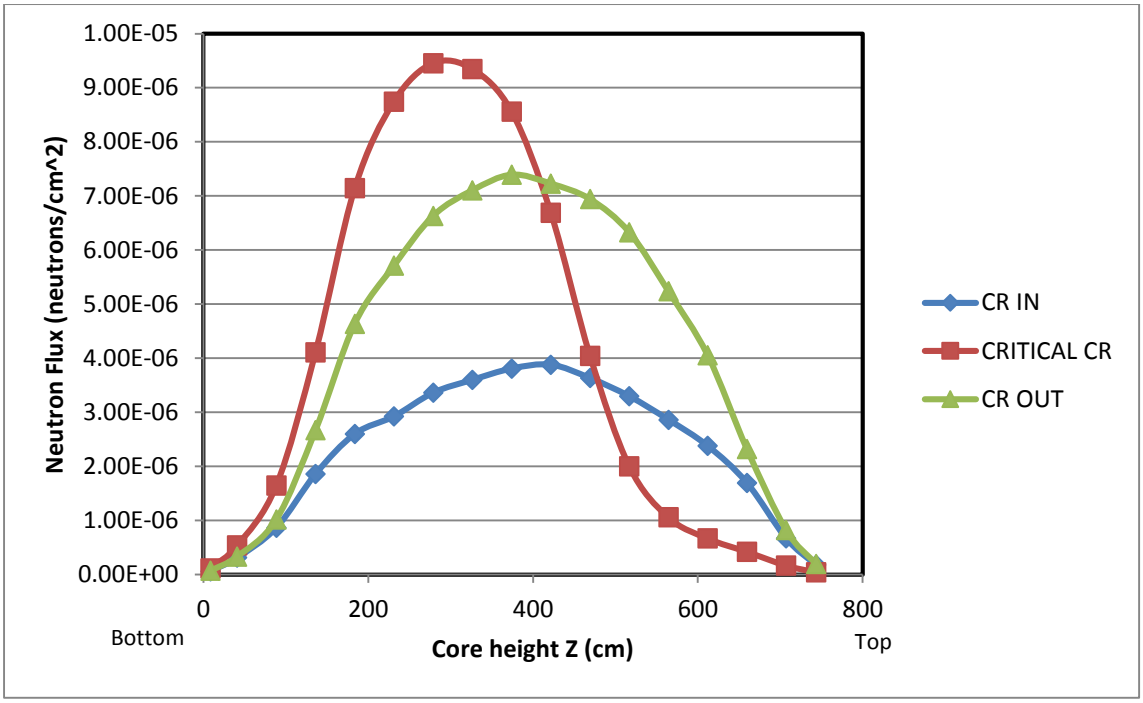

Figure 4-15: Comparison of the effect of the control rod position on flux

Figure 4-15 shows a depressed flux when the control rods are fully inserted (CR-IN), in comparison to the CR OUT plot and CRITICAL CR plot. The CRITICAL CR plot shows a depression at around a core height of $Z > 516.85$. This is where the operating control rods that are placed one third into the core are situated.

One sixth of the core is divided into 26 tally bins in the theta direction and some of these angles coincide with or are in the vicinity of the operational control rod. There are two control rods in the region of 162 < R < 198. The plots are shown in Figure 4-16 and Figure 4-17.

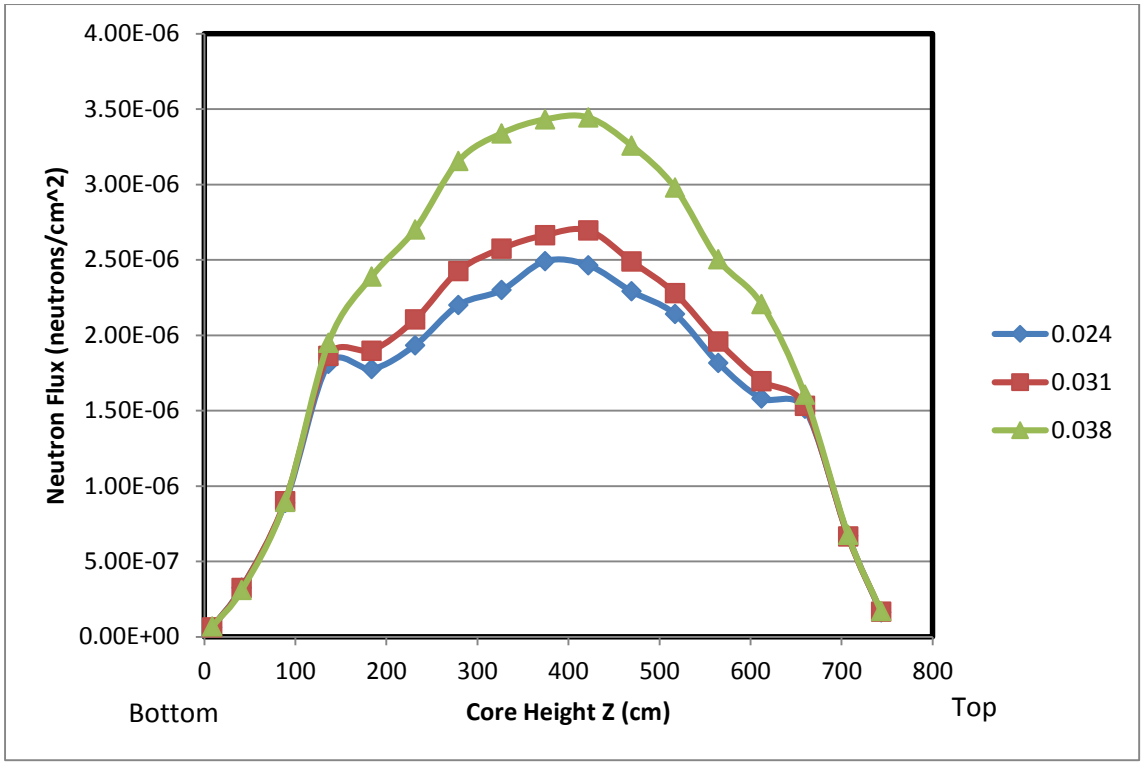

Figure 4-16: Neutron flux vs. core height for the controls rods fully inserted at different thetal directions

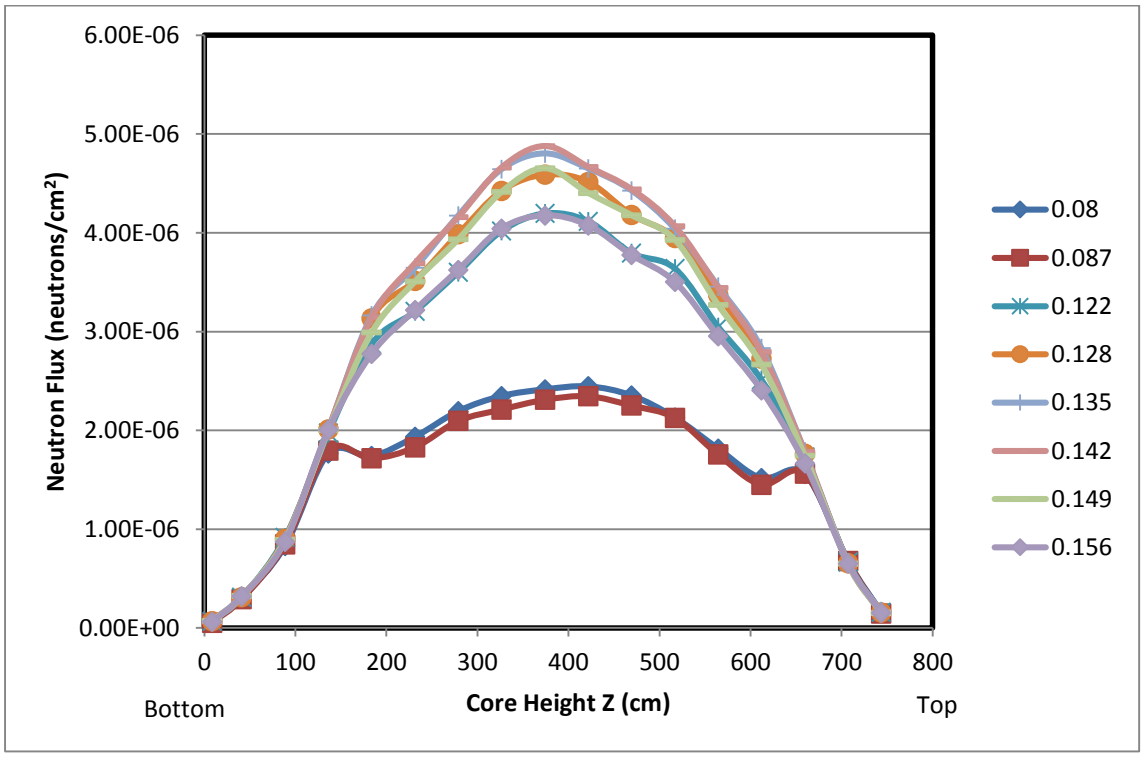

Figure 4-17: Neutron flux vs. core height for the controls rods fully inserted at multiple thetal directions

Figure 4-16 shows the location of the first control rod, where $\theta = 0.024$ and $\theta = 0.031$ are in the vicinity of the control rod in comparison to $\theta = 0.038$. Figure 4-17 shows the location of the second control rod. The flux at $\theta = 0.08$ and $\theta = 0.087$ is depressed in comparison to other positions. This shows the presence of a control rod in that region. A depression in flux is also observed at $\theta = 0.08$ for the critical control rod position, as shown in Figure 4-18. In Figure 4-19 the neutron fluxes are shown when there is no control rod in the reactor. The neutron flux plots coincide. These plots clearly show that the presence of the control rods has marked effects on the shape of the fluxes.

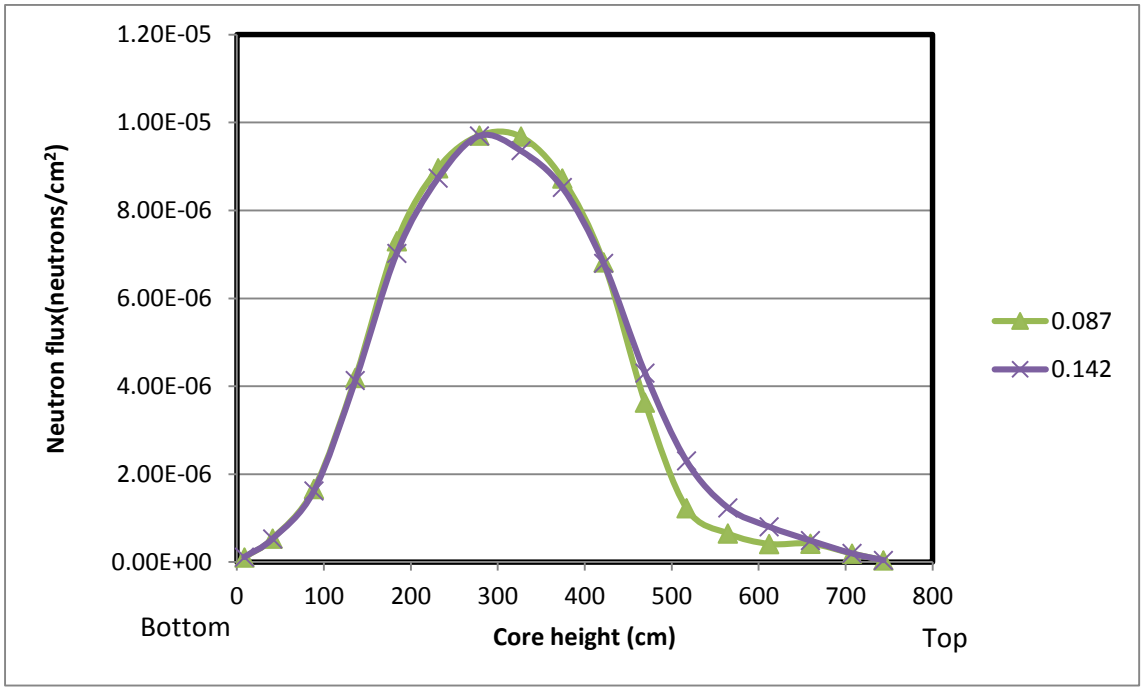

Figure 4-18: Neutron flux for the controls placed at the critical rod control position

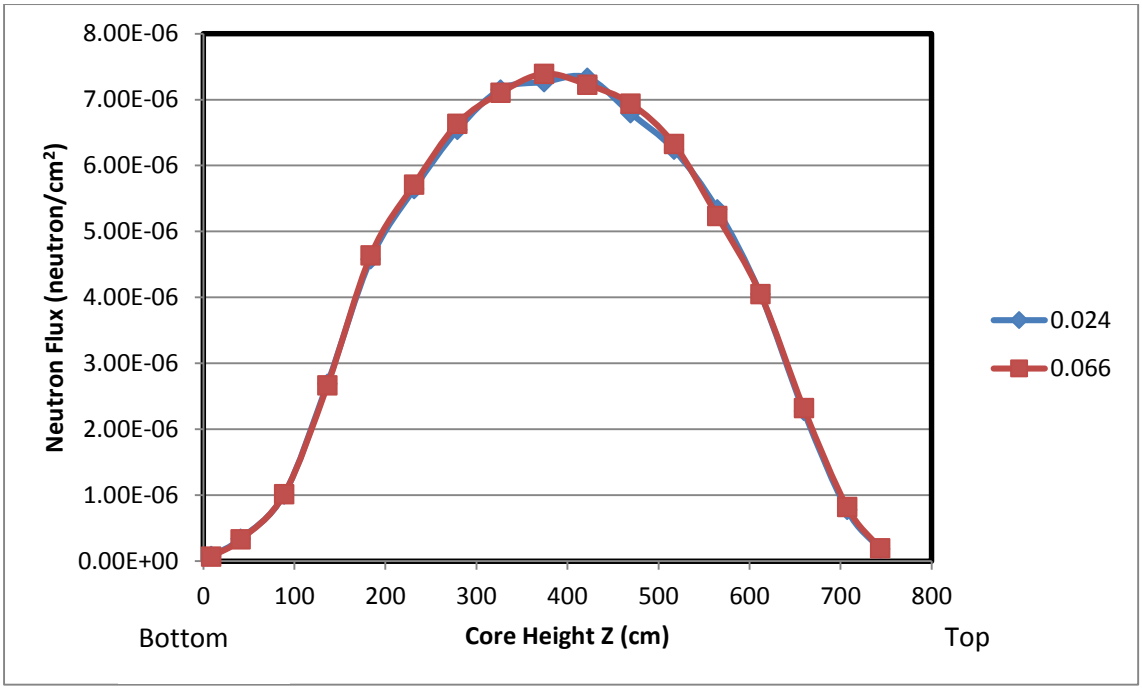

Figure 4-19: Comparison of control rod position vs. no control rod position for the control rods fully withdrawn

Adjusting the control rod B_4C

The neutron flux is evaluated at three different mass fractions of B_4C in the B_4C-C composite of the control rods. This is done to evaluate the effect of B_4C on the neutron economy. The mass fraction of B_4C is 1.241% in (c1), doubled to 2.482% in (c2) and tripled to 3.732% in (c3). The effect of the increase in the mass fraction of B_4C in the control rods can be observed in Figure 4-20.

The concentration of the neutron absorbers is increased in Figure 4-20 solely for the purpose of analysis. In reality, increasing the amount of neutron absorbers in the control rods is undesirable due to the possibility of the uncontrolled withdrawal of a control bank or the ejection of a control rod. This could increase the reactivity more than is desired.

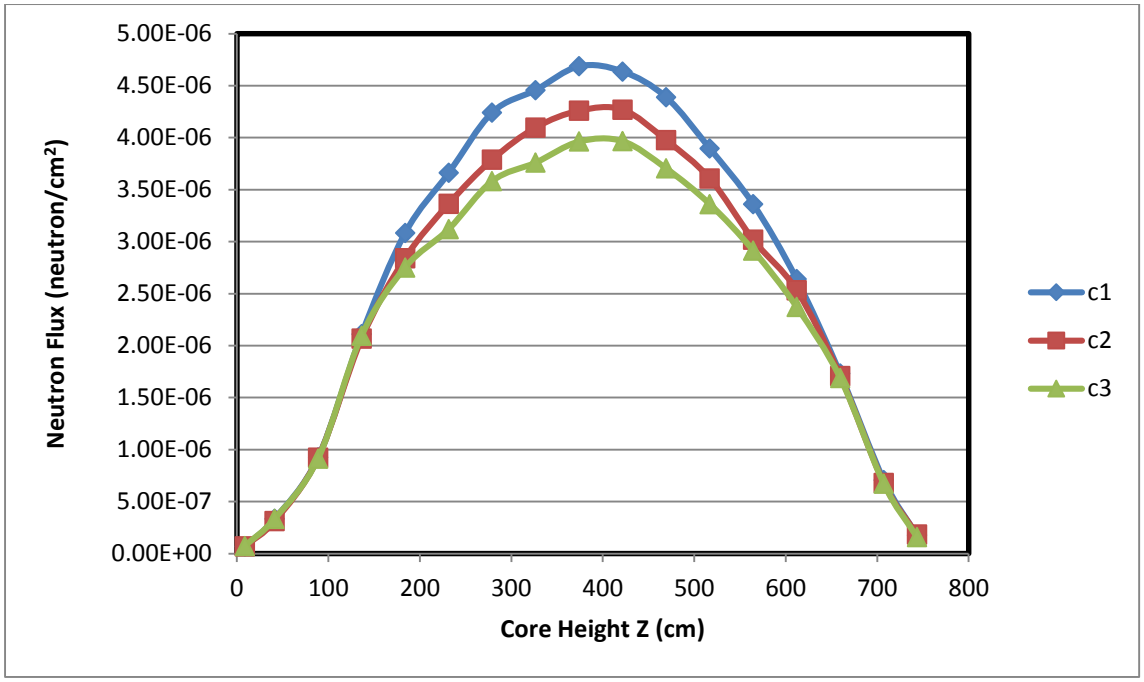

Figure 4-20: Comparison of different concentrations of B_4C in control rods

4.3.Time Economy of MCNP5

In this section the time expense of MCNP for each calculation is analysed. The calculations are run on two different machines to save time. The information for one of the machines is listed below.

Machine	Hp Probook 6570b
Processor	*i5-3210M*
Operating System	Windows 7
RAM	4.00GB

MCNP calculation	Time in minutes	Time in hours
Full core model without tallies	2345.46	39hrs 6 minutes
Full core model with tallies	11741.14	195hrs 41 minutes

The full core model requires a CPU time of 1.62 days and the full core model takes approximately 8 days of CPU time.

5. Conclusion

The PMR200 is a prismatic modular HTGR and the prismatic modular design is a strong candidate for NGNP. The reactor is in a pre-conceptual design phase and it is imperative to perform a neutronic analysis on a theoretical reactor design to verify the safety reactor. The choice of of the HTGR and Gen IV reactors is based on the inherent safety features, which include the retention of fission products, a negative temperature coefficient and a core that will not melt.

Calculations such as control rod reactivity worth and temperature coefficients are performed for safety analysis. These calculations are performed using MCNP5 for developing the core model. The code offers a practically real model of the HTGR since the hexagonal fuel assemblies are accommodated and the double-heterogeneity of the core is treated. However MCNP is not time efficient. It is imperative to perform convergence analysis before beginning the calculations so that there is no bias in the effective neutron multiplication factor and the source distribution. It is found that 110 skipped cycles is sufficient for convergence.

The initial criticality neutron effective multiplication factor for the pre-conceptual design is *1.21136.* Operating control rods placed at an active core depth of 158.6 cm and a B_4C mass fraction of 4.2% define the criticality condition of the reactor and the multiplication factor is determined to be 1.0002 at the critical state.

Doppler coefficients are computed for the TRISO particle and the fuel compact at temperature increments of 20 K, 30 K and 50 K. The initial temperature is 300 K. Both Doppler coefficients are found to be negative. The moderator coefficient is also found to be negative for the same temperature increments. The total temperature coefficient and isothermal temperature coefficients are found to be negative.

Two methods are presented to assess the effect of the control rods. The first method is the reactivity worth and the second is assessment of the effect of the control rods on the flux. Reactivity worth is analysed by placing the entire bank of operating control rods at different depths in the active core. Later the SCRAM reactivity of the RSS is analysed and found to be sufficient for emergency shutdown. Reactivity is also assessed for the full insertion of all three banks of control rods.

The effect of the B_4C in the control rods is compared for the critical control rod position, for the fully inserted control rods and for the fully withdrawn control rods. The flux is also analysed for the graphite blocks and the fuel blocks. The controls rods significantly depress the flux.

The CPU time economy of MCNP is analysed and each run requires substantial CPU time to complete. Using one CPU-core the full core takes approximately 1 day and 15 hours on an i5-3210M processor.

6. Recommendations for Future Work

The first recommendation is that the MCNP5 calculations be done on a High Performance computer to reduce CPU time.

Secondly the thermal fluid analysis of the PMR core must be coupled with the neutronics.

The third recommendation is that the convergence for the tallies is analysed. This was omitted in this study due to time constraints but it is crucial in terms of thermal fluid coupling. *Montwedi* did a study on a *"Neutronic Simulation of a European Pressurized Reactor"*, the effect of the number of cycles on tallies is analysed for 600, 800, 1200 and 3000 runs. It is found that the flux profile for 600 runs is not in agreement with 800, 1200 and 3000 runs and depending on the required precision; a minimum of 800 cycles is sufficient (Montwedi, 2014) .

Doppler coefficients of the fuel kernel require analysis, the coefficients were found to be positive and require recalculation and testing. In this regard, more histories could be run, and shorter temperature increments could be considered.

Uncontrolled control rod withdrawal is the most common type of initiator for a reactivity insertion accident. Analysis of this will complete the safety evaluations with regard to the control rods.

Finally, the accuracy of the model can be increased by considering the stochastic geometry of the fuel kernels in the compact and by making use of a finite lattice in defining the kernels in the compact.

7. Bibliography

Areva HTGR. (2014, March). Retrieved from High Temperature Gas-Cooled Reactor: https://us.areva.com

Bae, Y.-y., Hong, S.-D., & Kim, Y.-W. (2012, May 17-18). Scaling Analysis of Reactor Cavity Cooling System for PMR200. *Transactions of the Korea Nuclear Society Spring Meeting*. Jeju, Korea.

Brown, F. (2005). Fundamentals of Monte Carlo Particle Transport. *Lecture Notes for Monte Carlo course*. Report Reference: LA-UR-05-4983.

Brown, F. (2009, September 13-17). A Review of Best Practices for Monte Carlo Criticality Calculations. *2009 Nuclear Critucality Safety Topical Meeting*. Richland: American Nuclear Society.

Brown, F. B. (2006, September 10-14). On the Use of Shannon Entropy of the Fission Distribution for Assessing Convergence of Monte Carlo Criticality Calculations. *PHYSOR-2006, ANS Topical Meeting on Reactor Physics, Organized and hosted by the Canadian Nuclear Society.* Vancouver, BC,, Vancouver, Canada.

Brown, F. B., & Martin, W. R. (2004). Stochastic geometry capability in MCNP5 for the analysis of particle fuel. *Annals of Nuclear Energy 31*, 2039–2047.

Brown, F. B., Martin, W. R., Conlin, J. L., & Lee, J. C. (2005, April 17-21). Stochastic Geometry and HTGR Modeling with MCNP5. *Proc.Monte Carlo 2005 Topical meeting*. Chattanooga, Tennessee: American Nuclear Society.

Brown, F. B., Mosteller, R. D., & Sood, A. (2003). Verification of MCNP5. *Nuclear Mathematical and Computational Sciences: A Century in Review, A Century Anew*.

Brown, F. B., Mosteller, R. D., & Sood, A. (2003, April 6-11). Verification of MCNP5. *Nuclear Mathematical and Computational Sciences: A Century in Review, A Century Anew*. Tennessee, Gatlinburg, USA: American Nuclear Society.

Brown, F., Nease, B., & Cheatham, J. (2007, April 15-19). Convergence Testing For MCNP5 Monte Carlo Eigenvalue Calculations. *Joint International Topical Meeting in Mathematics & Computation in Nuclear Applications (M&C + SNA 2007)*. Monterey, California: American Nuclear Society.

Calldo, F. (2008, February 13). Eskom Power Crisis: Reasons, impact and possible solution. *Solidarity*. Centurion.

Chang, J. (2007, April 16-19). Status of Nuclear Hydrogen Production Technology Development Project in Korea. *International Conference on Non-electrical, Applications of Nuclear Power*. Korea: KAERI- Nuclear Hydrogen Development and Demonstration Plant.

Chang, J., Kim, Y.-W., Lee, K.-Y., Lee, Y.-W., Lee, W. J., Noh, J.-M., . . . Jung, K.-D. (2007, March 26). A Study of a Nuclear Hydrogen Production Demonstration Plant.

Chiang, M.-H., Wang, J.-Y., Sheu, R.-J., & Liu, Y.-W. H. (2013). Evaluation of the HTTR criticality and burnup calculations with continuous-energy and multigroup cross-sections. *Nuclear Engineering and Design*.

Chirayath, S. (2013). *Personal communication*. Texas A&M University.

Cop17 fact sheet. (2011, August). Retrieved February 11, 2015, from www.eskom.co.za

Criekgen, S. V. (2004, June). Mixed-Hybrid Dicretization Methods for the Linear Transport Eqaution. *Northwestern University*. Evanston, Illinois.

Employment, unemployment,skills and economic growth. (2014). *An exploration of household survey evidence on skills development and unemployment between 1994 and 2014*. Statistics South Africa.

Eskom. (2015). Retrieved from Eskom: www.eskom.co.za/OurCompany/CompanyInformation/Pages/Company_Information_1.aspx

Evaluation of High Temperature Gas Cooled Reactor Performance: Benchmark Analysis Related to Intial Testing of the HTTR and HTR-10. (2003). *Nuclear Power Technology Development Section, International Atomic Agency*. Vienna, Austria: IAEA-TECDOC-1382.

Gee, D. (2002, March 16). The Pebble Bed Modular. *Spring 2002: EEE 460 WebProject*.

Han, T. Y., Lee, H. C., Jo, C. K., & Noh, J. M. (2013). Homogenized cross section generation considering axial heterogeneity for VHTR fuel block. *Nucl.Eng.Des*.

Hendricks, J. S., Adams, K. J., Booth, T. E., Briesmeister, J. F., Carter, L. L., Cox, L. J., . . . Prael, R. E. (2000). Present and future capabilities of MCNP. *Applied Radiation and Isotopes 53*, 857-861.

Hussein, E. (1997, April 8). *Monte Carlo Method for Particle Transport Simulation, Course1.6 [Chapter11 : Uncertainity Analysis in MCNP].* Retrieved from Chulalongkorn University: www.nuceng.ca

IAEA. (2010). *High Temperature Gas Cooled Reactor.* Vienna: International Atomic Energy Agency.

Intergrated Resource Plan For Electricity 2010-2030. (2011, March 25). Retrieved from doe-irp.co.za

International Atomic Energy Agency, I. (n.d.). *General Atomic's Prismatic Modular Temperature Gas Cooled Reactor.* Retrieved from http://www-pub.iaea.org/MTCD/publications/PDF/TE_1645_CD/PDF/TECDOC_1645.pdf

Jo, C. K., Noh, J. M., & Chang, J. (2005, October 27-28). Preliminary Analysis of Temperature Coefficients for a 600MWth. *Transactions of the Korean Nuclear Society Autumn Meeting*. Busan, Korea.

Kessler, G. (2012). *Sustainable and Safe Nuclear Fission Energy.* Berlin Heidelerg: Springer.

Kim, K.-S., Cho, J.-Y., Lee, H. C., Noh, J. M., & Zee, S. Q. (2007). Development of a physics analysis procedure for prismatic very high temperature gas-cooled reactor. *Annals of Nuclear Energy 34*, 849-860.

Kim, K.-S., Cho, J.-Y., Lee, H. C., Noh, J. M., & Zee, S. Q. (2007). Developmental of a physics analysis procedure for the prismatic very high temperature gas-cooled reactor. *Annals of Nuclear Energy 34*, 849-860.

Kim, M.-H., & Lim, H.-S. (2011). Evaluation of the influence of bypass flow gap distribution on the core hot spot in. *Nuclear Engineering and Design 241*, 3076– 3085.

Kissane, M. P. (2009). A Review Of Radionuclide behaviour in the primary system of a very high temperature reactor. *Nuclear Engineering and Design*, 3076-3091.

Kodochigov, N., Sukharev, Y., Marova, E., Ponomarev-Stepnoy, N., Glushkov, E., & Fomichenko, P. (2003). Neutronic features of the GT-MHR reactor. *Nuclear Engineering and Design*, 161–171

Kuijper, J. C., Paepsaet, X., de Haas, J. M., von Lensa, W., Ohlig, U., Ruetten, H. J., . . . Seiler, R. (2006). HTGR reactor physics and fuel cycle studies. *Nuclear Enginnering and Design 236*, 615-634.

Kulikowska, T. (2000). An Introduction to neutron transport phenomena. *Lecture given at the Workhop on Nuclear Data and Nuclear Reactors: Physics, design and Safety*. Trieste, Italy.

Kunitomi, K., Katanishi, S., Takada, S., Takizuka, T., & Yan, X. (2004). Japan's Future HTR- the GTHTR300. *Nuclear Enginnering and Design 233*, 309-327.

Kuppers, C., Hahn, L., Heinzel, V., & Weil, L. (26 March 2014). The AVR Experimental Reactor-Development, Opeartion, and Incidents. *Final Report of the AVR Expert Group*. Julich.

LaBar, M. P., Simon, W. A., Shenoy, A. S., & Campbell, E. M. (n.d.). The Gas-Turbine Modular Helium Reactor. *Nuclear Energy Materials and Reactors - Vol.II*.

Lamarsh, J. R. (2nd edition). *Introduction to Nuclear Engineering.* Massachusetts: Addison-Wesley Publishing Compony.

Lee, H. C., Jo , C. K., Shim, H. J., Kim, Y., & Noh, J. M. (2010). Decay heat analysis of VHTR cores by Monte Carlo core depletion calculation. *Annals of Nuclera Energy 37*, 1356-1368.

Lewis, E. E. (2008). *Fundamentals of Nuclear Reactor Physics.* Academic Press.

Lewis, E. E., & Miller, W. F. (1985). *Computational Methods of Neutron Transport.* NY: John Wiley and Sons.

Lin, B., & Wesseh Jr., P. K. (2014). Energy consumption and Economic growth in South Africa reeaximined: A nonparametric testing apporach. *Renewable and Sustainable Energy Reviews 40*, 840-850.

Lohnert, G. (2004). Topical issue on "Japan's HTTR". *Nuclear Engineering and Design 233*, 1-3.

Mansour, H., Saad, H. M., & Aziz, M. (2013). Analysis of Reactivity - Intiated Accident for Control Rods Ejection. *Journal Of Nuclear and Particle Physics*, 45-54.

Mantahantsha, S. (2014, March 10). *Eskom CEO, chairman at odds over power crisis*. Retrieved from BusinessDay BD live: www.bdlive.co.za/business/energy/2014/03/10/eskom-ceo-chairman-at-odds-over-power crisis

Martin, W. (June 2012). *Creation of a Full-core HTR Benchmark with the Fort St. Vrain Initial Core and Assessment of Uncertainties in the FSV Fuel Composition and Geometry.* Ann Arbor: University of Michigan, Department of Nuclear Engineering and Radiological Sciences.

Matthews, C. (2014, Septemper 23). *Rosatom announces SA nuclear power deal.* Retrieved from Business Day BDLive: www.bdlive.co.za/business/energy/2014/09/23

Mcdowell, B. K., Mitchell, M. R., Pugh, R., Nickolaus, J. R., & Swearingen, G. L. (2011). *High Temperature Gas Reactors: Assement of Applicable Codes and Standards.* Richland, Washington: Pacfic Northwest National Laboratory.

Menyah, K., & Wolde-Rufael, Y. (2010). Energy consumption, pollutant emmisions and economic growth in South Africa. *Energy economics 32*, 1374-1382.

Mez, L. (2012). Nuclear energy–Any solution for sustainability and climate protection? *Energy Policy 48*, 56–63.

Montwedi. (2014, North-West University). Neutronic simulation of a European Pressurised Reactor. *MSc Thesis*. Potchefstroom, South Africa.

Moormann, R. (2008). Fission Product Transport and Source Terms in HTRs: Experience from AVR Pebble Bed Reactor. *2008*.

Mosteller, R. D. (n.d.). *Validation Suits for MCNP.* Retrieved from Los Alamos National Laboratory: http://lib-www.lanl.gov/cgi-bin/getfile?00796677.pdf

Mulder, E., & Teuchert, E. (2004, April 25-29). Plutonium disposition in the PBMR-400 High-Temperature Gas-Cooled Reactor. Chicago, Chicago, Illinois: on CD-ROM, American Nuclear Society.

Naicker, V., du Toit, M. H., & Nyalunga, G. P. (2015). NWURCS User Guide. North West University.

NUCL 878 course. (2014). *HTR technology Lecture Notes, Lecture Presented by Dr Cilliers*. North-West University, Potchefstroom, South Africa.

Pavlou, A. T., Betzler, B. R., Burke, T. P., Lee, J. C., Martin, W. R., & Pappo, W. N. (2012). Eigenvalue sensitivity studies for Fort St Vrain high temperature gas-cooled reactor to account for fabrication and modeling uncertainties. *Physor* .

Reitsma, F. (2012). Reactivity considerations for the on-line refuelling of a pebble bed modular. *Nuclear Engineering and Design 251*, 18– 29.

Reitsma, F. (2012). Reactivity considerations for the on-line refuelling of a pebble bed modular. *Nuclear Engineering and Design 251* , 18– 29.

Reitsma, F. (2014). *Personal communication*. North West University, Potchefstroom, South Africa.

Saurwen, J. (2007). *Preconceptual Engineering Services For The Next Generation Nuclear Plant (NGNP) with Hydrogen Production.* General Atomics for the Battelle Energy Alliance, LLC.

Schwarz, A. L., Schwarz, R. A., & Carter, L. L. (2011, March). MCNP/MCNPX Visual Editor Computer Code for Vised Version 24E. [Distributed on transmittal DVD in MCNP5\mcnp5_dist.tgz; will be extracted to MCNP5\utilities\VISUAL_EDITOR.]: Documentation on the MCNPDATA libraries may be found in Appendix G of the MCNPX manual and on the web http://www-xdiv.lanl.gov/projects/data/nuclear/mcnpdata.html .

Seker, V., & Colak, U. (2003). HTR-10 full core first criticality analysis with MCNP. *Nuclear Enginnering and Design 222*, 263-270.

Silva, F. C., Pereira, C., Veloso, M., & Costa, A. L. (2012). Shifting study of a VHTR using reprocessed fuel with various TRISO packing fractions. *Nuclear Engineering and Design 248*, 42-47.

Simulations, N. -M. (2010, November 17). MCNP Modeling of the very high temperature reactor (VHTR).

Slabber, J. (2004, September 22-24). Pebble Fuel Advantages. *2nd Topical Meeting on High Temperature Reactor Technology*. Beijing.

Sousa, R., Tanure, L., Costa, D. F., Pereira, C., Veloso, M., & Oliviera, A. (2014). A preliminary neutronic evaluation of the high temperature nuclear reactor (HTTR) using reproccessed fuel. *Annals of Nuclear Energy*, 232-238.

Southworth, F. H., MacDonald, P. E., Harrell, D. j., Shaber, E. L., Park, C. V., Holbrook, M. R., & Petti, D. A. (2003, November 16-30). The Next Generation Nuclear Plant (NGNP) Project. *global*, (pp. 276-287).

Stacey, W. M. (2007). *Nuclear Reactor Physics.* Atlanta: Wiley-VCH Verlag GmbH.

Tak, N.-i., Kim, M.-H., Hong, S. L., & Noh, J. M. (2011). A practical method for whole-core thermal analysis of Prismatic gas-cooled reactor. *Korea Atomic Research Institute*. 1045 Daedok street, Yuseong-gu, Daejeon 305-353, Korea.

Tak, N.-i., Kim, M.-H., Lim, H.-S., Jun, J. S., & Jo, C. K. (2010, October 21-22). Whole-Core Thermal Analysis of Prismatic Very High Temperature Reactor. *Transactions of the Korean Nuclear Society Autumn Meeting*. Jeju, Korea.

Trollip, H., Butler, A., Burton, J., Caetano, T., & Godinho, C. (2014). *Energy Security in South Africa.* Cape Town: MAPS.

Tyobeka, B., Ivanov, K., & Pautz, A. (2008). Evaluation of PBMR control rod worth using full. *Annals of Nuclear Energy 35*, 1050–1055.

van Wyk, J.-A. (2013, June). South Africas Nuclear Future. *SAIIA Occasional Paper No 150*.

X-5 Monte Carlo Team. (2003). *MCNP Version 5, Vol 1: Overview and Theory, LA-UR-03-1987*.

Zakova, J., & Talamo, A. (2008). Criticality assesment for prismatic high temperature reactors by fuel stochastic Monte Carlo modeling. *Annals of Nuclear Energy, 35*, 856-860.

8. Appendices

Appendix 1: Boltzmann equation

The Boltzmann equation was introduced by Ludwig Boltzmann in 1872. This equation has numerous applications including radioactive transfer in planetary and stellar atmospheres, electron transport in plasmas and neutron transport in nuclear reactors (Criekgen, 2004). It describes the statistical behaviour of neutrons in a fluid. The time-independent linear Boltzmann transport equation can be expressed as follows. All details are from (Brown, 2005).

$$\Psi(r,v) = \int \left[\int \Psi(r',v') C(v' \to v, r') dv' + Q(r',v) \right] T(r' \to r, v) dr'$$

$\Psi(r,v) =$ particle collision density

$Q(r',v)$= source term

$C(v' \to v, r')$= collision kernel, change in velocity at a fixed position

$T(r' \to r, v)$= transport kernel, change at fixed velocity

The source term is given by

$$Q(r,v) = \begin{cases} S(r,v) & \leftarrow Fixed\ source \\ S(r,v) + \int \Psi(r,v') F(v' \to v, r) dv' & \leftarrow Fixed\ Source + Fission \\ \frac{1}{K} \int \Psi(r,v') F(v' \to v, r) dv' & \leftarrow Eigenvalue \end{cases}$$

where

$S(r,v)$= fixed source

K= eigenvalue

$F(v' \to v, r)$ = creation operator (due to fission): a particle at (r,v') creates a particle at (r,v)

Assumptions

- Time independent

- Particles don't interact with each other
- Particle interactions don't interfere with material composition
- No long-range forces
- Markovian next event depends only on current(r,v,E) not previous events
- Relativistic effects are neglected
- Material properties are not affected by particle reactions

Appendix 2: Probability distribution function

$$\int_a^b f(x)dx = 1 \tag{1}$$

$f(x)dx$ is the probability that a variable x assumes a value within dx about x.

$f(x)$ is the probability distribution function, pdf

x is a variable that assumes a range of values that lie in the interval $a \leq x \leq b$

Appendix 3: Cumulative distribution function

The $F(x)$ is a monotonically increasing function of x termed the cumulative distribution function *(CDF)* and is defined as the probability that the variable x assumes a value less than or equal to x (details from (Stacey, 2007)).

$$F(x) = \int_a^x f(x')dx' \tag{2}$$

The probability that a neutron takes on a value between x and $x + dx$ is $F(x + dx) - F(x) = f(x)dx$

Appendix 4: URAN card in MCNP5

The URAN card in MCNP offers the user the option of random geometry modelling for the coated fuel particles. The URAN card has the following form. All details are from (X-5 Monte Carlo Team, 2003, pp. 3-33).

URAN n_1 dx_1 dy_1 dz_1 n_2 dx_2 dy_2 dz_2

n_1 is the universe which is flagged stochastic and the stochastic transformation is applied. dx_1, dy_1 and dz_1 are the maximum values in the positive or negative x-direction, y-direction and z-direction respectively. The second set of parameters n_2, dx_2, dy_2 and dz_2 are a second optional transformation.

When a neutron enters a stochastic embedded universe, the coordinates of the universe are determined by

$$x = x + (2\xi_x - 1).\delta_x$$

$$x = x + \left(2\xi_y - 1\right).\delta_y$$

$$x = x + (2\xi_z - 1).\delta_z$$

where ξ_x, ξ_y, ξ_z are random numbers uniformly distributed on (0,1) and δ_x, δ_y and δ_z are the user defined parameters supplied on the URAN card.